공학박사 학위논문

Development of Bismuth/Graphene Nanocomposite-Modified Electrodes and Their Application for Electrochemical Detection of Trace Heavy Metal Ions

비스무스/그래핀 나노복합체로 개질된 전극 개발 및 미량 중금속 이온의 전기화학적 검출 응용

2017년 2월

서울대학교 융합과학기술대학원

융합과학부 나노융합전공

이 소 희

Abstract

Development of Bismuth/Graphene Nanocomposite-Modified Electrodes and Their Application for Electrochemical Detection of Trace Heavy Metal Ions

Sohee Lee
Program in Nano Science and Technology
Graduate School of Convergence Science & Technology
Seoul National University

Heavy metals are considered one of the main sources of environmental pollution. Their main source is industrial activity, which directly or indirectly discharge the heavy metal species into the

environment. Certain heavy metals (e.g., mercury, cadmium, chromium, and lead) are highly toxic and affect several human organs, even at trace levels. For example, mercury and lead are known to cause damage to the nervous system, cadmium causes kidney and bone disease, and excessive absorption of zinc affects multiple aspects of the immune system. Heavy metal pollution is of great concern for global sustainability. It is therefore essential to monitor heavy metals in the environment, drinking water, food, and biological fluids. Traditional analytical methods include atomic absorption spectroscopy (AAS), inductively coupled plasma mass spectrometry (ICP-MS), and inductively coupled atomic emission spectrometry (ICP-AES). Although these techniques are highly sensitive and selective, they require laborious pre-treatment processes, expensive instruments, and professional personnel. In contrast, analytical electrochemical stripping techniques have attracted great interest in the detection of heavy metals. Owing to properties including short analytical time, low cost, and high sensitivity, electrochemical detection methods have been widely recognized as powerful techniques for the detection of heavy metals. In particular, anodic stripping voltammetry (ASV), a technique that consists of deposition

and stripping steps, is used very frequently. Mercury electrodes have proven to be valuable tools for this technique. However, considering their toxicity and the difficulty involved in the handling of mercury, these electrodes have recently been replaced by mercury-free electrodes. Several elements have been tested for their capacity to replace mercury (e.g., bismuth, gold, silver, antimony, and carbon). In recent years, bismuth electrodes have been attracting increasing attention in ASV analysis. The remarkable stripping performance of bismuth electrodes is attributed to the ability of bismuth to form ‘fused alloys’ with heavy metals. These alloys are analogous to the amalgams formed by mercury. Additionally, because of their fast electron transfer rate, unique structural characteristics, and high surface area, carbon-based nanomaterials are employed extensively as sensing materials to detect heavy metals.

This dissertation aims at presenting the fabrication of bismuth-based nanocomposites that can be employed in the development of electrochemical sensors for the detection of heavy metals.

Firstly, chemically activated reduced graphene (AG) was used with Nafion as a sensing material for the first time. This material was placed on a glassy carbon electrode (GCE, modified by *in-situ*-

deposited bismuth) to fabricate an electrochemical platform for the simultaneous and individual determination of three heavy metals in solution. Next, the graphene was prepared by electrochemical deposition directly onto a GCE surface. The bismuth film was then deposited *in situ* on the surface of the electrochemical sensor electrode that was used for sensitive determination of trace heavy metals. Finally, an iron oxide/graphene nanocomposite was directly produced by heat treatment of a mixture of iron oleate and graphene. The GCE was modified with the as-prepared nanocomposite, and employed as an electrochemical sensing platform for sensitive analysis of heavy metal ions. The generated iron oxide nanoparticles were homogeneously embedded in the graphene layers. These act as mutual spacers in the nanocomposite, preventing restacking of the graphene, and enhancing the detection sensitivity towards heavy metals.

These bismuth-based nanocomposites enable the electrochemical sensing of heavy metals with graphene- or nanoparticle-modified electrodes. The results suggest that these nanocomposites can improve the sensitivity and stability of the system.

Keywords: Bismuth, nanocomposite, Heavy metal detection, Graphene, Anodic stripping voltammetry, Electrochemical sensor, Modified electrode.

Student Number: 2011-22758

Contents

List of Figures

List of Tables

Chapter 1. Introduction: Bismuth/Graphene Nanocomposite-Modified Electrodes for Detection of Trace Heavy Metal Ions and Dissertation Overview

1.1 Introduction

Heavy metal pollution is one of the most serious environmental problems hindering global sustainability. Although some heavy metals (iron, selenium, cobalt, copper, manganese, and zinc) play vital roles in biological functions, many others are toxic [1]. Moreover, they tend to form complexes, especially with ligands in biological matter containing nitrogen, sulfur, and oxygen. This may lead to changes in the molecular structure of proteins, breaking of hydrogen bonds, or enzyme inhibition [2]. For example, mercury (sources: coal burning, as well as mining and industrial waste) and lead (sources: automobile exhaust, old paints, mining wastes, incinerator ash, and water from lead pipes) are both known to cause damage to the nervous system; cadmium, whose sources include the electroplating

and mining industries, is associated with kidney disease; and arsenic (sources: herbicides and the mining industry) is known to cause damage to the skin, eyes, and liver [3].

They are non-biodegradable and therefore can accumulate in the food chain and persist in ecological systems, exposing top-level predators to very high levels of pollution. Thus, safe limits or maximum contaminant levels for drinking water have been defined by different organizations worldwide. Table 1.1 summarizes the standards and guidelines for heavy metals in drinking water recommended by the World Health Organization [4]. These guidelines are based on toxicity data and scientific studies. Heavy metal pollution has become of great concern for global sustainability. Therefore, it is essential to monitor heavy metals in the environment, drinking water, food, and biological fluids.

Conventional methods for trace heavy metal analysis require sophisticated analytical techniques, including atomic absorption spectroscopy (AAS) [5], inductively coupled plasma-mass spectrometry (ICP-MS) [6], inductively coupled plasma-atomic emission spectrometry (ICP-AES) [7], and ultraviolet−visible (UV-vis) spectroscopy [8]. Although these techniques are highly sensitive and

selective, they require tedious sample preparation and preconcentration procedures, expensive instruments, and professional personnel. Moreover, they cannot be carried out using portable devices for on-site detection. Efforts are ongoing for the preparation of rapid and inexpensive techniques for heavy metal detection. Thus, techniques including colorimetry, fluorimetry, and voltammetry have been adapted to allow miniaturization and on-site application.

Electrochemical measurements have exhibited numerous advantages for the detection of trace heavy metals. These include rapid analysis, good selectivity, and sensitivity. Because heavy metals have a defined redox potential, selectivity toward specific heavy metal ions can be achieved by bare electrodes without the need of a molecular recognition probe. Several techniques have been employed in electrochemical sensing, including voltammetry, amperometry, potentiometry, impedemetry, and conductometry [10]. In particular, the anodic stripping voltammetry (ASV) method is readily amendable for the determination of heavy metals. Its remarkable sensitivity is attributed to the combination of an effective preconcentration step with advanced measurement procedures. This generates an extremely favorable signal-to-background ratio. Four to six metals can be

measured simultaneously in various matrices at concentration levels as low as 10^{-10} M. Moreover, this technique utilizes relatively inexpensive and portable instrumentation. Proper choice of the working electrode is crucial for the success of the stripping operation. The ideal working electrode should offer effective preconcentration, a favorable redox reaction of the target metal, a reproducible and renewable surface, and a low background current over a wide potential range. Owing to the high overpotential of hydrogen that allows its use at useful negative potentials, mercury became established as the preferred electrode for electrochemical stripping analysis. Two basic electrode systems, the mercury film electrode and hanging mercury electrode, have gained wide acceptance in the development of ASV [11]. While these mercury electrodes provide an attractive stripping performance, new alternative electrode materials with a similar performance are desirable for addressing growing concerns regarding the toxicity, handling, volatility, and disposal of mercury. The recent trend towards green chemistry aims to reduce and eliminate the use and generation of hazardous substances. Thus, several countries have banned the export and storage of metallic mercury. In this context, the search for alternative materials that can

be applied to the fabrication of heavy metal electrochemical sensors has spurred considerable research during the last decade. Several metals such as bismuth, gold, silver, antimony, carbon, and boron-doped diamond have been tested for their capacity to replace mercury. The proposed alternative, touted as an environmentally green species, is bismuth. This metal has been widely adapted by researchers as a replacement for mercury film electrodes. Moreover, the use of an *ex-situ*- or *in-situ*-modified bismuth electrode has been reported to give rise to significant electroanalytical improvements over that of a bare electrode. The advantageous analytical properties of bismuth-film electrodes, roughly comparable to those of mercury-film electrodes, are attributed to the property of bismuth to form "fused alloys" with heavy metals. This may be analogous to the amalgams that mercury forms with a similar sensitivity [12]. The design of the bismuth electrode plays a major role in the resulting stripping performance. In most cases, a carbon substrate is used to support the bismuth film. A variety of carbon electrodes of different sizes and geometries can be used. The choice of substrate affects the final results and is therefore a crucial factor in the production of bismuth film electrodes. Thus, very different results can be obtained from different electrode substrates,

even when the same conditions to form the bismuth film are applied. Although these electrodes have been used in ASV analysis of heavy metals, the limit of detection and the sensitivity of bismuth film electrodes cannot meet the need for the detection of trace heavy metals. An effective way to solve these issues is the surface modification of bismuth electrodes with nanomaterials. Nanomaterials (for example, nanoparticles, carbon-based materials such as carbon nanotubes and graphene, and nanostructures) possess a higher surface area, improved electron transfer rate, and increased mass transport. Such nanomaterial-modified electrodes, employed for the stripping analysis of heavy metals, exhibit dramatically increased sensitivity due to their unique chemical, physical, and electronic properties.

The combination of bismuth with nanomaterials such as nanoparticle- or carbon-based materials possesses a high degree of specificity. This makes the developed sensing formats attractive for the design and fabrication of integrated detection systems for real sample application.

This chapter introduces a classification of electrochemical sensors and presents synthetic methods of bismuth-based electrodes suitable

for the detection of heavy metals. In the succeeding section, various types of bismuth-based nanocomposite electrodes are introduced. The final section is an overview of the fabrication of bismuth-based nanocomposite electrodes, and the application of these electrodes for the detection of heavy metals.

Metal	World Health Organization (mg/L)
Nickel	0.07
Copper	2
Zinc	3
Cadmium	0.003
Mercury	0.001
Lead	0.010
Arsenic	0.010

Table 1. 1 Standards and guidelines for heavy metals in drinking water recommended by the World Health Organization.

1.2 Electrochemical Sensors

The oldest electrochemical sensors date back to the 1950s and were used for oxygen monitoring. More recently, many efforts have been made to develop new and better electrochemical sensors for the monitoring of toxic materials in environment. Electrochemical measurements have shown numerous advantages for trace heavy metal detection, including rapid analysis, good selectivity, and sensitivity. Several techniques are employed in electrochemical sensing, including voltammetry, amperometry, potentiometry, impedemetry, and conductometry [13]. In particular, the ASV method is readily amendable for determination of heavy metals.

The electrochemical analysis techniques are discussed in the next section.

Stripping step	Accumulation step	Measure	Technique
Linear or staircase anodic voltage scan	Electrolytic reduction	*i* vs *E*	Anodic stripping voltammetry
	Adsorption	*i* vs *E*	Adsorptive anodic stripping voltammetry
Pulsed anodic voltage scan	Electrolytic reduction	*Δi vs E*	Differential pulse anodic stripping voltammetry
	Adsorption	*Δi vs E*	Differential pulse adsorptive anodic stripping voltammetry
Linear or staircase cathodic voltage scan	Electrolytic oxidation	*i* vs *E*	Cathodic stripping voltammetry
	Adsorption	*i* vs *E*	Adsorptive cathodic stripping voltammetry
Constant anodic current	Electrolytic oxidation	*E* vs *t*	Anodic chronopotentiometric stripping analysis
Constant cathodic current	Adsorption	*E* vs *t*	Cathodic chronopotentiometric stripping analysis
Constant current	Adsorption	*E* vs *t*	Adsorptive chronopotentiometric stripping analysis
Chemical oxidation or reduction	Electrolytic reduction or oxidation	*E* vs *t*	Potentiometric stripping analysis

Table 1. 2 Classification of electrochemical stripping techniques [4].

1.2.1 Electrochemical Stripping Techniques

Electrochemical stripping techniques are among the most sensitive of instrumental analytical techniques. Because of their high sensitivity and selectivity, they are important in trace analysis and speciation studies. With detection limits generally in the 10^{-11} to 10^{-9} mol L^{-1} range and in a few cases as low as 10^{-12} mol L^{-1}, they are three or four orders of magnitude more sensitive than the simple polarographic methods. The high sensitivity and selectivity of stripping techniques arises because two distinct controlled electrochemical steps are involved.

In the first step the analyte is transferred to the electrode surface in one of two ways namely; (i) by electrolytic oxidation or reduction which results in the analyte forming a deposit on the working electrode or (ii) by the adsorption of the analyte directly or in combination with other reagents onto the electrode surface. This first step, which is a pre-concentration, enrichment or accumulation step, is carried out while the working electrode is held at a constant potential. In the accumulation process a fraction of the analyte is transferred from the test solution matrix and forms a phase on or in the electrode in which its

concentration is orders of magnitude higher than it is in the test solution. On completion of the accunulation step, a rest period of 10 to 30 s is observed so that the test solution can come to rest before the second step is commenced.

In the second step, the amount of analyte accumulated at the working electrode is determined by monitoring the electrical response produced as this accumulated material is either oxidised or reduced from the electrode. This process is referred to as the stripping step since the material accumulated during the first step is stripped from the electrode and normally passes back into solution. The stripping is carried out in one of three ways namely: (i) varying the potential on the working electrode and monitoring the current response (voltammetry), (ii) passing a constant current through the cell and measuring the potential that the working electrode develops as a function of time (chronopotentiometry), or (iii) chemically and monitoring the potential of the working electrode during the stripping process (potentiometry). In the voltammtric methods the potential applied to the working electrode in the stripping step may be in the form of a linear scan, staircase, A.C. modulated linear scan or staircase, square wave modulated linear scan or staircase, or a pulsed

linear scan or staircase voltage [9].

Because the different accumulation and determination procedures may be combined in a variety of ways, a whole family of electrochemical stripping techniques has been developed many of which are listed in Table 1.2.

1.2.2 Voltammetric Stripping

Stripping voltammetry comprises a group of various techniques including Anodic stripping voltammetry (ASV), Cathodic stripping voltammetry (CSV) and Adsorptive stripping voltammetry (AdSV). It is an ultrasensitive detection technique based on electrochemical measurements similar to polarography. Stripping voltammetry is a two-step technique that allows simultaneous detection of various inorganic and organic species in the sub-nanomolar range. The first step consists of the electrolytic deposition of a chemical species onto an inert electrode surface at a constant potential. This preconcentration step explains the remarkable sensitivity of the technique. It can involve either an anodic or cathodic process. However, the most common use of stripping voltammetry involves a

cathodic process for deposition in which the metal ionic species are reduced from the solution to the electrode surface. The second step consists of the application of a voltage scan to the electrode. At a specific potential, it causes the stripping of a specific species accumulated onto the electrode surface as amalgam or thin films, into the solution. The resulting faradic current is proportional to the concentration of the chemical species [12].

In particular, ASV method is readily amendable for determination of heavy metals. ASV analysis typically involves two steps; (i) electrochemical deposition or accumulation of heavy metals at a constant potential to preconcentrate the analyte onto the electrode surface, and (ii) stripping or dissolution of the deposited analyte from the electrode surface (Figure 1.1 and 1.2).

Cathodic stripping voltammetry is used for the indirect determination of inorganic and organic anions which form sparingly soluble salts with Hg(I) or Ag(I). When a mercury (or silver) electrode is anodically polarized, Hg_2^{2+} (or Ag^+) are produced and react with the analyte to form the sparingly soluble Hg(I) or Ag(I) salt which accumulates on the electrode surface. The accumulation potential depends on the supporting electrolyte, the solubility product

of the Hg(I) or Ag(I) salt, and the concentration of the analyte in the test solution. For mercury electrodes E_{acc} is usually in the range $+0.4$V to -0.2V (vs Ag/AgCl). In the determination step, a cathodic potential scan is applied to reduce the Hg(I) or Ag(I) in the sparingly soluble salt accumulated on the electrode surface which gives rise to the voltammetric current peak.

In AdSV, conversely to ASV, the preconcentration step of the metal ions at the surface of the electrode is made by a non-electrochemical process, in the form of complexes. Notably, Ni and Co were quantified by AdSV after complexation with dimethylglyoxime [13], Cr after complexation with cupferron [14] and Al after complexation with cupferron [15]. In analytical practice, stripping voltammograms are recorded in the differential pulse or square wave modes, which are generally more sensitive than normal scan mode.

Differential pulse voltammetry is comparable to normal pulse voltammetry in that the potential is also scanned with a series of pulses. However, it differs from normal pulse voltammetry because each potential pulse is fixed, of small amplitude (10 to 100 mV), and is superimposed on a slowly changing base potential. Current is measured at two points for each pulse, the first point (1) just before

the application of the pulse and the second (2) at the end of the pulse. These sampling points are selected to allow for the decay of the non-faradaic (charging) current. The difference between current measurements at these points for each pulse is determined and plotted against the base potential. The excitation signal in square wave voltammetry consists of a symmetrical square-wave pulse of amplitude Esw superimposed on a staircase waveform of step height ΔE, where the forward pulse of the square wave coincides with the staircase step. The net current, i_{net}, is obtained by taking the difference between the forward and reverse currents ($i_{for} - i_{rev}$) and is centered on the redox potential. The peak height is directly proportional to the concentration of the electroactive species and direct detection limits as low as 10^{-8} M are possible [16].

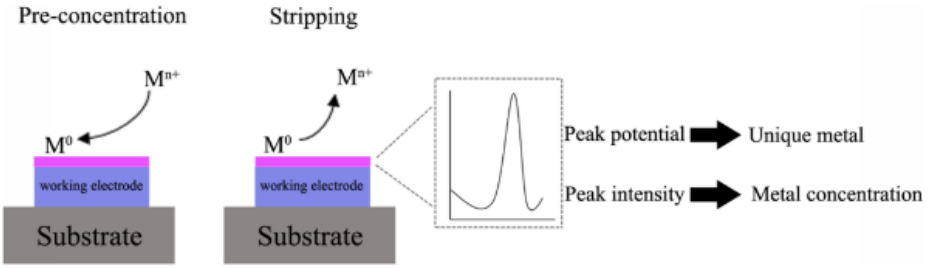

Figure 1. 1 Anodic stripping voltammetry principle. (Reprinted with permission from Ref. Biosensors, 5, 2015, 241)

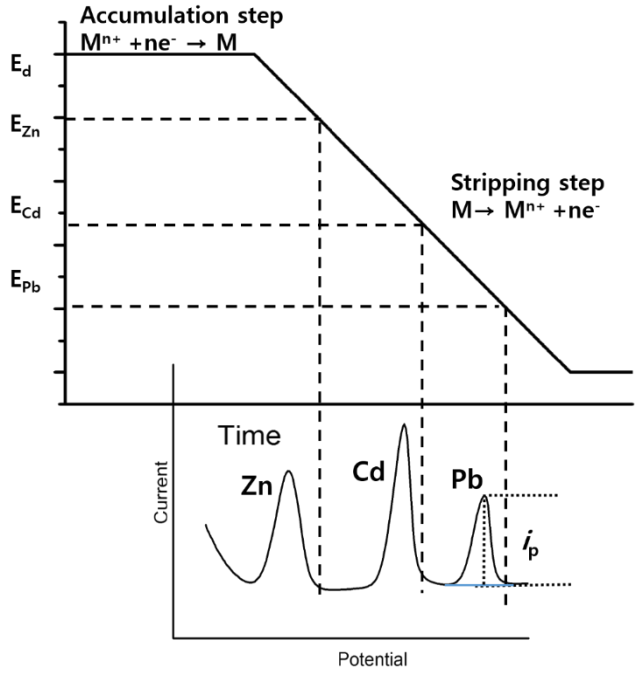

Figure 1. 2 Principle of anodic stripping voltammetry illustrated by the potential–time waveform for a solution containing zinc, cadmium and lead.

1.2.3 Electrode Materials for Stripping Voltammetry

1.2.3.1 Mercury Electrodes

Mercury has been the electrode materials of choice for many stripping applications [2c]. The use of mercury electrodes for metal detection has been reported since the middle of the 20th century. The mercury-based electrode was the first one that received attention for electrochemical detection of heavy metals because it brought high sensitivity, good reproducibility, and a wide cathodic potential range for heavy metal detection [17]. Two basic electrode systems, the mercury film electrode (MFE) and hanging mercury electrode (HMDE), have gained wide acceptance in the development of anodic stripping voltammetry (Figure 1.3) [18]. The hanging mercury drop electrode has been used successfully in countless applications involving reduction of organic and inorganic electroactive compounds. However successful, the HMDE, consisting of a renewable drop of mercury at the end of a fine capillary, has some drawbacks: it is bulky, requires a mercury reservoir and regular maintenance of the capillary and incorporates complicated electronics

for precise drop generation and disposal. Besides, the HMDE, unlike solid electrodes, is mechanically unstable (i.e. the mercury drops are easily dislodged) so that it is not particularly suitable for on-site analysis (e.g. shipboard operations that involve vibrations) or for flow-through applications (where the electrode is subject to high flow rates). Finally, the HMDE is not the ideal substrate for permanent modification by chemical reagents or permselective coatings that improve the analytical properties. Although, in principle it is possible to modify the surface of the HMDE, such procedures have only been occasionally used due to the electrode sensitivity to mechanical handling and to its very principle of operation (one drop for each measurement). Mercury film electrodes (MFE), prepared by coating a suitable substrate with a thin 'film' of metallic mercury, have come into use in order to address some of these limitations. MFEs can be of fairly small size, do not require any ancillaries, provide a larger surface-to-volume ratio, are mechanically more stable than mercury drops and offer great scope for different cell configurations and for chemical modification of their surface. Additionally, the mercury film can be pre-plated and reused for some time. However, greatest sensitivity is obtained using *in situ* deposition of mercury: the

mercury is then plated simultaneously with the heavy metals, giving a thinner mercury film with a higher internal metal concentration, and which is less affected than the pre-plated film by interference by surfactants which are known to occur in natural waters. Glassy carbon is the usual conductive substrate for the electrode as it is inert and relatively easy to polish [18-19].

However, despite the excellent performance of mercury electrodes, future regulations and occupational health considerations may severely restrict or even ban the use of mercury as an electrode material because of its high toxicity. Indeed, mercury compounds that are characterized by a high toxicity, like mercuric ions (Hg^{2+}) or organic compounds (e.g. dimethyl mercury), can be formed by immersion of metallic mercury (Hg^{0}) in natural waters in the presence of dissolved oxygen or by the mean of bacterial activity. A few years ago, Yosypchuk and Novotný [20] described the use of "non-toxic" electrodes of solid mercury amalgams (Ag, Cu, Au) for stripping analysis. However, despite these electrode materials can be considered as "non-toxic" for laboratory use, it is not the case for environmental on-site monitoring. Indeed, mechanical and/or bacterial corrosion can lead to mercury release from amalgams, as

mercuric ions or metallic mercury. As a result, electrode materials that can potentially replace mercury are continually sought. Different bare carbon, gold, silver or iridium electrodes have been used as possible alternatives to mercury [1, 21].

1.2.3.2 Gold and Silver Electrodes

Gold and silver materials exhibit unique electrical, optical and catalytic properties. Meanwhile, various detection methods with high specificity have been designed for heavy metal sensing. Kirowa-Eisner et al. used gold and silver electrodes to detect cadmium, lead and copper [22]. They showed that gold is unsuitable for mixtures of lead and cadmium because of overlapping of the two stripping peaks. Silver exhibits excellent characteristics for lead and cadmium detection: high repeatability and long-term stability without the need of any pretreatment, with limits of detection (LOD) in the nM range. The sensitivity can be further improved by using advanced procedures or electrode surfaces. For example, Compton's group has detected arsenic(III) with a LOD of 1 ppb on gold [23]and silver [24] electrodes using ASV assisted with ultrasound. Note that Compton et

al. have also shown that gold electrodes are highly sensitive for the detection of chromium (VI) even with cyclic voltammetry, with a LOD of 228 ppb and have proven superior performances compared to glassy carbon [25]. For real application, more and more heavy metal electrochemical sensors have been fabricated on gold-based screen-printed electrodes due to its nature of inexpensiveness, portability and easy to mass production [26].

1.2.3.3 Carbon-based Electrodes

Although carbon materials used in electrochemistry share some of the electronic properties of metals, their structures and chemistry differ dramatically from all metallic electrodes. The well-known materials of carbon include graphite, diamond, and fullerenes, each of which can exist in a variety of materials with differing electrochemical properties. The simplest graphite material is a two-dimensional graphene sheet, which is essentially a very large polyaromatic hydrocarbon. The synthesis and properties of a wide variety of graphene structures were recently reviewed [27].

Carbon fibers have been used in electrochemistry since

approximately the early 1980s, and their structures and properties relevant to electrochemical applications were reviewed in 1991. There has been significant activity since that time due to the utility of carbon fibers for making ultramicro electrodes and for in vivo voltammetry. Furthermore, the discovery of carbon nanotubes provided a completely new type of carbon "fiber" with distinct electrochemical properties [28].

An electrochemically important variant on the graphite structure is glassy carbon (GC), which is made by heat treating various polymers, often poly acrylonitrile. By heating the polymer under pressure in an inert atmosphere to 1000-3000 ℃, the heteroatoms are evaporated until only carbon remains. Glassy carbon should be distinguished from a variety of other disordered graphitic materials, such as "diamond-like carbon", amorphous carbon, polycrystalline graphite, and carbon black. While the properties of the materials vary greatly with preparation and pretreatment, some generalizations based on their origins are useful.

In the year 2008, it was exactly a half of a century since R. N. Adams published a short one-page report, in which he had introduced a new type of electrode, carbon paste electrode (CPE) [29]. The

respective assembly, i.e., an electrode holder (body) filled with carbon paste, used in the pioneering studies was already viewed and described in Adams's initial report [29]. The proper construction had been based on short Teflon rod with a well drilled in and a Pt-wires electrical contact. Their main advantages are the simplicity and variability in size, whereas the renewal of carbon paste or its total exchange is less convenient. As possible alternatives to commonly used configurations with solid electrodes (glassy carbon or gold disks) in electrochemical stripping analysis of heavy metals, the individual carbon paste variants are then as follows; i) the bare carbon paste plated with mercury film and bismuth film, ii) bulk modified carbon pastes with bismuth or antimony oxide, or fine metal powders [30].

The discovery of numerous nanoscale materials, specifically carbon-based ones continue to add new dimensions to the rapid development of nanotechnology (Figure 1.4). At such small scales, materials adopt certain properties resulting in unique optical, electrical, chemical and mechanical characteristics. Nanoscale carbon-based materials include single walled carbon nanotubes (SWNTs), multiwalled carbon nanotubes (MWNTs), fullerenes and graphene among many others. Carbon has

the ability to hybridize into sp, sp^2 and sp^3configurations depending on the bonding relationships with neighboring atoms. This is due to the narrow gap between the 2s and 2p electron shells. These hybrid states are responsible for the diversity of organic compounds as well as the ability to fabricate a wide variety of nanoscale carbon-based materials. Hexagonal sp^2 hybridization seems to be the most preferred conformation in nanoscale carbon-based materials. The distinctive properties of sp^2 hybridized carbon in particular and unique behavior of nanoscale materials in general create very versatile materials that exhibit distinct properties in terms of size, surface area, strength, optical and electrical properties. Further, the sensitivity of carbon's structure to perturbations in synthetic conditions, allow for tailored manipulations to a degree not yet matched by inorganic nanostructured [31].

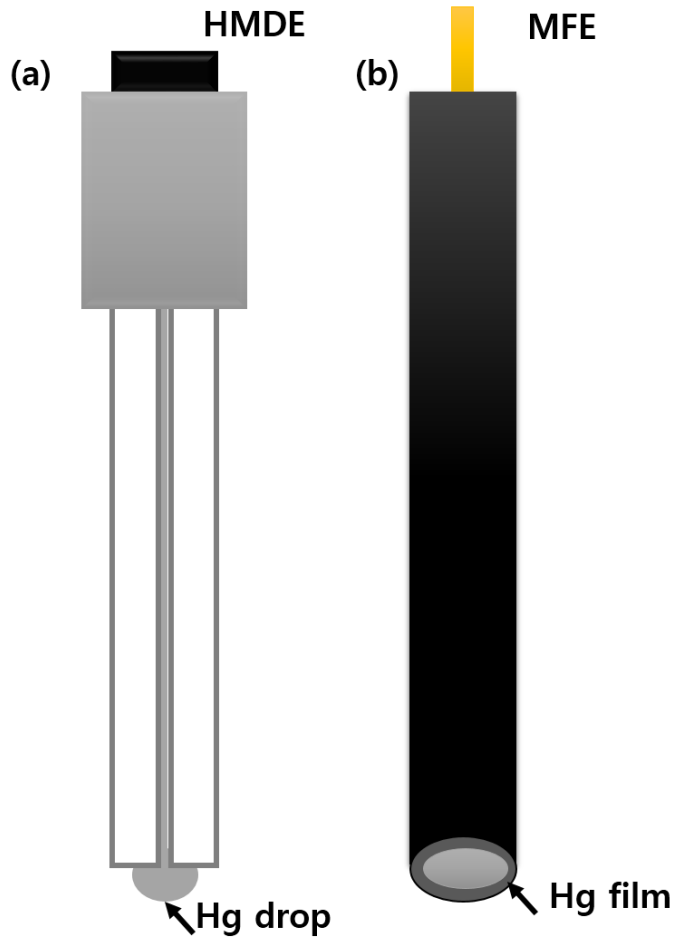

Figure 1. 3 Two examples of mercury electrodes; (a) hanging mercury drop electrode (HMDE); (b) mercury film electrode (MFE).

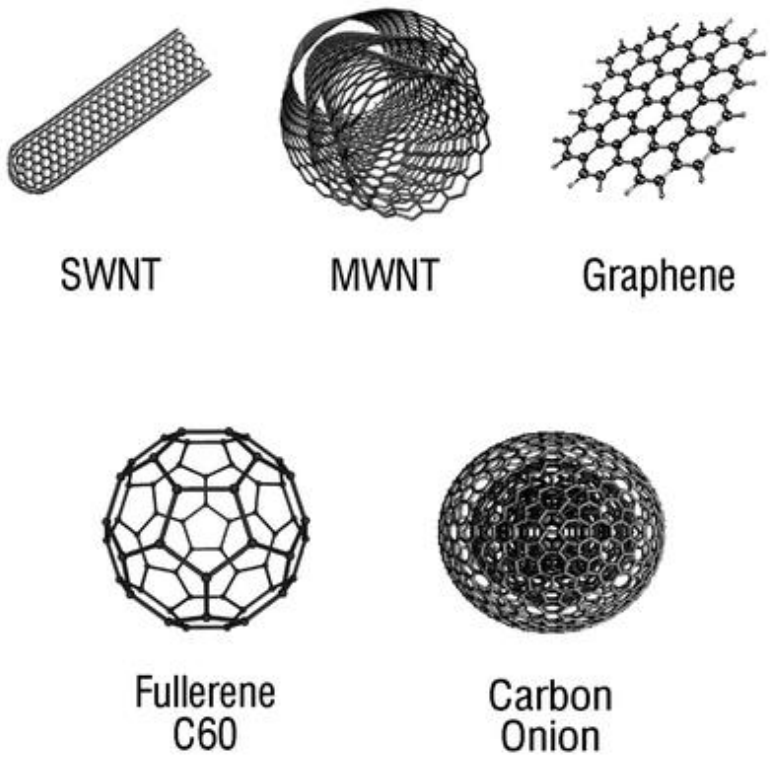

Figure 1. 4 Some examples of nanoscale carbon-based materials (Reprinted with permission from Ref. Environ. Sci. Technol., 42, 2008, 5843)

1.2.3.4 Bismuth Electrodes

In 2000, Wang, for the first time, reported a Bi-coated carbon electrode as a sensor for the stripping voltammetric analysis of lead, cadmium and zinc [32]. Bismuth is known to form binary – or multicomponet (low-temperature melting) 'fusible' alloys with numerous heavy metal, including lead, cadmium, thallium, antimony, indium, or gallium. Such formation of low-temperature alloys facilitates the nucleation process during the deposition of heavy metals. Moreover, bismuth has the advantage of not requiring the removal of dissolved oxygen during stripping analysis, and it is also characterized by a wide negative potential window, which is a good analytical advantage, as reported in several papers [33].

Bismuth electrodes used for the electrochemical-stripping analysis. The technique is based on two different steps: i) a preconcentration step, where heavy metal ions (M^{n+}) are reduced to form a M-Bi alloy; ii) in the second step, the heavy metals are re-oxidized and go back in solution $M(Bi) \rightarrow M^{n+} + ne^{-}$. In this step, the amount of metal present is determined by use of sensitive electrochemical techniques.

Electrode	Underlying Electrode	*In-/Ex situ*	Target Analyte(s)	LOD (µg/L)	Technique	Ref.
BiF	GCE	In-situ	Pb	1.1	ASV	[2a]
BiF	GCE	In-situ	Cd, Pb ,Zn	0.2 ,0.2, 0.7	SW-ASV	[13]
BiF	Carbon film resisitor	In-situ	Cd, Pb, Zn	0.11, 0.16, 0.008	SW-ASV	[14]
BiF	Edge-plane pyrolytic graphite	In-situ	Cd, Pb	0.062, 0.084	SW-ASV	[15]
BiF	Graphite-epoxy composite	In-situ	Cd, Pb, Zn	2.2, 23.1, 600	SW-ASV	[16]
BiF	Multi-Walled Carbon Nanotubes	In-situ	Cd, Pb, Zn	0.7, 1.3, 12	SW-ASV	[17]

ASV;Anodic stripping voltammetry, BiF;Bsmuth film, BiO;Bismuth oxide, G;Graphene,GCE;Glassy carbon electrode SW-ASV; Square-wave anodic stripping voltammetry, SPE;Screen printed electrode

Table 1. 3 Comparison of different electrodes for determination of heavy metal ions.

1.3 Preparation of Bismuth-based Electrochemical Electrodes

1.3.1 Design of Bismuth Electrodes

From the early 2000, bismuth has emerged as a promising electrode material in electroanalysis field being with interest overall in electrochemical stripping, voltammetric and amperometric-based sensors [34]. Bismuth-based nanomaterials are proposed to achieve better analytical performance in heavy metal detections (Table 1.3). The role of bismuth in electrode modification to be used for heavy metal detection is well known as an alternative to mercury. In addition, the development of new sensing platforms using bismuth-based electrode is a focus of recent research for detection trace heavy metal. Bismuth-based nanomaterials play an important role in this field being the principal function its use for the surface modification of working electrode. Different types of bismuth-based sensors have been reported but the most used configurations are based on the co-deposition (*in situ*) of bismuth during electrochemical stripping analysis and the use of bismuth modified (*ex situ*) electrodes. Also,

various strategies for the synthesis of bismuth nanoparticles have been reported for modifying electrode for heavy metal detection.

1.3.2 Synthesis of Bismuth Nanoparticles

Different ways to obtain bismuth nanoparticles (BiNPs) have been reported. In general, BiNPs are synthesized by a thermal plasma method, aerosol quenching, electron beam irradiation and chemical reduction, etc. On one hand, the obtaining of BiNPs can be performed form bulk metallic bismuth by using thermal decomposition; however, this method usually is not efficient enough in terms of production yield [35]. On the other hand reductive methods to synthesize BiNPs also have been reported. Various reducing agents, including ethylene glycol [36], sodium borohydride [37], aqueous hydrazine solution [38], ethylene-diamine [39] and, recently, sodium hyposphite [40] have been used to prepare Bi crystals. The use of an organometallic complex of bismuth as a precursor for the decomposition also has been reported [41]. In addition, photochemical activation has been used to synthesize BiNPs [42]. The use of reductive methods provides not only advantages in terms of size and shape control but also the efficiency

of BiNP preparation in terms of massive production. Among the many synthesis strategies reported so far, chemical, physical and electrochemical methods are described in the next sections.

1.3.2.1 Chemical Methods

Chemical methods have been developed for synthesizing BiNPs. The most popular chemical approaches, including chemical reduction using a variety of organic and inorganic reducing agents, physicochemical reduction, and radiolysis are widely used for synthesis of BiNPs. Reducing reagents such as ethylene glycol, sodium borohydride, hydrazine solution, sodium hyposphite have been used to prepare BiNPs. Most of these methods are still in development stage and the experienced problems are the stability and aggregation of NPs, control of crystal growth, morphology, size and size distribution. Furthermore, purification of these nanomaterials is often challenging due to the necessity of removing the excess of potentially toxic reagents, such as tris[bis(trimethylsilyl)amino]bismuth, prior to their application in further applications [42b, 43] (Figure 1.5 and 1.6).

1.3.2.2 Physical Methods

Another different way to synthesize BiNPs is focused on the physical method. One of the first attempts was based on solution dispersion of melted bismuth, taking advantage of their low melting point. The production of monodispersed bismuth particles was realized by emulsifying molten drops of bismuth in boiling di(ethylene glycol) (the top-down approach), followed by quenching with cold ethanol. Bi powders (100 mesh, Aldrich) were directly added to boiling di(ethylene glycol) (DEG, with a bp of 241 ℃) and melted to produce big drops. PVP was also added as a stabilizer. After the reaction mixture had been vigorously stirred and thus emulsified for 20 min, uniform spherical colloids of bismuth were obtained as the hot mixture was poured into a cold ethanol bath. Depending on the concentration of Bi and the stirring rate, the diameters of these uniform spherical colloids could be readily varied from 100 to 600 nm. This procedure was schematically resumed in the Figure 1.7 [44].

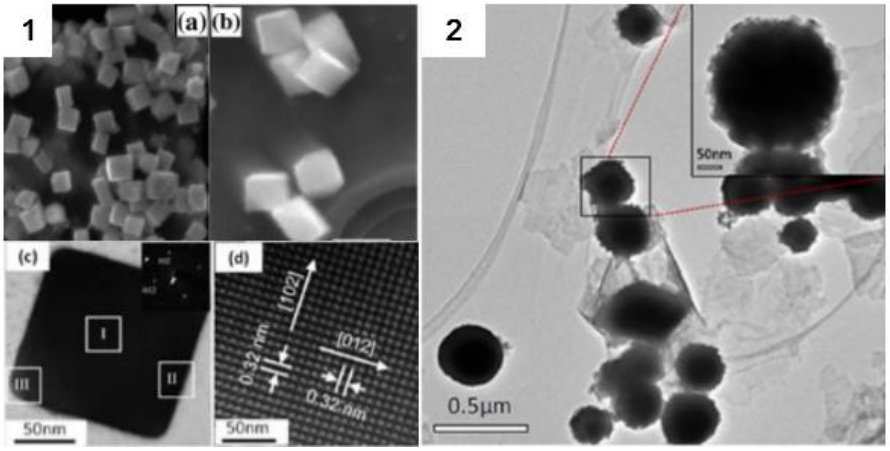

Figure 1. 5 TEM images of different examples of bismuth nanostructures generated through polyol process in presence of different amounts of PVP. (Reprinted with permission from Ref. 1) J. Phys. Chem. B, 51, 2006, 25702, 2) Biosens. Bioelectron. 40, 2013,57)

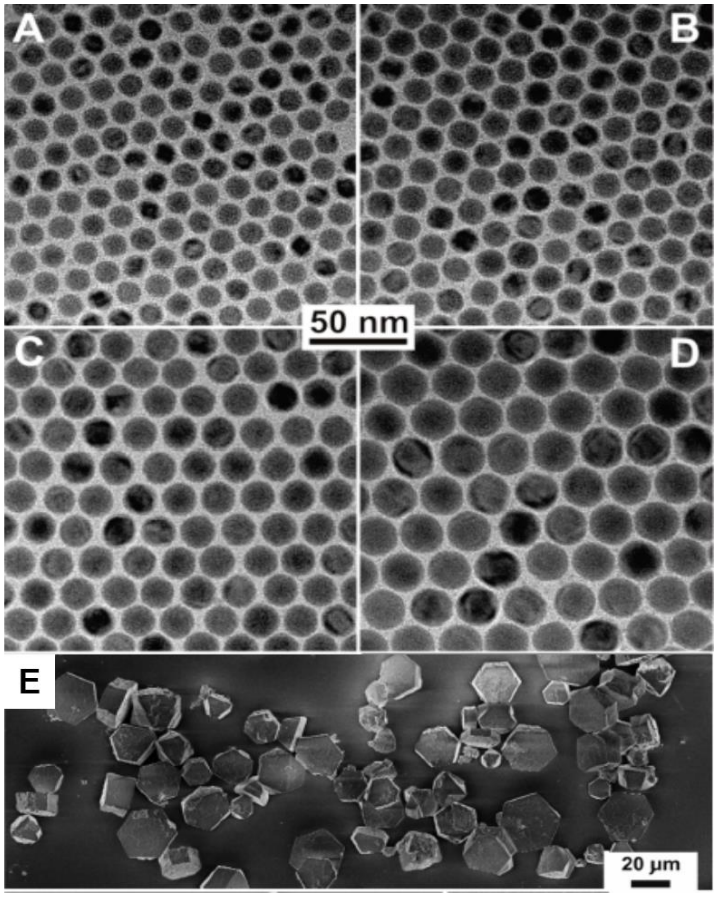

Figure 1. 6 TEM images of Bi nanoparticles of various sizes in the range 11-22 nm (A-D). SEM images of various colloidal crystals grown by slow destabilization of dispersions of Bi nanoparticles (E). (Reprinted with permission from Ref. J. Am. Chem. Soc. 2010, 132, 15158)

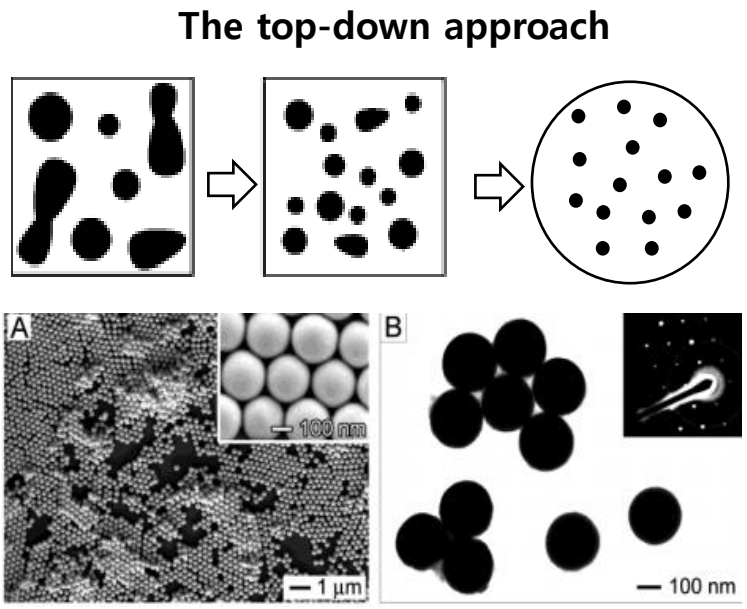

Figure 1. 7 Schematic illustration of the top down approach to monodispersed spherical colloids of metals with relatively low melting points. SEM and TEM images of sample that was prepared using the top-down route. (Reprinted with permission from Ref. Nano. Lett. 4, 2004, 2047)

1.3.2.3 Electrochemical Methods

The fabrication of nanostructured materials has recently received much attention due to their interesting optical, electronic, chemical and electrochemical properties [45]. The use of electrochemical methods has resulted in a plethora of interesting shaped metals such as spheres, cubes, prisms, dendrites, stars, spikes, rods and flowers [43, 46] (in Figure 1.9). The electrodeposition of nanostructured metals is an intense area of research interest with a significant advantage as it is known that shape plays a critical role in analytical applications [47]. One obvious advantage is the ability to create deposits with high surface areas that are rigidly attached to a substrate. This is often problematic using chemically synthesized nanomaterials due to poor attachment and agglomeration effects. It also alleviates any influence of capping agents which may adversely affect the surface chemistry of the material for specific applications and in particular sensing of trace analytes [48]. Other advantages include the ease of fabrication, low cost, and precise control over the amount of material electrodeposited. This kind of synthesis process can be controlled by a number of electrodeposition techniques, such as cyclic voltammetry

(CV), step methods such as chronoamperometry (CA), chronopotentiometry (CP) and chronocoulometry (CC), pulsed plating at a fixed or varying potential or using AC methods [49].

Many researchers have chosen to electrodeposit metals onto untreated substrates in order to maintain an overall clean surface, thereby avoiding possible complications in later applications with surface capping organic moieties. In particular, a good way to improve the properties of bismuth nanostructures obtained during electrochemical methods is the use of noble metals or carbon substrate as a sensing layer.

In 2000, bismuth film electrodes were introduced as an alternative to mercury film electrode. Bismuth film electrodes are prepared by plating thin bismuth films on suitable electrode materials. They can be plated on the same substrate as mercury; glassy carbon, gold, silver, and boron-doped diamond electrode. Among the carbon substrates for bismuth film electrodes, glassy carbon generates a low background current [50]. In addition, carbon fibers[51] or gold[51] and platinum[52] wires have been used. This process can be carried out in two different ways (*ex situ* and *in situ*). The first method, pre-plating or *ex situ* plating, involves electroplating the bismuth-film ions before

transferring the electrode to the sample solution for analysis. The reported plating conditions of the bismuth film are rather variable; an acidic media is always recommended (as Bi(III) is easily hydrolyzed at higher pH, as discussed below) containing 5–200 mg/l Bi(III) with a deposition potential in the range −0.5 to −1.2 V and a deposition time of 1–8 min under conditions of forced convection (electrode rotation or stirring)[50, 53]. *In situ*, bismuth ions are added directly into the solution to be analyzed, and the analyte is incorporated as the bismuth film is formed [54]. Stripping potentiograms obtained with analyte sample by using the Autolab potentiostats are shown in Figure 1.8. In *in situ* plating, a general practical rule is that the Bi(III) concentration must be at least 10-fold higher than the expected analyte concentration to avoid saturation effects. When this method of preparing the bismuth coating is selected, the plating conditions (plating potential and time) are necessarily dictated by the conditions used for the actual analytical cycle. In preparing bismuth film electrodes, the *ex situ* approach can be suitable when the plating can be carried out in a medium different from that of the target metal ions analysis. The choice of substrate is a crucial factor in the case of bismuth film electrodes, because very different results can be

obtained even when applying the same conditions on different electrode substrates to form the bismuth film. Recently Bi-based composite electrodes for heavy metal detection were developed using carbon paste[55], glassy carbon[56] or silver[57]. The major advantage of composite electrodes, as in the case of *ex situ* plating, includes simplicity of analytical measurements. Moreover, three-dimensional nanostructures with large specific surface area and high surface free energy, which is superior to the film in the chemical sensor applications, have aroused much attention in recent years. In addition, electrochemistry offers convenient and elegant techniques for the fabrication of nanostructures. Z. Zhang et al.[46e] reported a single-crystalline bunch-like bismuth nanostructure using a two-step electrodeposition in anodic alumina membranes for the first time. The growth mechanism of the bunch-like Bi as follows: at the beginning of deposition, bismuth nanowires embedded in the anodic alumina membrane were fabricated by pulsed electrodeposition. After the nanowires grew out of the membranes, the bismuth nanowire array formed the nano electrode array, which acted as the cathode in the following deposition. The growth of these Bi nanoparticles proceeds to nanowires, self-assembly, and finally to the bunch-like bismuth,

which is depicted in the Figure 1.10.

In the case of bismuth electrodes developed by the *in situ* approach, the concentration of bismuth is an important parameter to be investigated. The concentration of bismuth controls the thickness of the bismuth film. The thickness of the film usually does not affect the peak position of heavy metal but rather affects the peak height. The results of Kefala et al. showed a decrease of current intensity of the peak with increasing thickness of the bismuth film [50]. For the usual *in-situ* deposition method under the conditions employed and assuming a uniform distribution of the bismuth film on the electrode surface (which is only a rough approximation), the average bismuth film thickness, l_{Bi}, can be calculated using the equation:

$$\boldsymbol{l_{Bi} = \frac{m_{Bi}}{\pi R^2 d_{Bi}} = \frac{Q_{Bi} M_{Bi}}{nF\pi R^2 d_{Bi}}}$$

where m_{Bi} is the amount of metallic bismuth deposited on the electrode surface, Q_{Bi} is the charge for bismuth deposition, M_{Bi} is the formal weight of bismuth (209 g mol^{-1}), n is the number of electrons per molecule of Bi during Bi(III) reduction (3 eq mol^{-1}), F is the

Faraday constant (96,487 Cb eq^{-1}), R is the electrode radius (1.5 mm) and d_{Bi} is the density of metallic Bi (9.8 g cm^{-3}). Specifically, at concentrations of bismuth of 0.01–1 mg/L, the heavy metal signal increases significantly. This behavior was attributed to the increased number of nucleation sites and increased alloy formation. However, at bismuth concentrations greater than 2 mg/L, it was found that a too high concentration of bismuth ions led to a substantial decrease in sensitivity, which was ascribed to the formation of a thick layer of bismuth on the electrode surface that partially blocks the conductive surface of the electrode, reducing the number of sites (Figure 1.11) [46a].

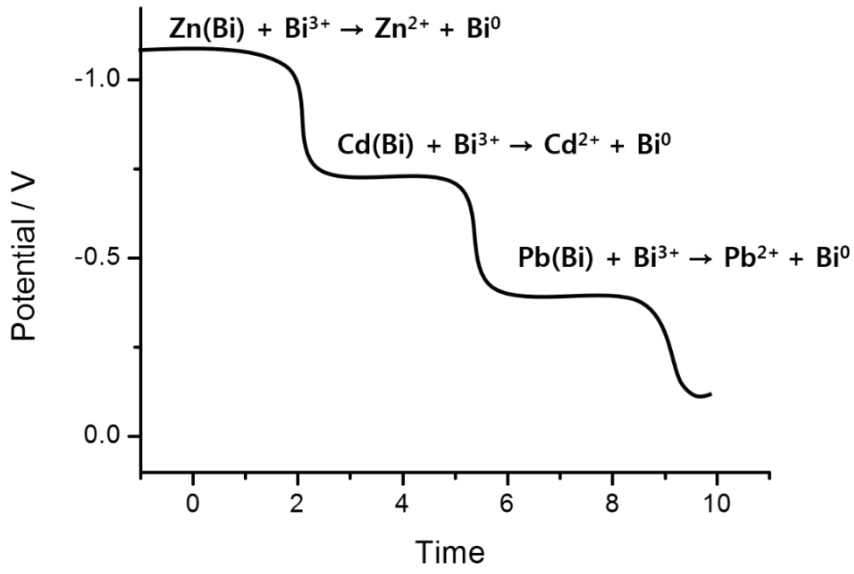

Figure 1. 8 Stripping potentiogram for a solution containing zinc, cadmium, lead and bismuth.

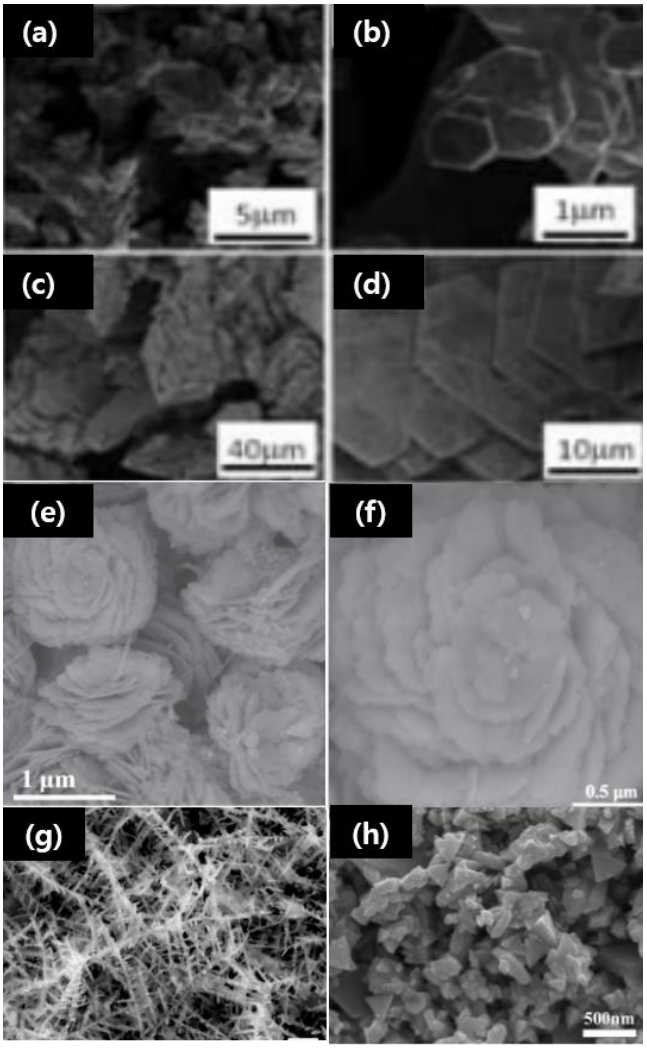

Figure 1. 9 Examples of bismuth nanostructures generated by electrodeposition. (a)-(d) hexagonal discs, (e), (f) nanofloweres, (g) dendrites, and (h) prisms. (Reprinted with permission from Ref. Chem. Lett., 42, 2013, 150, CrystEngComm., 13, 2011, 794, ChemPhysChem., 13, 2012, 2162, J. Mater. Chem., 21, 2011, 3119, J. Ceram. Process. Res., 10, 2009, 190)

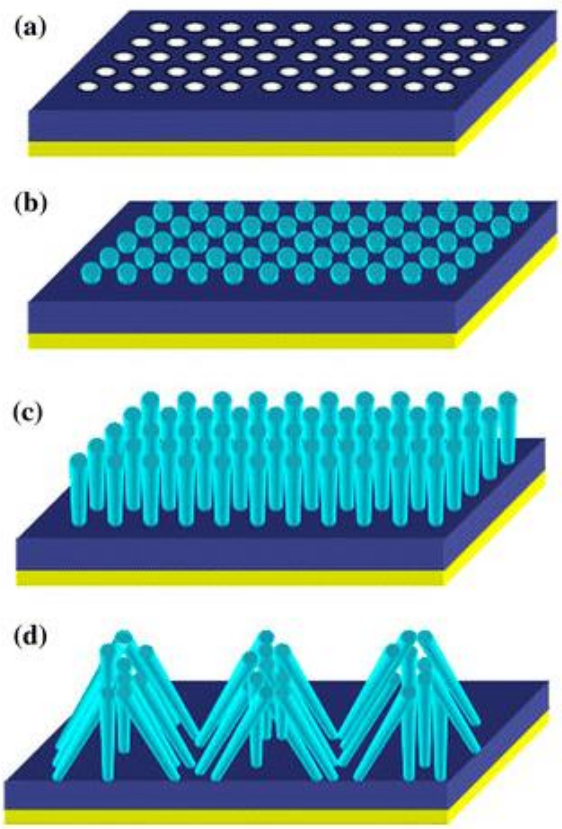

Figure 1. 10 Schematic for the synthesis of bunch-like bismuth that can be achieved via two-step electrodeposition. (Reprinted with permission from Ref. Nanoscale Res. Lett. 5, 2009, 398)

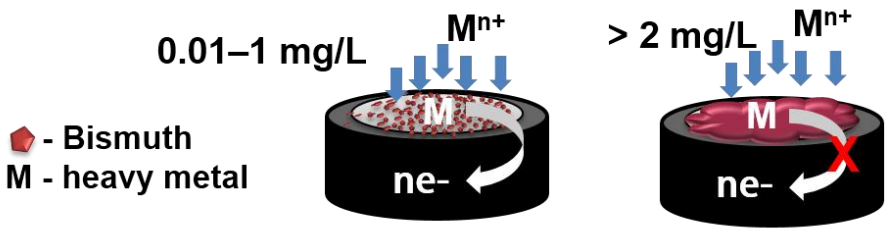

Figure 1. 11 Illustration of the effect of bismuth concentration.

1.3.3 Bismuth-based Modifications and Nanocomposite for Detection of Heavy Metal Ions

Benefiting from the potential advantages of chemical and thermal stability, high surface reaction activity and catalytic efficiency, nanomaterials are often used for electrode modification. In particular, metal, metal oxide, and carbon based nanomaterials are the most commonly used nanomaterials in electrochemical detection of heavy metal ions.

1.3.3.1 Metal Nanoparticles

Metal nanoparticles have interesting electrical, optical and catalytic properties, depending not only on their size but also on their shape, composition, crystal structure and surface properties [58]. The interest in metal nanoparticles for sensing applications is growing nowadays due to their strong emission and stability to photobleaching and also thanks to their possibility to be easily functionalized by specific receptors to afford water compatibility and increase target specificity [2].

Gold nanoparticle-modified electrodes possess higher surface area, improved electron transfer rate, and increased mass-transport rate. By co-deposition of bismuth and target heavy metals on the gold nanoparticle-modified glassy carbon electrode. The nanocomposite modified electrode significantly lowered the limit of detection toward Hg^{2+} [59]. It has also been reported that the sensitivity of gold nanoparticle-modified electrodes was an order of magnitude higher than that of the macro electrode counterpart when used for As^{3+} detection [60].

By layer-by-layer assembly, multi-layer of gold nanoparticles can be immobilized on the surface of gold electrode to construct sensitive sensor for As^{3+} detection [61]. Combining with ASV detection, this sensor can detect 4.36 $\mu g\ L^{-1}$ level of As^{3+}. Based on the facile wet-chemical process, a composite of bimetallic Au–Pt nanoparticles/organic nanofibers with uniform three-dimensional porous nanostructure has been prepared [62]. Benefiting from the large effective surface area and good conducting property of the nanocomposite, this sensor shows a low detection limit of 0.008 $\mu g\ L^{-1}$ for Hg^{2+}.

Similar to bismuth, antimony nanoparticles have also been proven

to be highly sensitive and reliable for tracing analysis of heavy metals in conjunction with anodic stripping voltammetry (ASV). For example, Toghill et al. prepared an antimony nanoparticles modified boron doped diamond electrode for simultaneous electrochemical determination of Pb^{2+} and Cd^{2+} over the range of 50–500 mg L^{-1} [63].

Metal nanoparticles modified electrodes have also been constructed by the composites that combine two to three materials together to provide synergistic contribution from individual components. Zhu et al. has been developed based on the gold nanoparticle-graphene-cysteine composite (Au-GN-Cys) modified bismuth film glassy carbon electrode using square wave anodic stripping voltammetry [64]. The synergistic effect of cysteine as well as the enlarged, activated surface and good electrical conductivity of gold nanoparticles and graphene contributed to the deposition of Cd(II) and Pb(II) on the electrode surface [65].

1.3.3.2 Carbon Nanotubes

Carbon nanomaterials such as carbon nanotubes (CNTs), carbon

nanofibers, and graphene have been explored as the electrode materials for detection of heavy metals. For electrochemical sensing applications, CNTs have many advantages including a large surface area, small size, excellent electron transfer ability, and easy surface-modification [2, 31, 66]. In addition, CNTs have been recognized as excellent sorbents for heavy metal ions. Therefore, it is promising to construct electrochemical sensors using the CNT-modified electrodes for heavy metal detection because they are capable of simultaneous pre-concentration and detection of multiple heavy metal ions. Hwang et al. has been reported a bismuth-modified carbon nanotube electrode (Bi-CNT electrode) was employed for the determination of trace lead, cadmium and zinc. Bismuth film was prepared by in situ plating of bismuth onto the screen-printed CNT electrode. The Bi-CNT electrode presented well-defined, reproducible and sharp stripping signals [67]. Xu et al. reported a multiwall carbon nanotubes (MWCNTs) were dispersed in Nafion solution and used in combination with bismuth for fabricating composite sensors to determine trace Pb(II) and Cd(II) by differential pulse anodic stripping voltammetry. The synergistic effect of MWCNTs and bismuth composite film was obtained for Pb(II) and Cd(II) detection

with improved sensitivity and reproducibility. Linear calibration curves ranged from 0.05 to 100 μg/L for Pb(II) and 0.08 to 100 μg/L for Cd(II) [68]. Figure 1.14 shows a scheme of the structure of the CNT nanoelectrode array. CNTs have been employed to prepare nanoelectrode arrays (NEAs) by using plasma-enhanced chemical vapor deposition [69]. CNTs-NEAs have the properties of low background current and a high signal-to-noise ratio, and can be used for ultrasensitive voltammetric detection of trace Cd^{2+} and Pd^{2+}. A detection limit of 0.04 ng L^{-1} (40 ppt) in connection with a 240 s accumulation time is reported (Figure 1.12).

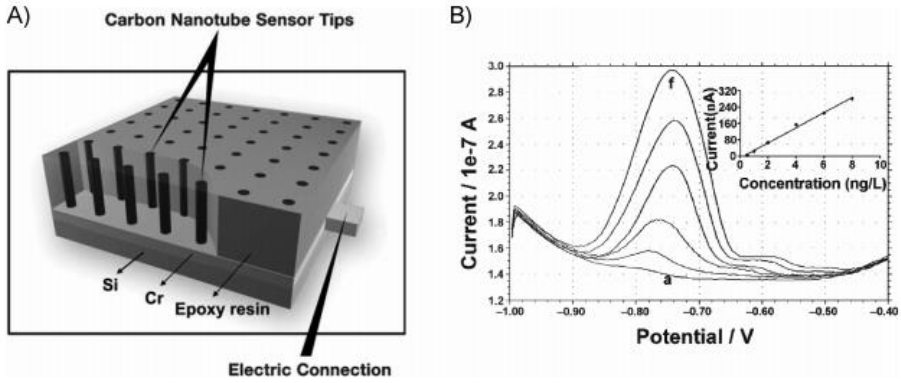

Figure 1. 12 (A) Structure of carbon nanotubes nanoelectrode array. (B) Square wave voltammetric response for an increasing Cd^{2+} the concentration of 0.5, 1, 2, 4, 6, 8 mg L^{-1}. Also shown (inset) is the resulting calibration plot. (Reprinted with permission from Ref. Analyst, 130, 2005, 1098）

1.3.3.3 Other Nanomaterials

The use of nanostructurated materials combined with a unique three-dimensional network structure and particular multi adsorbing sites results in an improved electrochemical sensing platform toward heavy metals with high sensitivity and excellent selectivity for stripping analysis.

Wu et al. reported mesoporous nickel oxide nanosheets and chitosan composite system for detection of Hg^{2+} with a linear range of 0.8 to 500 μM in pH 6.0 phosphate-buffered solutions [70]. Mesoporous carbon also used for detection of heavy metals. Zhu et al. proposed based on an ordered mesoporous carbon and Nafion composite film (OMC/Nafion) coated glassy carbon electrode. The analysis of Pb^{2+} using anodic stripping voltammetry (ASV) includes two steps. OMC can provide higher electrical conductivity, enlarged active surface area, and more coordinate sites to the interface so that enhance the detection sensitivity of lead. Linear calibration curve was found to be from 20 nM to 2 μM for Pb^{2+} with a sensitivity of 17.4±1.38 μA/μM [71].

A similar work presented by Huang et al. for trace detection of

mercury ions combining the use of 2-mercaptobenzothiazole adapters in a SiO_2 3D gold micro/nanopore array has been recently reported showing an excellent linear range (0.05-10 nM) and a good repeatability (relative standard deviation of 2.10%) [72].

1.4 Preparation of Bismuth/Graphene Nanocomposite Electrodes

1.4.1 Graphene

Graphene is a two-dimensional, single-layer sheet of sp^2-hybridized carbon atoms that are closely packed into a hexagonal lattice structure [73]. Graphene is an ideal materials for electrochemistry because of its very large 2-D electrical conductivity, large surface area and fast electron transfer rate, etc [74]. Several electrochemical sensor based on graphene and graphene composites for heavy metal detection have been developed. Li et al. reported that Nafion-graphene composite film based electrochemical sensors not only exhibits improved sensitivity for the metal ion (Pb^{2+} and Cd^{2+}) detections, but also alleviates the interferences due to the synergistic

effect of graphene nanosheets and Nafion [75]. The stripping current signal is greatly enhanced on graphene electrodes. The detection limits (S/N =3) are 0.02 mg L^{-1} for both Cd^{2+} and Pb^{2+}, which are more sensitive than those of Nafion film modified bismuth electrode. Willemse et al. also reported a Nafion-graphene nanocomposite solution in combination with an in situ plated mercury film electrode as a highly sensitive electrochemical platform for the determination of Zn^{2+}, Cd^{2+}, Pb^{2+}, and Cu^{2+} by square-wave anodic stripping voltammetry (SWASV) [3]. Although the Nafion-graphene composite electrochemical sensors discussed above showed high sensitivity for the detection of metal ions, this simple mixture method to make nanocomposites could easily lead to irreversible agglomerates and even restacking of graphene to form graphite after the drying of dispersion solutions, due to van der Waals forces and π–π stacking interactions among individual graphene sheets [76]. One strategy to minimize aggregation problems of graphene sheets is to incorporate nanoparticles into graphene sheets. Recently, graphene decorated with metal or metal oxide has been used for detection of heavy metals. A SnO_2/graphene nanocomposite with highly uniform size has been used to modify electrode and fabricate sensor for heavy metal

detection. As the SnO_2/graphene nanocomposite can act as electrochemical catalyst in detecting heavy metal ions with SWASVs, the sensor can simultaneously detect Cd^{2+}, Pb^{2+}, Cu^{2+}, and Hg^{2+} with the limits of detection of 0.1, 0.18, 0.23, and 0.28 nM, respectively [77]. Gao et al. reported the preparation, characterization, and electrochemical behavior toward heavy metal ions of the AlOOH-reduced graphene oxide nanocomposites. This composite material was synthesized through a green one-pot hydrothermal method. Due to the strong affinity of AlOOH to heavy metal ions and the fast electron-transfer kinetics of graphene, the combination of solid-phase extraction and stripping voltammetric analysis allowed fast and sensitive determination of Cd(II) and Pb(II) [78]. Recently, Huang et al. reported agaphene-MWCNTs based electrochemical sensor was used to detect heavy metal ions for the first time. Graphene-MWCNTs nanocomposites with excellent conductivity were obtained conveniently by the direct electrochemical reduction of graphene oxide–MWCNTs nanocomposites. The electrochemical results demonstrate that the graphene-MWCNTs nanocomposites can act as a kind of practical sensing material to simultaneously determine Pb^{2+} and Cd^{2+} ions in terms of anodic stripping voltammetry [79].

Cyclodextrins are toroidal in shape, which can bind selectively many kinds of organic, inorganic and biological molecules into their cavities to form stable host-gust inclusion complexes due to the unique structure. Meijiao et al. reported the hydroxypropyl-β-cyclodextrin-reduced graphene oxide hybrid nanosheets (HP-β-CD-RGO) were synthesized by microwave irradiation. The hybrid nanosheets, combining Nafion and in situ deposited bismuth film, were used as the sensing material for the simultaneous determination of Pb^{2+} and Cd^{2+} for the first time [80] (Figure 1.13). This sensor exhibited two well-defined and sharp stripping peaks for $Pb^{2+}$and Cd^{2+} and improved the sensitivities and limits of detection. The limit of detection (S/N = 3) were estimated to be 9.42×10^{-11} mol L^{-1} for Pb^{2+} and 6.73×10^{-11} mol L^{-1} for Cd^{2+}, respectively.

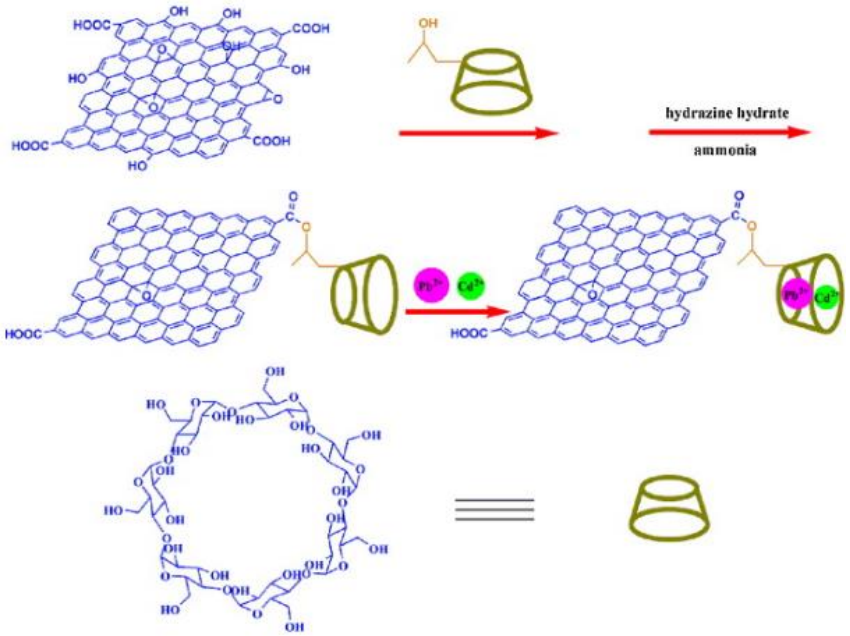

Figure 1. 13 Schematic of the synthesis procedure of HP-β-CD-RGO hybrid nanosheets and the interaction between HP-β-CD-RGO and the heavy metal ions (Pb^{2+}, Cd^{2+}). (Reprinted with permission from Ref. Electrochim. Acta, 108, 2013, 412)

1.5 Dissertation Overview

The development of bismuth-based nanocomposite electrode materials for the detection of heavy metal ions is thought to result in better analytical performance, thus attracting much interest in the field of electrochemical analysis. Additionally, these nanocomposites should simplify the existing configurations and improve their performance. Therefore, this work presents extensive research carried out toward the design and fabrication of bismuth-graphene nanocomposites with advanced properties using efficient synthetic methods. Subsequently, the obtained nanocomposite-modified electrode was employed in electrochemical sensors for the detection of heavy metal ions.

This dissertation is composed of three parts. The first part (Chapter 2) reports on the chemically activated reduced graphene and its use in combination with an *in situ* plated bismuth composite film to fabricate a sensitive mercury-free electrochemical platform for the analysis of zinc, cadmium, and lead. We report the first-time fabrication of an activated graphene/Nafion/bismuth composite (AG-NA/Bi) film electrode for the detection of trace heavy metal ions

using differential pulse anodic stripping voltammetry (DPASV). The surface and electrochemical properties of the AG-NA/Bi composite-film-modified electrode were investigated by SEM and TEM imaging. The experimental variables such as deposition potential, deposition time, bismuth concentration, and stirring speed during pre-concentration were optimized for determining trace metal levels in a 0.1 M acetate buffer (pH 4.5). The detection limits for simultaneous analysis were 0.60, 0.08, and 0.05 μg L^{-1} for Zn^{2+}, Cd^{2+}, and Pb^{2+}, respectively, while the individual analysis limits were 0.57 (Zn^{2+}), 0.07 (Cd^{2+}), and 0.05 μg L^{-1} (Pb^{2+}). The composite film, displaying integrated advantages of activated graphene, Nafion, and bismuth, enhanced the sensitivity toward trace metal ions, especially zinc. The produced AG-NA/Bi composite film electrodes were successfully applied to the trace metal analysis of a real sample.

The second part (Chapter 3) describes a greatly enhanced sensing platform (based on the direct electrochemical reduction of graphene oxide on glassy carbon electrodes) developed for the determination of zinc, cadmium, and lead by DPASV. The goal of this work was the improvement of analytical performance and fabrication of a sensitive mercury-free electrochemical platform, combining the advantages of

electrochemically deposited graphene (EG) and the glassy carbon electrode coated with an in-situ-plated bismuth nanocomposite film. Owing to the enlarged active surface area, high electronic conductivity, and strong absorptivity of graphene, the modified composite electrode exhibited enhanced electron transfer properties and excellent stripping performance in the analysis of trace heavy metal ions. The linear calibration curve ranges for Zn^{2+}, Cd^{2+}, and Pb^{2+} were 1 to 100 μg L^{-1}. The detection limits of metal ions were determined at a signal-to-noise ratio (S/N) of three. The simultaneous analysis detection limits were 1.80, 0.18, and 0.11 μg L^{-1} for Zn^{2+}, Cd^{2+}, and Pb^{2+}, respectively. In the case of individual analysis, the limits of detection were 2.05 (Zn^{2+}), 0.14 (Cd^{2+}), and 0.13 μg L^{-1} (Pb^{2+}). The above method offers several advantages over other graphene sheet fabrication techniques, being simple, fast, and free of reduction agents. This green preparation method greatly expands the scope of graphene-based electrochemical sensing devices and holds promise for wide application in environmental analysis.

The last part (Chapter 4) describes the solvent-free thermal decomposition used to prepare iron oxide/graphene nanocomposites for electrochemical sensing materials. These nanocomposites can be

easily prepared by simple heating of a mixture of the iron oleate precursor and graphene. The as-synthesized nanocomposite-modified electrode was used in combination with in-situ-plated bismuth as an electrochemical sensor for the detection of heavy metal ions, and the electrochemical properties of the iron oxide/graphene/Bi composite electrode were also investigated. Due to the synergetic effect between graphene and iron oxide nanoparticles, the modified electrode showed improved electrocatalytic activity, with high sensitivity toward trace heavy metal ions. Under optimized conditions, the electrode exhibited a linear range of 1–100 μg L^{-1} for Zn^{2+}, Cd^{2+}, and Pb^{2+}, with the respective detection limits being 0.11, 0.08, and 0.07 μg L^{-1} (S/N = 3). The simple solvent-free thermal decomposition method used in the synthesis of nanocomposite electrode materials can be extended to the synthesis of nanocomposites and promising electrode materials for the determination of heavy metal ions.

The above bismuth-based nanocomposites enable successful electrochemical sensing of heavy metal ions with graphene- or nanoparticle-modified electrodes, and the results suggest that these nanocomposites lead to improved sensitivity and stability.

References

[1] Wang, J.; Tian, B. *Analytical Chemistry* **1993**, *65*, 1529.

[2] Aragay, G.; Pons, J.; Merkoçi, A. *Chemical Reviews* **2011**, *111*, 3433.

[3] Willemse, C. M.; Tlhomelang, K.; Jahed, N.; Baker, P. G.; Iwuoha, E. I. *Sensors* **2011**, *11*, 3970.

[4] Organization, W. H. *Guidelines for drinking-water quality*, Geneva: world health organization **2011**.

[5] Willis, J. *Anal. Chem.* **1962**, *34*, 614.

[6] Caroli, S.; Forte, G.; Iamiceli, A. L.; Galoppi, B. *Talanta* **1999**, *50*, 327.

[7] Schramel, P.; Wendler, I.; Angerer, J. *Int. Arch. Occup. Environ. Health* **1997**, *69*, 219.

[8] Li, M.; Gou, H.; Al-Ogaidi, I.; Wu, N. *ACS Sustainable Chemistry & Engineering* **2013**, *1*, 713.

[9] Thomas, F. G.; Henze, G. n. *Introduction to Voltammetric Analysis : Theory and Practice*, CSIRO PUBLISHING, Collingwood, Vic **2001**.

[10] Wang, J. *Stripping Analysis*, Vch, Deerfiled Beach, FL **1985**.

[11] a) Kimmel, D. W.; LeBlanc, G.; Meschievitz, M. E.; Cliffel, D. E. *Analytical Chemistry* **2012**, *84*, 685. b) Krawczyński vel Krawczyk, T.; Moszczyńska, M.; Trojanowicz, M. *Biosensors and Bioelectronics* **2000**, *15*, 681.

[12] March, G.; Nguyen, T. D.; Piro, B. *Biosensors* **2015**, *5*, 241.

[13] Hutton, E. A.; van Elteren, J. T.; Ogorevc, B.; Smyth, M. R. *Talanta* **2004**, *63*, 849.

[14] Chatzitheodorou, E.; Economou, A.; Voulgaropoulos, A. *Electroanalysis* **2004**, *16*, 1745.

[15] Kefala, G.; Economou, A.; Sofoniou, M. *Talanta* **2006**, *68*, 1013.

[16] Settle, F. A. *Handbook of instrumental techniques for analytical chemistry*, Prentice Hall PTR **1997**.

[17] Aragay, G.; Puig-Font, A.; Cadevall, M.; Merkoçi, A. *The Journal of Physical Chemistry C* **2010**, *114*, 9049.

[18] a) Fischer, E.; van den Berg, C. M. *Analytica Chimica Acta* **1999**, *385*, 273. b) Economou, A.; Fielden, P. *Analyst* **2003**, *128*, 205.

[19] a) Florence, T. *Journal of Electroanalytical Chemistry and Interfacial Electrochemistry* **1970**, *27*, 273. b) Kounaves, S.; O'Dea, J.; Chandresekhar, P.; Osteryoung, J. *Analytical Chemistry* **1986**, *58*, 3199.

[20] Yosypchuk, B.; Novotný, L. *Critical Reviews in Analytical Chemistry* **2002**, *32*, 141.

[21] Bonfil, Y.; Kirowa-Eisner, E. *Analytica Chimica Acta* **2002**, *457*, 285.

[22] a) Bonfil, Y.; Brand, M.; Kirowa-Eisner, E. *Analytica chimica acta* **1999**, *387*, 85. b) Bonfil, Y.; Brand, M.; Kirowa-Eisner, E. *Analytica chimica acta* **2002**, *464*, 99. c) Brand, M.; Eshkenazi, I.; Kirowa-Eisner, E. *Analytical Chemistry* **1997**, *69*, 4660. d) Kirowa-Eisner, E.; Brand, M.; Tzur, D. *Analytica chimica acta* **1999**, *385*, 325.

[23] Simm, A. O.; Banks, C. E.; Compton, R. G. *Electroanalysis* **2005**, *17*, 335.

[24] Simm, A. O.; Banks, C. E.; Compton, R. G. *Electroanalysis* **2005**, *17*, 1727.

[25] Welch, C. M.; Nekrassova, O.; Compton, R. G. *Talanta* **2005**, *65*, 74.

[26] a) Niu, X.; Lan, M.; Zhao, H.; Chen, C.; Li, Y.; Zhu, X. *Analytical Letters* **2013**, *46*, 2479. b) Laschi, S.; Palchetti, I.; Mascini, M. *Sensors and Actuators B: Chemical* **2006**, *114*, 460.

[27] McCreery, R. L. *Chem. Rev* **2008**, *108*, 2646.

[28] Bard, A. J.; Rubenstein, I. *Electroanalytical chemistry: a series of advances Vol. 17*, CRC Press **1996**.

[29] Adams, R. N. *Analytical Chemistry* **1958**, *30*, 1576.

[30] Švancara, I.; Vytřas, K.; Kalcher, K.; Walcarius, A.; Wang, J. *Electroanalysis* **2009**, *21*, 7.

[31] Wanekaya, A. K. *Analyst* **2011**, *136*, 4383.

[32] Wang, J.; Lu, J.; Hocevar, S. B.; Farias, P. A. M.; Ogorevc, B. *Analytical Chemistry* **2000**, *72*, 3218.

[33] a) Wang, J. *Electroanalysis* **2005**, *17*, 1341. b) Economou, A. *TrAC - Trends in Analytical Chemistry* **2005**, *24*, 334. c) Kokkinos, C.; Economou, A. *Current Analytical Chemistry* **2008**, *4*, 183.

[34] Economou, A. *TrAC Trends in Analytical Chemistry* **2005**, *24*, 334.

[35] Zhao, Y.; Zhang, Z.; Dang, H. *Materials Letters* **2004**, *58*, 790.

[36] Wang, W. Z.; Poudel, B.; Ma, Y.; Ren, Z. F. *The Journal of Physical Chemistry B* **2006**, *110*, 25702.

[37] Wang, Y.; Chen, J.; Chen, L.; Chen, Y.-B.; Wu, L.-M. *Crystal Growth & Design* **2010**, *10*, 1578.

[38] Ma, D.; Zhao, J.; Li, Y.; Su, X.; Hou, S.; Zhao, Y.; Hao, X.; Li, L. *Colloids and Surfaces A: Physicochemical and Engineering Aspects* **2010**, *368*, 105.

[39] Fu, R.; Xu, S.; Lu, Y.-N.; Zhu, J.-J. *Crystal growth & design* **2005**, *5*, 1379.

[40] Ma, D.; Zhao, J.; Chu, R.; Yang, S.; Zhao, Y.; Hao, X.; Li, L.; Zhang, L.; Lu, Y.; Yu, C. *Advanced Powder Technology* **2013**, *24*, 79.

[41] a) Carotenuto, G.; Hison, C. L.; Capezzuto, F.; Palomba, M.; Perlo, P.; Conte, P. *Journal of Nanoparticle Research* **2008**, *11*, 1729. b) Son, J. S.; Park, K.; Han, M.-K.; Kang, C.; Park, S.-G.;

Kim, J.-H.; Kim, W.; Kim, S.-J.; Hyeon, T. *Angewandte Chemie International Edition* **2011**, *50*, 1363.

[42] a) Luz, A.; Feldmann, C. *Journal of Materials Chemistry* **2009**, *19*, 8107. b) Warren, S. C.; Jackson, A. C.; Cater-Cyker, Z. D.; DiSalvo, F. J.; Wiesner, U. *Journal of the American Chemical Society* **2007**, *129*, 10072.

[43] Jin, C. G.; Jiang, G. W.; Liu, W. F.; Cai, W. L.; Yao, L. Z.; Yao, Z.; Li, X. G. *Journal of Materials Chemistry* **2003**, *13*, 1743.

[44] Wang, Y.; Xia, Y. *Nano Letters* **2004**, *4*, 2047.

[45] a) Burda, C.; Chen, X.; Narayanan, R.; El-Sayed, M. A. *Chemical reviews* **2005**, *105*, 1025. b) Schuller, J. A.; Barnard, E. S.; Cai, W.; Jun, Y. C.; White, J. S.; Brongersma, M. L. *Nat Mater* **2010**, *9*, 193.

[46] a) Haifeng, Y.; Yan, Y.; Junfang, L.; Xiaojing, L.; Guangcheng, X.; Qing, Z.; Chao, W. *Chemistry Letters* **2013**, *42*, 150. b) Ni, Y.; Zhang, Y.; Zhang, L.; Hong, J. *CrystEngComm* **2011**, *13*, 794. c) Som, T.; Simo, A.; Fenger, R.; Troppenz, G. V.; Bansen, R.; Pfänder, N.; Emmerling, F.; Rappich, J.; Boeck, T.; Rademann, K. *ChemPhysChem* **2012**, *13*, 2162. d) Yang, M. *Journal of Materials Chemistry* **2011**, *21*, 3119. e) Zhang, Z.; Yu, K.; Bai, D.; Zhu, Z. *Nanoscale Research Letters* **2009**, *5*, 398.

[47] Solla-Gullon, J.; Vidal-Iglesias, F. J.; Lopez-Cudero, A.; Garnier, E.; Feliu, J. M.; Aldaz, A. *Physical Chemistry Chemical Physics* **2008**, *10*, 3689.

[48] Plowman, B. J.; Bhargava, S. K.; O'Mullane, A. P. *Analyst* **2011**, *136*, 5107.

[49] a) Therese, G. H. A.; Kamath, P. V. *Chemistry of Materials* **2000**, *12*, 1195. b) Wu, M.-S.; Lee, J.-T.; Wang, Y.-Y.; Wan, C.-C. *The Journal of Physical Chemistry B* **2004**, *108*, 16331. c) Hwanga, G. H.; Hana, W. K.; Kima, S. J.; Honga, S. J.; Parkb, J. S.; Parka,

H. J.; Kanga, S. G. *Journal of Ceramic Processing Research* **2009**, *10*, 190.

[50] Kefala, G.; Economou, A.; Voulgaropoulos, A.; Sofoniou, M. *Talanta* **2003**, *61*, 603.

[51] Hočevar, S. B.; Ogorevc, B.; Wang, J.; Pihlar, B. *Electroanalysis* **2002**, *14*, 1707.

[52] Baldo, M.; Daniele, S.; Bragato, C., in *Journal de Physique IV (Proceedings), Vol. 107*, EDP sciences, **2003**, pp. 103.

[53] a) Królicka, A.; Pauliukaitappproaches the limit, R.; Svancara, I.; Metelka, R.; Bobrowski, A.; Norkus, E.; Kalcher, K.; Vytřas, K. *Electrochemistry Communications* **2002**, *4*, 193. b) Wang, J.; Lu, J. *Electrochemistry Communications* **2000**, *2*, 390. c) Hutton, E. A.; Ogorevc, B.; Hočevar, S. B.; Weldon, F.; Smyth, M. R.; Wang, J. *Electrochemistry Communications* **2001**, *3*, 707. d) Hutton, E. A.; Hočevar, S. B.; Ogorevc, B.; Smyth, M. R. *Electrochemistry Communications* **2003**, *5*, 765.

[54] Arduini, F.; Calvo, J. Q.; Palleschi, G.; Moscone, D.; Amine, A. *TrAC Trends in Analytical Chemistry* **2010**, *29*, 1295.

[55] Hočevar, S. B.; Švancara, I.; Vytřas, K.; Ogorevc, B. *Electrochimica Acta* **2005**, *51*, 706.

[56] Hwang, G.-H.; Han, W.-K.; Hong, S.-J.; Park, J.-S.; Kang, S.-G. *Talanta* **2009**, *77*, 1432.

[57] Skogvold, S. M.; Mikkelsen, Ø .; Schrøder, K. H. *Electroanalysis* **2005**, *17*, 1938.

[58] a) Kelly, K. L.; Coronado, E.; Zhao, L. L.; Schatz, G. C. *The Journal of Physical Chemistry B* **2003**, *107*, 668. b) Lamprecht, B.; Schider, G.; Lechner, R.; Ditlbacher, H.; Krenn, J.; Leitner, A.; Aussenegg, F. *Physical review letters* **2000**, *84*, 4721. c) Daniel, M.-C.; Astruc, D. *Chemical reviews* **2004**, *104*, 293. d) Sun, Y.; Xia, Y. *Science* **2002**, *298*, 2176.

[59] Abollino, O.; Giacomino, A.; Malandrino, M.; Piscionieri, G.; Mentasti, E. *Electroanalysis* **2008**, *20*, 75.

[60] Dai, X.; Compton, R. G. *Electroanalysis* **2005**, *17*, 1325.

[61] Ottakam Thotiyl, M. M.; Basit, H.; Sánchez, J. A.; Goyer, C.; Coche-Guerente, L.; Dumy, P.; Sampath, S.; Labbé, P.; Moutet, J. C. *Journal of Colloid and Interface Science* **2012**, *383*, 130.

[62] Gong, J.; Zhou, T.; Song, D.; Zhang, L.; Hu, X. *Analytical Chemistry* **2010**, *82*, 567.

[63] Toghill, K. E.; Xiao, L.; Wildgoose, G. G.; Compton, R. G. *Electroanalysis* **2009**, *21*, 1113.

[64] Zhu, L.; Xu, L.; Huang, B.; Jia, N.; Tan, L.; Yao, S. *Electrochimica Acta* **2014**, *115*, 471.

[65] Zhu, L.; Xu, L.; Huang, B.; Jia, N.; Tan, L.; Yao, S. *Electrochimica Acta* **2014**, *115*, 471.

[66] a) Shao, Y.; Wang, J.; Wu, H.; Liu, J.; Aksay, I. A.; Lin, Y. *Electroanalysis* **2010**, *22*, 1027. b) Xu, H.; Zeng, L.; Xing, S.; Xian, Y.; Shi, G.; Jin, L. *Electroanalysis* **2008**, *20*, 2655.

[67] Hwang, G. H.; Han, W. K.; Park, J. S.; Kang, S. G. *Talanta* **2008**, *76*, 301.

[68] Xu, H.; Zeng, L.; Xing, S.; Xian, Y.; Shi, G.; Jin, L. *Electroanalysis* **2008**, *20*, 2655.

[69] Liu, G.; Lin, Y.; Tu, Y.; Ren, Z. *Analyst* **2005**, *130*, 1098.

[70] Stankovich, S.; Dikin, D. A.; Dommett, G. H.; Kohlhaas, K. M.; Zimney, E. J.; Stach, E. A.; Piner, R. D.; Nguyen, S. T.; Ruoff, R. S. *nature* **2006**, *442*, 282.

[71] a) Brownson, D. A.; Banks, C. E. *Analyst* **2010**, *135*, 2768. b) Shan, C.; Yang, H.; Song, J.; Han, D.; Ivaska, A.; Niu, L. *Analytical Chemistry* **2009**, *81*, 2378. c) Brownson, D. A.; Kampouris, D. K.; Banks, C. E. *Chemical Society Reviews* **2012**, *41*, 6944.

[72] Li, J.; Guo, S.; Zhai, Y.; Wang, E. *Analytica Chimica Acta* **2009**, *649*, 196.

[73] Liu, J.; Fu, S.; Yuan, B.; Li, Y.; Deng, Z. *Journal of the American Chemical Society* **2010**, *132*, 7279.

[74] Wei, Y.; Gao, C.; Meng, F.-L.; Li, H.-H.; Wang, L.; Liu, J.-H.; Huang, X.-J. *The Journal of Physical Chemistry C* **2011**, *116*, 1034.

[75] Gao, C.; Yu, X.-Y.; Xu, R.-X.; Liu, J.-H.; Huang, X.-J. *ACS applied materials & interfaces* **2012**, *4*, 4672.

[76] Huang, H.; Chen, T.; Liu, X.; Ma, H. *Analytica chimica acta* **2014**, *852*, 45.

[77] Lv, M.; Wang, X.; Li, J.; Yang, X.; Zhang, C. a.; Yang, J.; Hu, H. *Electrochimica Acta* **2013**, *108*, 412.

[78] Wu, Z.; Jiang, L.; Zhu, Y.; Xu, C.; Ye, Y.; Wang, X. *Journal of Solid State Electrochemistry* **2012**, *16*, 3171.

[79] Zhu, L.; Tian, C.; Yang, R.; Zhai, J. *Electroanalysis* **2008**, *20*, 527.

[80] Fu, X.-C.; Chen, X.; Guo, Z.; Kong, L.-T.; Wang, J.; Liu, J.-H.; Huang, X.-J. *Electrochimica Acta* **2010**, *56*, 463.

Chapter 2. Synthesis of Activated Graphene/Bismuth Nanocomposite for Electrochemical Detection of Trace Heavy Metal Ions

2.1 Introduction

Among environmental pollutants, heavy metals, such as lead, cadmium, and zinc, are considered to be the most important that cause major public-health concerns owing to their high stability and bio-accumulation [1]. Heavy metals affect several human organs in even very low concentrations. It is important to develop a simple and highly sensitive analytical method for assessing environmental pollutants in soil, water, and air to improve the quality of environment and human life. Analytical methods, such as electrothermal atomic absorption spectrometry (ET-AAS), inductively coupled plasma mass spectrometry (ICP-MS), flame atomic absorption spectrometry (FAAS), and electrochemical (EC) techniques, have been developed for trace metal determination [2].

However, spectrometric methods are cumbersome, time consuming, expensive, and unsuitable *in situ* measurements owing to the required complex instrumentation. In contrast, electrochemical techniques are attractive because of their remarkable sensitivity, portability, and low cost. Among the electrochemical methods, anodic stripping voltammetric analysis is recognized as a powerful tool for the determination of trace metal ions [3]. In stripping voltammetry, mercury is commonly used as the working electrode because of the resultant of excellent reproducibility and high sensitivity. However, owing to the toxicity, various attempts have been made to design a mercury-free replacement. In recent years, bismuth film electrodes have attracted attention to the stripping technique because of remarkable low toxicity and environmentally friendly material. Moreover, it can be formed with alloy with many metals and has a wide potential window, which is an analytical advantage [4].

Graphene, which comprises two-dimensional nanostructures of sp^2-bonded carbon atoms in a hexagonal configuration, is an excellent nanomaterial for electrochemistry owing to its good electrical conductivity, low cost, mechanical properties, and high specific surface area [5]. In 2004, Geim and co-workers [6] reported

graphene sheets prepared by mechanical exfoliation [7]. Since then, more studies were researched focusing on developing attractive applications in electroanalytical chemistry as a unique electrode material for manifolds [8]. Moreover, chemical modification of graphene oxide could be further improve in its electrochemical performance [9].

Graphene formed through chemical activation of graphene oxide (GO) with KOH has a very high specific surface area and in-plane electrical conductivity resulting in its good electrochemical performance as an electrode material. A chemically activated graphene has been proven to be excellent applications, including lithium-ion batteries and supercapacitors [10]. However, to the best our knowledge, activated graphene has never investigated in electrochemical analysis of heavy metal ions.

In this paper, we synthesized chemically activated reduced graphene (AG) with a Brunauer-Emmett-Teller (BET) surface area of up to 2335 m2 g-1. AG was used in combination with an *in situ* electrochemically deposited bismuth composite film to fabricate a sensitive and mercury-free electrochemical platform for the analysis of zinc, cadmium, and lead ions. Nafion acts as an effective

solubilizing agent for activated graphene (AG-NA) and anti-fouling coating to reduce the influence of surface-active macromolecules [4d]. Both AG and Nafion provide negative charge to bind positively charged Bi^{3+} to drive the formation of homogeneous, and stable nanocomposite materials [9b]. In this work, we report the first example of the fabrication of an AG-NA/Bi composite film electrode for the detection of trace heavy metal ions using DPAVS; its performance was compared with that of synthesized reduced graphene oxide (RGO). Thus, the increased analytical performance of the AG-NA/Bi composite film electrode was verified: It showed the combined advantages of electrical conductivity and large specific surface area together with the unique features of *in situ* plated bismuth. Bismuth and the target metal ions nucleate on the surface of the electrode, and form a "fused alloy," which facilitates the nucleation process during the deposition of heavy metals; they also can be anodically stripped during the stripping step, resulting in well-defined peaks for trace metals [3a, 11].

2.2 Experimental Section

2.2.1 Chemicals

All the chemicals used were of analytical reagent grade, and the water was double-distilled. Bi^{3+}, Zn^{2+}, Cd^{2+}, and Pb^{2+} were prepared from 1000 mg L^{-1} atomic absorption standard solutions via dilution. Nafion (NA, 5 wt% solution in a mixture of water and lower aliphatic alcohols) was purchased from Sigma-Aldrich (USA), and sodium acetate and acetic acid were purchased from Aldrich (USA). The working supporting electrolyte comprised 0.1 mol L^{-1} acetate buffer (pH 4.5), which was prepared by mixing appropriate amounts of acetic acid and sodium acetate.

2.2.2 Characterization Methods

The BET specific surface area was determined via N_2 adsorption using a Micromeritics ASAP 2010 (USA) analyzer at the temperature of liquid nitrogen. A high resolution transmission electron microscope (HR-TEM; JEM-3010, JEOL) and field-emission

scanning electron microscope (FE-SEM; JSM-6700F, JEOL) were used to check the morphologies of the AG and AG-NA/Bi composites.

2.2.3 Apparatus

The electrochemical experiments were performed using an Autolab potentiostat (Metrohm, USA) with conventional three electrode system. A modified glassy carbon electrode (3 mm in diameter, Bioanalytical Systems, Inc.) served as the working electrode, while a Ag/AgCl electrode (Bioanalytical Systems, Inc.) and platinum wire were used as the reference and counter electrodes, respectively.

2.2.4 Preparation of the Activated Graphene and Reduced Graphene Oxide

Graphite oxide (GO) was synthesized from graphite powder according to the modified Hummers method [12]. Graphite oxide (500 mg) was dispersed in de-ionized water (20 mL) and sonicated for 20 min, and then KOH (3 g) was added to the dispersion. The mixture was stirred at room temperature for 6 h and dried in an oven at

120 ℃ for 6 h. The dry mixture was then heated at 800 ℃ for 1 h in a horizontal tube furnace under nitrogen flow. After several washings and drying at 80 ℃, AG was obtained [10]. The as-prepared GO was thermally expanded to synthesize RGO by rapid heating to 250 ℃ in a tube furnace (heating rate: 13℃ min^{-1}) [13], and the final products were washed several times with ethanol.

2.2.5 Preparation of the AG/Nafion (NA) Nanocomposite Modified Electrode

Prior to use, the glassy carbon electrode was carefully polished with wet 0.3 and 0.05 μm alumina slurries on a felt pad in succession and then rinsed with double-distilled water. AG (1 mg) was sonicated in a solution containing H_2O (1 mL), isopropyl alcohol (3.4 mL), and Nafion solution (0.1 mL) for 15 min to form the AG dispersion. Then, a 6 μL aliquot of the mixture was coated onto the glassy carbon electrode to prepare the AG-NA composite-film–modified electrode. The modified electrode was dried for 5 min under an infrared heat lamp**.**

2.2.6 Fabrication of Bismuth (Bi)-coated the AG/NA Nanocomposite Modified Electrode

The AG-NA–coated glassy carbon electrode modified (AG-NA/GCE) with bismuth was plated *in situ* using the following procedure: The AG-NA/GCE, Ag/AgCl, and Pt wire electrodes were immersed in an electrochemical cell containing 0.1 mol L^{-1} acetate buffer (pH 4.5), 1 mg L^{-1} of bismuth, and the target metals ions; Bi and the target metals were simultaneously deposited on the surface of the electrode by treatment at −1.4 V for 300 s with stirring.

2.2.7 Procedure for Differential Pulse Anodic Stripping Voltammetry Analysis

After deposition, the solution was left in quiescence for ~10 s. Differential pulse voltammetry was performed via a potential scan from −1.4 to 0.0 V with an amplitude of 50 mV, pulse width of 50 ms, potential step of 4 mV, and pulse period of 0.2 s (without stirring). The scan was terminated at 0.0 V. Prior to the next cycle, the electrode was cleaned for 60 s at 0.3 V in fresh supporting electrolyte

with stirring to remove the target metals and bismuth. All potentials are given versus the Ag/AgCl electrode.

2.3 Results and Discussion

2.3.1 Characterization of the AG and AG/NA/Bi composite

Figure 2.1 is illustrates the synthetic approach for preparing the AG through of process of chemical activation of graphene oxide (GO) with KOH to create pores. The structure and morphology of AG were characterized using a TEM and SEM. Figure 2.2 (a) shows the TEM image of reduced graphene oxide. Figure 2.2 (b) and (c) shows the HR-TEM and SEM images of chemically activated graphene oxide and demonstrate its porous structure. As seen in Figure 2.2 (a) the sheet of RGO has a smooth and wrinkled monolayer. Figure 2.2 (b) shows that the morphology of AG is markedly different from that of RGO and contains many pores, which are advantageous for the transport of electrons. TEM images of the AG-NA/Bi composite are shown in Figure 2.3 (a) and (e). For further investigation, TEM observations and energy dispersive X-ray (EDX) mapping

measurements were performed. Figure 2.3 shows the TEM images and EDX mapping of the bismuth distribution in the composite sample; Figure 2.3 (b) and (c) shows the results of carbon and bismuth, respectively, while Figure 2.3 (d) shows a mapping overlay of (b) and (c). Figure 2.3 (e) also shows that bismuth was deposited on the AG surface. Based on these results, the bismuth particles were well distributed.

N_2 adsorption–desorption isotherms of AG are shown in Figure 2.4 (a) and (b). The specific surface area, total pore volume, and average pore size of AG and RGO are shown in Table 2.1. The BET specific surface areas of AG and RGO were 2335.0 and 370.0 $m^2 g^{-1}$ (as calculated from the linear relative pressure range between 0.1 and 0.5). Compared with that of RGO, the surface area of AG is much larger, which indicates the degree of activation of GO by KOH. The isotherm of AG can be classified as having typical type IV isotherm hysteresis, which indicates a narrow distribution of mesopores. Generally, the pore diameters of mesopores are within the range of 2 – 50 nm. The average pore diameter and total pore volume of AG are 3.06 nm and 1.54$m^3 g^{-1}$, respectively. These pores could provide sufficient mass-transport pathways for reactants and products.

Figure 2. 1 Schematic of preparation of an activated graphene.

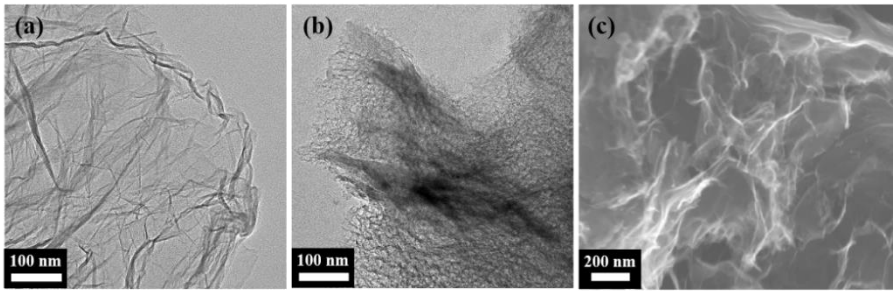

Figure 2. 2 TEM and SEM images of reduced graphene oxide (a), chemically activated graphene oxide (b), (c).

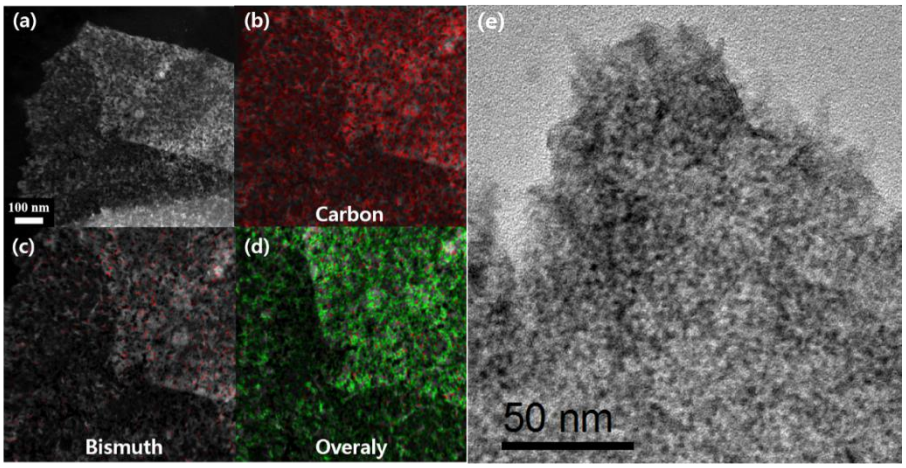

Figure 2. 3 TEM images of activated graphene / Bi composite film (a), (e) and the corresponding elemental mapping of carbon (b), bismuth (c) and overlay (d) for AG-NA/Bi composite film.

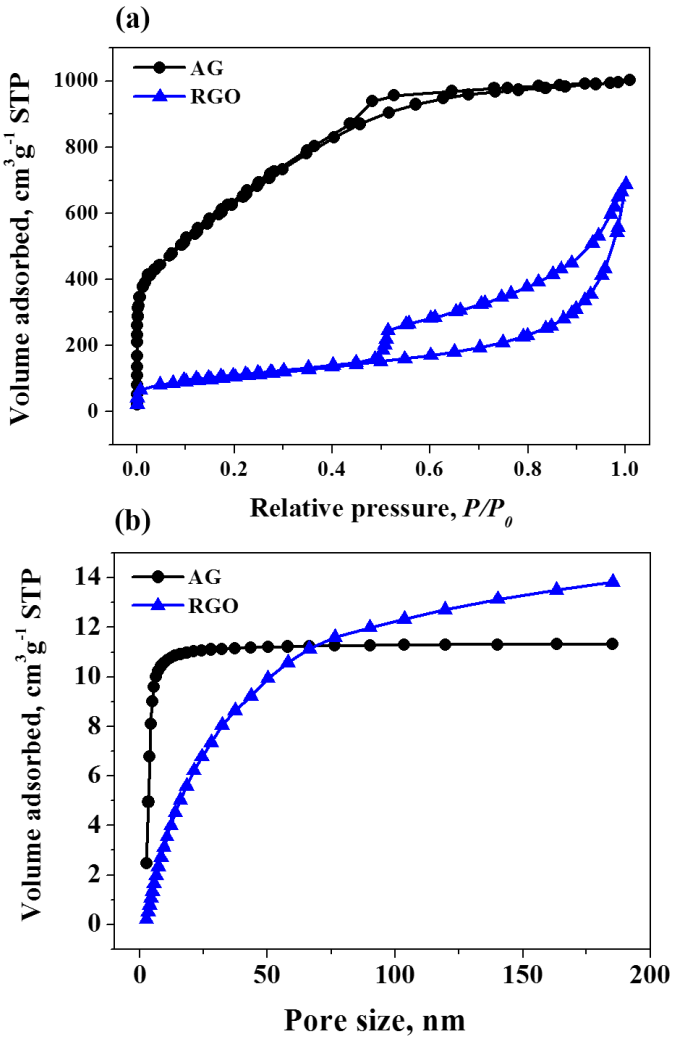

Figure 2. 4 Nitrogen adsorption–desorption analysis of activated graphene oxide and reduced graphene oxide. (a) N2 isotherm curves at 77.4 K. (b) Cumulative pore volume and pore size distribution obtained from the adsorption isotherm in (a).

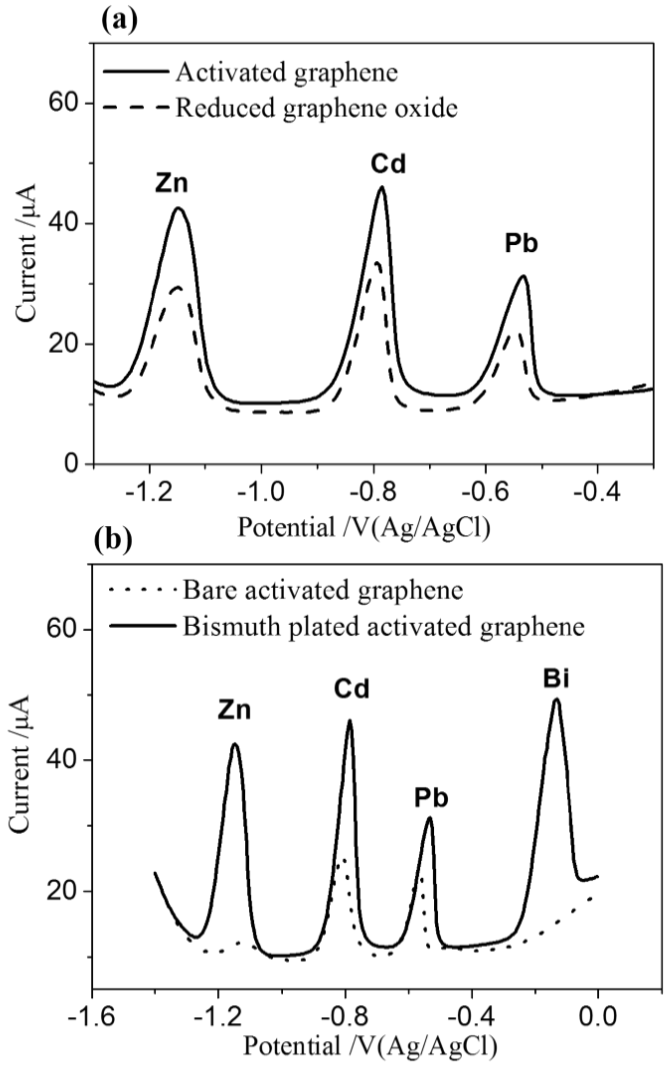

Figure 2. 5 Anodic stripping voltammograms of 50 μg L^{-1} Zn^{2+}, Cd^{2+} and Pb^{2+} at *in situ* plated bismuth film on AG and RGO (a), at bare AG and *in situ* plated bismuth film on AG (b).

	Reduced graphene oxide	Activated graphene
Specific surface area(m^2g^{-1})	370.0	2335.0
Total pore volume(m^3g^{-1})[a]	0.99	1.54
Average pore diameter (nm)[b]	11.93	3.06

[a] Total pore volumes measured at P/P_0 = 0.992. [b] BJH desorption averate pore diameters.

Table 2. 1 The specific surface area, total pore volume and average pore diameter of samples.

2.3.2 Electrochemical Characterization

To prove the performance of AG for trace metal ion determination, the voltammetric behaviors of the AG- and RGO-modified electrode were investigated with an *in situ* plated bismuth film electrode using DPASV in 0.1 mol L^{-1} acetate buffer solution (pH 4.5). Stripping voltammograms of the different film-coated GC electrodes with bismuth are shown in Figure 2.5 (a) (RGO: dashed line; AG: solid line). The stripping voltammograms were obtained in a solution containing 50 μg L^{-1} of Zn^{2+}, Pb^{2+}, and Cd^{2+}. Sharper and higher peak currents for the target metal ions were obtained by using the AG-modified electrode. Compared with RGO-modified electrode, the sensitivity of the AG-coated electrode was higher by ~67%. This enhanced signal indicates that the unique properties of highly conductive AG result from the extensive conjugated sp^2 carbon network and porous structure. Thus, the AG-based electrode had much better sensitivity than the other electrodes for anodic stripping voltammetry.

Figure 2.5 (b) shows the stripping voltammograms of 50 μg L^{-1} of Zn^{2+}, Cd^{2+}, and Pb^{2+} on the bare AG-NA–coated glassy carbon

electrode and AG-NA/Bi composite-film–coated electrode in an acetate buffer. Although the AG-NA/GCE shows separate peaks for Zn^{2+}, Cd^{2+}, and Pb^{2+}, the sensitivity of the AG-NA/Bi composite-film electrode for trace metal ion detection was much higher with well-defined, sharp, and separate peaks for the analytes. Relative to the bare AG-NA/GCE, the stripping signals on the AG-NA/Bi composite film electrode were notably improved by about 15 times for zinc, 2 times for cadmium, and 1.5 times for lead. This enhanced signal is attributed to the capacity of bismuth to form a “fused alloy” with trace metal ions resulting in easier reduction of zinc, cadmium, and lead [2b]. In addition, the large electroactive area and strong absorption of AG result from attracts trace metal ions and bismuth the bulk solution to the electrode surface [10]. Graphene has a narrow potential window and the hydrogen evolution potential is more positive than the reduction potential of zinc (around –1.3 V). However, when bismuth was plated onto the AG/NA electrode, the voltammetric analytical curve of the electrode depends on the bismuth film. In these experiments, zinc was successfully determined at the AG-NA/Bi composite electrode. Therefore, AG could be used as a substrate for the bismuth film, which is appropriate for the

determination of most heavy trace metal ions including zinc.

2.3.3 Effect of Experimental Variables

In order to get the best detection results, a solution containing 50 μg L^{-1} each of trace metal ions was utilized to investigate the effect of different parameters. The influence of pHs of buffer solutions on the stripping peak currents was studied in the pH range 3.0 and 6.0 by DPASV. As shown in Figure 2.6 (a), the stripping peak currents were significantly influenced by pH values of acetate buffer solutions. The optimum pH ranges were 4.5 ~ 5.5 for trace heavy metal ions, respectively. If the acidity was higher or lower than the best range above, the peak currents of trace heavy metal ions were decreased. The maximum peak current of Cd^{2+} and Pb^{2+} was observed at pH 4.5, which is mildly acidic condition. However, the peak current of Zn^{2+} was maximal at pH 5.5 and then decreased. The decrease of the peak currents at the lower pH than 4.5 can be attributed to the protonation on the graphene plan. At the pHs higher than 4.5, the decrease in the peak currents is due to the hydrolysis of cations. Thus, pH 4.5 was chosen as the optimal pH for the simultaneous determination of Zn^{2+},

Cd^{2+} and Pb^{2+}.

The effect of pre-concentration time is shown in Figure 2.6 (b). At shorter pre-concentration times, the peak currents for the three metal ions increased linearly with deposition time owing to the increased amount of metals ions on the AG-NA/Bi-modified electrode. However, the plot tended to curve with a diminished slope value up to 300 s. As the deposition time increased, the thickness of the bismuth film was also increased, which hindered the mass transfer of metal ions during the stripping step. Thus, 300 s was chosen to be the optimal pre-concentration deposition time.

The thickness of the bismuth film also depends on the ion concentration. Figure 2.6 (c) demonstrates the effect of bismuth concentration on the stripping responses. As shown, the peak currents of trace metal ions tend to increase with the increasing concentration of bismuth from 0 to 0.4 mgL^{-1}. However, for bismuth concentrations higher than 0.4 mgL^{-1}, the peak currents of trace metal ions decreased or in similar state. An excess concentration of bismuth ion did not lead to a substantial increase in sensitive over the bismuth concentration of 0.4 mgL^{-1}. Consequently, the optimized concentration of bismuth was chosen as 0.4 mgL^{-1}

The effect of the deposition potential on the peak currents of Zn^{2+}, Cd^{2+}, and Pb^{2+} was studied in the potential range from −1.6 to −0.8 V and the stripping response of the metal ions was obtained, as shown in Figure 2.6 (d). As the pre-concentration potential became increasingly negative, the peak current of Zn^{2+} increased to –1.4 V. The peak currents of Cd^{2+} and Pb^{2+} did not increase significantly and were not influenced by the pre-concentration potential owing to their more positive reduction potentials. The different trends observed for Zn^{2+}, Cd^{2+}, and Pb^{2+} may be due to their different standard potentials. To obtain better sensitivity for the simultaneous detection of trace heavy metal ions, −1.4 V was determined to be the optimal pre-concentration potential.

In Figure 2.6 (e), the effects of the variation of the stirring speed during pre-concentration step between 0 and 2500 rpm are shown, in order to investigate the mass transport behavior. As demonstrated by the Levich equation, the plot of the stripping current indicates that the mass transport behavior correlates linearly with the square root of the electrode stirring speed. The stripping peak currents for the metal ions were continuously increased with stirring speed. Therefore, a stirring speed of 2500 rpm was used during pre-concentration [14-15].

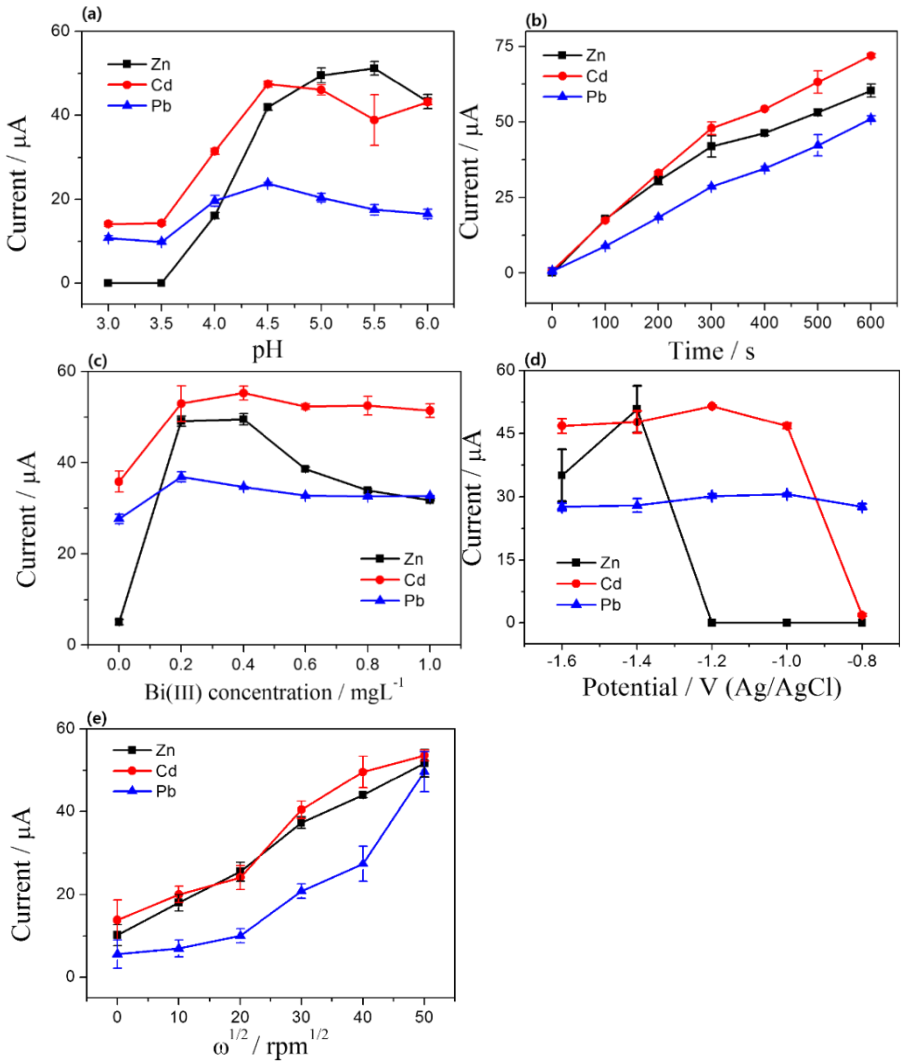

Figure 2. 6 Effect of pHs (a), deposition time (b), bismuth concentration (c), deposition potential (d), and stirring speed during pre-concentration (e) on the stripping peak current of 50 μg L^{-1} each of Zn^{2+}, Cd^{2+} and Pb^{2+} on an *in situ* plated AG-NA/Bi composite film coated electrode in solution.

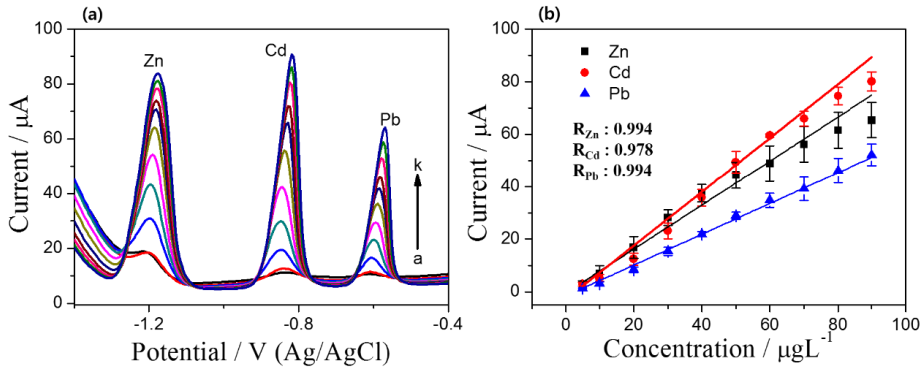

Figure 2. 7 Stripping voltammograms for the different concentrations of Zn^{2+}, Cd^{2+} and Pb^{2+} over a concentration range of 5, 10, 20, 30, 40, 50, 60, 70, 80, 90 µg L^{-1} from a to k in 0.1 M acetate buffer solution at pH 4.5 using the AG-NA/Bi composite film electrode (a). The right part show the calibration curves (b) for the simultaneous determination of Zn^{2+}, Cd^{2+} and Pb^{2+} in 5 to 90 µg L^{-1} concentration ranges. Error bar : *n*=3

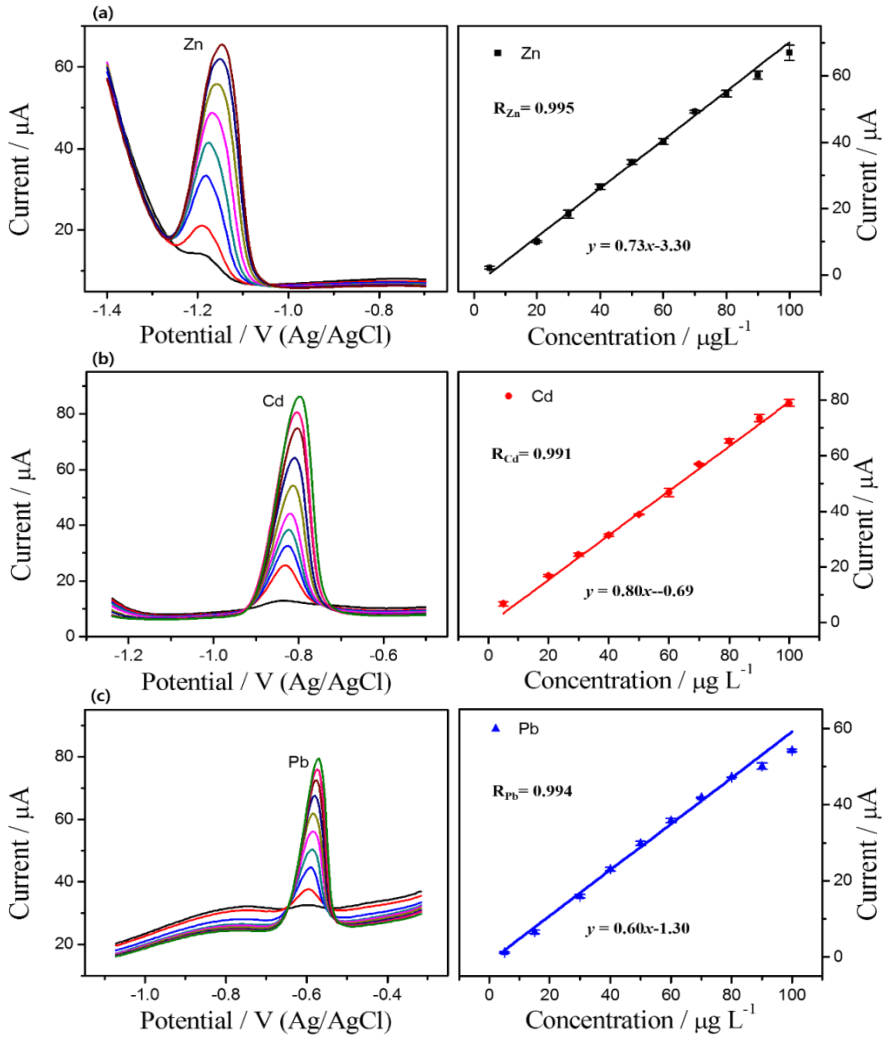

Figure 2. 8 Differential pulse anodic stripping voltammetry (left part) and corresponding calibration plots (right part) for individual analysis of Zn^{2+} (a), Cd^{2+} (b) and Pb^{2+} (b) obtained at AG-NA/Bi composite film electrode over 5 - 100 μg L^{-1}. Error bar: *n*=3.

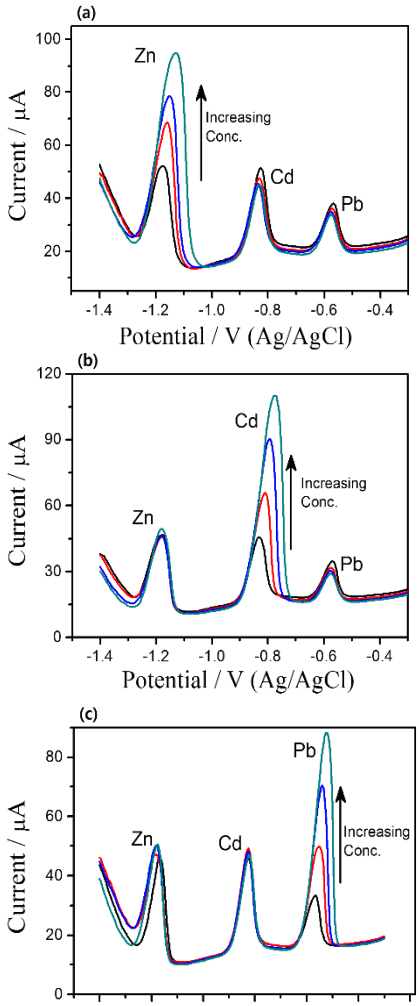

Figure 2. 9 DPASV response of the AG-NA/Bi nano composite modified GCE: (a) at 20, 50, 100, and 200 µg L^{-1} Zn^{2+} in the presence of 20 µg L^{-1} Cd^{2+} and Pb^{2+} in 0.1 M acetate buffer solution (pH 4.5); (b) at 20, 50, 100, and 200 µg L^{-1} Cd^{2+} in the presence of 20 µg L^{-1} Zn^{2+} and Pb^{2+} in 0.1 M acetate buffer solution (pH 4.5); (c) at 20, 50, 100, and 200 µg L^{-1} Pb^{2+} in the presence of 20 µg L^{-1} Zn^{2+} and Cd^{2+} in 0.1 M acetate buffer solution (pH 4.5).

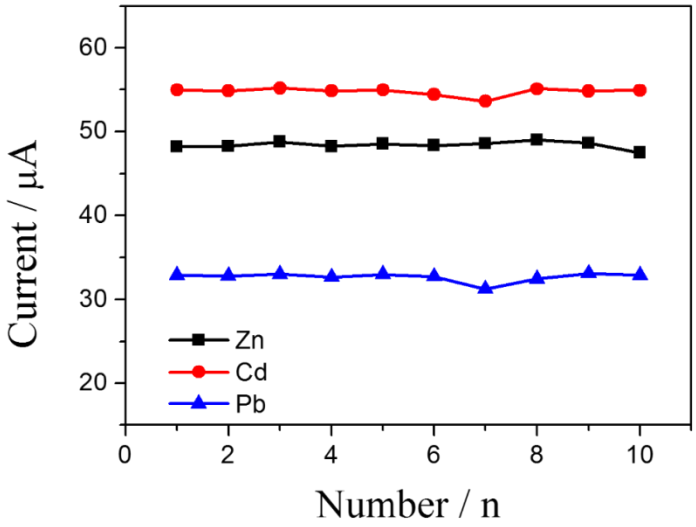

Figure 2. 10 The stability of 10 repetitive measurements of 50 μg L^{-1} Zn^{2+}, Cd^{2+} and Pb^{2+} on an *in situ* plated AG-NA/Bi composite film coated electrode in solution.

Electrodes	Linear range ($\mu g\ L^{-1}$)			Limit of detection ($\mu g\ L^{-1}$)			Ref.
	Zn^{2+}	Cd^{2+}	Pb^{2+}	Zn^{2+}	Cd^{2+}	Pb^{2+}	
RGO/NA/Hg	0.5 – 5.0	0.5 – 5.0	0.5 – 5.0	0.14	0.13	0. 07	[1]
RGO/NA/Bi	–	0.44 – 178	2.4 – 241	–	0.18	0.09	[4e]
CNT/Bi	20 – 100	20 –100	20 – 100	12	0.70	1.30	[14]
MWCNTs/NA/Bi	–	0.08 – 100	0.05 –100	–	0.04	0.03	[15]
RGO/AlOOH	–	200 – 800	200 – 800	–	0.03	0.09	[16]
ERGO/PG/Bi	10 – 100	10 – 100	10 – 100	0.26	0.10	0.16	[17]
AG/NA/Bi	5 – 100	5 – 100	5 – 100	0.57	0.07	0.05	This work

Table 2. 2 Comparison of different electrodes for determination of heavy metal ions.

2.3.4 Analytical Performance

The analytical performance of the AG-NA/Bi composite electrode was investigated for the simultaneous and individual determination of Zn^{2+}, Cd^{2+}, and Pb^{2+} using DPASV. Figure 2.7 show the voltammograms and calibration plots for simultaneous analyses. It was found that the peak current and the concentration of trace metal ion exhibited a favorable linear relation over the range from 5 to 90 μg L^{-1}. The corresponding calibration plots are shown in Figure 2.7 (b). The The corresponding calibration plots and correlation coefficients are $y = 0.586x - 1.623$ and R = 0.994 for Zn^{2+}, $y = 0.839x - 0.592$ and R = 0.978 for Cd^{2+}, and $y = 1.024x - 2.951$ and R = 0.994 for Pb^{2+} (x: concentration (μg L^{-1}), y: current (μA)). In comparing, the individual analysis of heavy metal ions was performed at the same conditions as shown in Figure 2.8. It was found that the peak current and the concentration of trace metal ion exhibited a favorable linear relation over the range from 5 to 100 μg L^{-1}. The corresponding calibration plots and correlation coefficients are $y = 0.737x - 3.302$ and R = 0.995 for Zn^{2+}, $y = 0.818x - 0.693$ and R = 0.991 for Cd^{2+}, and $y = 0.614x - 1.303$ and R = 0.999 for Pb^{2+} (x:

concentration (μg L^{-1}), *y*: current (μA)). The limits of detection were 0.60 μg L^{-1} for Zn^{2+}, 0.08 μg L^{-1} for Cd^{2+}, and 0.05 μg L^{-1} for Pb^{2+} for simultaneous analysis. In case of individual analysis, the limits of detection were were 0.57 μg L^{-1} for Zn^{2+}, 0.07 μg L^{-1} for Cd^{2+}, and 0.05 μg L^{-1} for Pb^{2+}; these values are comparable to those of the Nafion/CNT-coated bismuth film electrode (12 μg L^{-1} for Zn^{2+}, 0.7 μg L^{-1} for Cd^{2+}, and 1.3 μg L^{-1} for Pb^{2+} [11]) and RGO/Bi composite electrode (17 μg L^{-1} for Zn^{2+}, 2.8 μg L^{-1} for Cd^{2+}, and 0.55 μg L^{-1} for Pb^{2+} [18], which indicates that the present method shows similar sensitivity for the simultaneous detection of trace heavy metals.

Therefore, the AG-NA/Bi composite electrode with a well-defined stripping response could successfully applied to the determination of trace heavy metal ions. Mutual interference is a common problem existing in detection of several metal ions simultaneously. Thus, we studied the mutual interferences between trace metal ions at the modified electrode. When fixing the concentration of other cations, but increasing the concentration of Zn^{2+}, as shown in Figure 2.9 (a), the peak current of Zn^{2+} linearly increased while the peak current of other cations almost remains the same. Similarly, when fixing the concentration of other cations, but increasing the concentration of one

cation, as shown Figure 2.9 (b) and (c), the peak current of the one cation linearly increased while the peak current of other two cations almost remais the same. All the results indicate that, there is no mutual interferences among trace metal ions at the AG-NA/Bi nano composite modified electrode when detecting the target metal ions.

Furthermore, the detection limits obtained with the AG-NA/Bi composite electrode compares favorably with previously reported modified electrode listed in Table 2.2. The results indicate that the present method shows high sensitivity for the detection of trace heavy metals.

The reproducibility of AG-NA/Bi composite-film–modified glassy carbon electrode was studied by 10 repetitive measurements of 50 μg L^{-1} heavy metal ions, as shown in Fig. 8. The relative standard deviation (RSD) was 0.8 % for Zn^{2+}, 0.8 % Cd^{2+}, and 1.6 % for Pb^{2+}, respectively. Such good precision may be related to the controllable structure the Nafion film resulting from the interfusion of the AG nanosheets.

2.3.5 Application to Real Environments

To evaluate its accuracy in practical application, the AG-NA/Bi composite film electrode was also employed to the simultaneous determination of Zn^{2+}, Cd^{2+}, and Pb^{2+} in local tap-water sample by using standard addition method. Different concentrations of trace heavy metal ions were added to the tap water, and the samples were analyzed three times. The mean recoveries (% ± SD) of the method were calculated, and their values were summarized in Table 2. The result of DPAVS determination were compared with those obtained by inductively coupled plasma mass spectrometry (ICP-MS). The comparative results, shown in Table 2, all results indicated that the AG-NA/Bi composite electrode is potentially useful for the analysis of heavy metals in real samples.

Metal	Added ($\mu g\ L^{-1}$)	Found ($\mu g\ L^{-1}$)[a]	Recovery (%)[b]	Found by ICP-MS[a]
Zn	5	4.8 ±0.1	96.4 ± 4	6.5 ± 0.1
	10	9.8 ± 0.1	98.5 ± 3	10.6 ± 0.0
	15	16.2 ± 0.5	100.7 ± 7	15.2 ± 0.3
	20	19.9 ± 0.3	99.3 ± 2	19.9 ± 0.6
Cd	5	4.8 ± 0.2	87.4 ± 3	4.1 ± 0.0
	10	9.2 ± 0.4	93.8 ± 2	8.91 ± 0.1
	15	14.0 ± 0.5	93.6 ± 8	13.5 ± 0.3
	20	18.4 ± 0.2	92.1 ± 3	17.5 ± 0.3
Pb	5	4.3 ± 0.1	85.5 ± 6	3.2 ± 0.1
	10	9.3 ± 0.3	92.6 ± 3	6.7 ± 0.1
	15	13.8 ± 0.6	93.2 ± 4	11.7 ± 0.4
	20	18.2 ± 0.3	91.2 ± 2	16.8 ± 0.3

[a] Mean of three repetitive measurements at a 95 % confidence level

[b] Mean ± standard deviation %

Table 2. 3 Recoveries of trace heavy metal ions in tap water samples

2.4 Conclusion

We developed a method for the preparation of a new and enhanced sensing platform based on porous graphene through simple KOH activation of GO. The resultant AG has a unique structure that makes it attractive as a potential material for the electrochemical determination of trace metal ions. The AG-NA/Bi composite electrode was applied for the simultaneous determination of trace zinc, cadmium, and lead by DPASV. The composite film integrates the unique properties of AG and the advantages of bismuth electrodes, leading to enhanced sensitivity towards trace metal ions, especially zinc. The appearance of a zinc stripping peak reveals its superior sensitivity as compared to previous Bi electrodes. The AG-NA/Bi composite was also used as an electrode material for the sensitive determination of metal ions in a real sample. Thus, the proposed method facilitates the monitoring of trace heavy metals and can be expanded to detect other environmental pollutants.

References

[1] Willemse, C. M.; Tlhomelang, K.; Jahed, N.; Baker, P. G.; Iwuoha, E. I. *Sensors* **2011**, *11*, 3970.

[2] a) Korn, M. d. G. A.; de Andrade, J. B.; de Jesus, D. S.; Lemos, V. A.; Bandeira, M. L. S. F.; dos Santos, W. N. L.; Bezerra, M. A.; Amorim, F. A. C.; Souza, A. S.; Ferreira, S. L. C. *Talanta* **2006**, *69*, 16. b) Arduini, F.; Calvo, J. Q.; Palleschi, G.; Moscone, D.; Amine, A. *TRAC Trends in Analytical Chemistry* **2010**, *29*, 1295.

[3] a) Wang, J.; Lu, J.; Hocevar, S. B.; Farias, P. A. M.; Ogorevc, B. *Analytical Chemistry* **2000**, *72*, 3218. b) Achterberg, E. P.; Braungardt, C. *Analytica Chimica Acta* **1999**, *400*, 381. c) Batley, G. E. *Marine Chemistry* **1983**, *12*, 107.

[4] a) Li, H.; Li, J.; Yang, Z.; Xu, Q.; Hou, C.; Peng, J.; Hu, X. *Journal of Hazardous Materials* **2011**, *191*, 26. b) Torma, F.; Kádár, M.; Tóth, K.; Tatár, E. *Analytica Chimica Acta* **2008**, *619*, 173. c) De Vitre, R. R.; Tercier, M. L.; Tsacopoulos, M.; Buffle, J. *Analytica Chimica Acta* **1991**, *249*, 419. d) Li, J.; Guo, S.; Zhai, Y.; Wang, E. *Analytica Chimica Acta* **2009**, *649*, 196. e) Gadhari, N. S.; Sanghavi, B. J.; Karna, S. P.; Srivastava, A. K. *Electrochimica Acta* **2010**, *56*, 627.

[5] a) Wang, J.; Lu, J.; Kirgöz, Ü. A.; Hocevar, S. B.; Ogorevc, B. *Analytica Chimica Acta* **2001**, *434*, 29. b) Pumera, M.; Ambrosi, A.; Bonanni, A.; Chng, E. L. K.; Poh, H. L. *TRAC Trends in Analytical Chemistry* **2010**, *29*, 954. c) Pumera, M. *The Chemical Record* **2009**, *9*, 211. d) Liang, M.; Zhi, L. *Journal of Materials Chemistry* **2009**, *19*, 5871. e) Yang, W.; Ratinac, K. R.; Ringer, S. P.; Thordarson, P.; Gooding, J. J.; Braet, F. *Angewandte Chemie International Edition* **2010**, *49*, 2114.

[6] Shao, Y.; Wang, J.; Wu, H.; Liu, J.; Aksay, I. A.; Lin, Y.

Electroanalysis **2010**, *22*, 1027.

[7] Novoselov, K. S.; Geim, A. K.; Morozov, S. V.; Jiang, D.; Zhang, Y.; Dubonos, S. V.; Grigorieva, I. V.; Firsov, A. A. *Science* **2004**, *306*, 666.

[8] a) Fan, X.; Peng, W.; Li, Y.; Li, X.; Wang, S.; Zhang, G.; Zhang, F. *Advanced materials* **2008**, *20*, 4490. b) Wang, Y.; Li, Y.; Tang, L.; Lu, J.; Li, J. *Electrochemistry Communications* **2009**, *11*, 889.

[9] a) Sanghavi, B. J.; Sitaula, S.; Griep, M. H.; Karna, S. P.; Ali, M. F.; Swami, N. S. *Analytical Chemistry* **2013**, *85*, 8158. b) Li, Y.; van Zijll, M.; Chiang, S.; Pan, N. *Journal of Power Sources* **2011**, *196*, 6003. c) Liu, J.; Tang, J.; Gooding, J. J. *Journal of Materials Chemistry* **2012**, *22*, 12435. d) Zhu, Y.; Murali, S.; Cai, W.; Li, X.; Suk, J. W.; Potts, J. R.; Ruoff, R. S. *Advanced materials* **2010**, *22*, 3906. e) Sanghavi, B. J.; Wolfbeis, O. S.; Hirsch, T.; Swami, N. S. *Microchimica Acta* **2015**, *182*, 1. f) Sanghavi, B. J.; Varhue, W.; Chávez, J. L.; Chou, C.-F.; Swami, N. S. *Analytical Chemistry* **2014**, *86*, 4120.

[10] Zhu, Y.; Murali, S.; Stoller, M. D.; Ganesh, K. J.; Cai, W.; Ferreira, P. J.; Pirkle, A.; Wallace, R. M.; Cychosz, K. A.; Thommes, M.; Su, D.; Stach, E. A.; Ruoff, R. S. *Science* **2011**, *332*, 1537.

[11] Xu, H.; Zeng, L.; Xing, S.; Xian, Y.; Shi, G.; Jin, L. *Electroanalysis* **2008**, *20*, 2655.

[12] Wang, Z.-l.; Xu, D.; Huang, Y.; Wu, Z.; Wang, L.-m.; Zhang, X.-b. *Chemical Communications* **2012**, *48*, 976.

[13] Cassagneau, T.; Fendler, J. H. *Advanced materials* **1998**, *10*, 877.

[14] Hwang, G. H.; Han, W. K.; Park, J. S.; Kang, S. G. *Talanta* **2008**, *76*, 301.

[15] Kefala, G.; Economou, A.; Voulgaropoulos, A. *Analyst* **2004**, *129*, 1082.

[16] Gao, C.; Yu, X.-Y.; Xu, R.-X.; Liu, J.-H.; Huang, X.-J. *ACS applied materials & interfaces* **2012**, *4*, 4672.
[17] Pokpas, K.; Zbeda, S.; Jahed, N.; Mohamed, N.; Baker, P. G.; Iwuoha, E. I. *Int. J. Electrochem. Sci* **2014**, *9*, 736.
[18] Sahoo, P. K.; Panigrahy, B.; Sahoo, S.; Satpati, A. K.; Li, D.; Bahadur, D. *Biosensors and Bioelectronics* **2013**, *43*, 293.

Chapter 3. Development of an Electrochemically Reduced Graphene Oxide/Bismuth Modified Electrode for Stripping Analysis of Heavy Metal Ions

3.1 Introduction

Heavy metals such as lead, cadmium, and zinc are well-known undesirable constituents in groundwater, drinking water, and soil. Especially they can be accumulated in the human body through the food chain to induce a severe threat to human health [1]. The increase in concentration of heavy metals, resulting from anthropogenic activities such as mining and industrial processing, has become a global concern [2]. Accordingly, it is increasingly necessary to develop sensitive, rapid, and simple analytical methods required for continuous monitoring of these pollutants. Analytical methods, such as electrothermal atomic absorption spectrometry, flame atomic absorption spectrometry [3], inductively coupled plasma mass spectrometry (ICP-MS) [4], and electrochemical techniques, have

been developed for trace metal determination. However, spectrometric methods are unsuitable for *in situ* measurements owing to the complex instrumentation required. In addition, they are expensive, cumbersome mode of administration, and time consuming, requiring analysis to be performed by skilled personnel in a specialized manner. In contrast, electrochemical methods, especially electrochemical stripping analysis, have been widely recognized as convenient techniques for measuring heavy metal ions owing to good selectivity, low cost, portability and the ability to accurately determine multiple elements at trace level [5]. Until now, mercury and mercury film electrodes have been commonly used as materials in stripping voltammetric analysis for heavy metal determination, due to good reproducibility and high sensitivity [6]. Mercury is, however, a very hazardous material, its use raising serious health and environmental concerns. Numerous attempts have been made to replace it with new, more environmentally friendly mercury-free electrodes. Bismuth electrodes have recently been developed in the field of the stripping technique as a possible replacement for mercury electrodes. Bismuth electrodes have shown results comparable to mercury electrodes, which can form fused alloys with trace heavy

metals. Moreover, bismuth electrodes have many beneficial properties such as low toxicity, high sensitivity, good stripping signal, and simple preparation [5b, 7]. However, new materials with bismuth film for working electrodes are still needed for developing a high-sensitivity heavy metal-sensing platform [8].

Graphene, a one atom-thick planar sheet of sp^2-bonded carbon atoms, is attracting tremendous attention due to its large specific surface area, high thermal conductivity, and good electrical conductivity. Moreover, graphene exhibits remarkable electrochemical properties, such as a large potential window, low charge-transfer resistance, excellent electrochemical activity, and fast electron transfer rate [9]. The extraordinary properties of graphene enhance its application to electrochemical sensing [10]. Mechanical cleavage of graphite led to the discovery of graphene, but the low productivity of this approach makes it impractical for large-scale preparations [11]. Later, graphene sheets were grown on a single crystal of silicon carbide by vacuum graphitization [12], or produced continuously in microwave plasma reactors [13]. Furthermore, graphene has been made from rapid thermal expansion of graphite or chemical reduction of exfoliated graphite oxide (GO), a soft chemical

synthesis route [14]. All these methods suffer from limitations of high temperature, expensive special equipment, use of toxic chemicals or conditions, and tedious procedures. Therefore, a "green synthesis" of graphene under mild conditions is needed. Recently, electrochemical deposition has been reported as a simple method and green strategy for graphene synthesis [15]. For sensing applications, the modification of electrodes for depositing graphene is crucial. Graphene-modified electrodes are normally fabricated by drop-casting solution-based graphene obtained from chemical reduction of graphene oxide. However, this method has intrinsic limitations such as weak adhesion to substrate electrode, lack of control of film thickness, and agglomeration of the reduced graphene suspension through strong interactions and π-π stacking. Thus, a method for the direct electrochemical reduction of GO was proposed [16].

In this study, we carried out direct electrochemical reduction of GO on a glassy carbon electrode (GCE) from GO dispersion to determine trace heavy metal ions by differential pulse anodic stripping voltammetry (DPASV). This method can be used to control film thickness quantitatively and form a stable film on the electrode surface without any further treatment.

The objective of this work was to improve analytical performance and fabricate a sensitive, mercury-free, electrochemical platform combining the advantages of EG with the *in situ* plating bismuth nanocomposite film-coated GCE. Associated with an enlarged active surface area, high electronic conductivity, and strong absorptive ability of graphene, the modified composite electrode showed enhanced electron transfer properties and excellent stripping performance for the analysis of trace heavy metal ions. The experimental results indicated that this electrode exhibited excellent voltammetric response to heavy metal ions. This simple, fast, highly sensitive, reducing-agent-free, low-cost sensor was fabricated to determine the traces of lead, cadmium, and zinc in real samples.

3.2 Experimental Section

3.2.1 Chemicals

All chemicals were of analytical grade and used without further purification. Standard solutions of Bi^{3+}, Zn^{2+}, Cd^{2+}, and Pb^{2+} (1000 mg L^{-1}) were obtained from Sigma-Aldrich and diluted as required.

Graphite powder (<20 μm), sodium acetate, and acetic acid were purchased from Aldrich (USA). Sodium phosphate buffer (PBS) was used as supporting electrolyte to prepare the EG film. A 0.1 M acetate buffer (pH 4.5), prepared by mixing appropriate amounts of acetic acid and sodium acetate, was used to prepare solutions of the supporting electrolyte. All solutions were prepared with double-distilled water.

3.2.2 Characterization Methods

A transmission electron microscope (TEM; JEM-3010, JEOL) and field-emission scanning electron microscope (FE-SEM; JSM-6700F, JEOL) were used to check the morphologies of the GO, EG and EG/Bi composite. Raman analysis was performed using a Raman spectrometer (Dongwoo DM 500i) employing a 15 mW Argon laser at 514.5 nm.

3.2.3 Apparatus

Electrochemical measurements were performed on an Autolab

potentiostat (Metrohm, USA) with a conventional three-electrode system. A modified GCE (3 mm in diameter, Bioanalytical Systems, Inc.) served as the working electrode, while a Ag/AgCl electrode (Bioanalytical Systems, Inc.) and platinum wire were used as the reference and counter electrodes, respectively.

3.2.4 Preparation of Graphene Oxide

Graphite oxide (GO) was prepared from graphite powder according to an improved Hummers method [14a]. A mixture of 72 ml of H_2SO_4 and 8 ml of HCl was added to a beaker containing 3 g of graphite at room temperature. Then 18 g of $KMnO_4$ was added to the mixture slowly with stirring in an ice bath. After the reaction for 1 h at room temperature, the beaker was heated to 90 ℃ and maintained at this temperature for 24 h for further reaction. Finally, 300 ml of deionized water and 5 ml of H_2O_2 (30 wt% in H_2O) were sequentially added to dissolve insoluble materials. The color of the mixture immediately turned to bright yellow from dark purple. The resulting GO suspension was washed with 250 ml of 10 wt% HCl aqueous solution three times to remove residual metal ions and with deionized

water repeatedly until the solution pH reached a constant value of 7.

3.2.5 Preparation of Electrochemically Reduced Graphene Oxide (EG) Modified Electrode

The prepared graphite oxide powder was exfoliated into PBS solution (0.1 M, pH 7) by ultrasonication, forming a 5 mg ml^{-1} GO suspension [16c]. Prior to use, the GCE was carefully polished on a felt pad with successive 0.3 and 0.05 μm wet alumina slurries and rinsed with double-distilled water. Electrochemical reduction of GO on the GCE surface was performed in the GO dispersion solution with magnetic stirring using cyclic voltammetry (CV). The CV scan was performed between –1.5 and 0.8 V at a rate of 50 mV s^{-1}. After electrochemical reduction, the working electrode was washed with double-distilled water and dried under an infrared heat lamp for 2 min.

3.2.6 Preparation of EG/Bismuth (Bi) Nanocomposite Modified Electrode

The analysis of trace heavy metal ions by differential pulse anodic stripping voltammetry (DPASV) was performed in 0.1 M acetate buffer solution. The EG-coated CGE (EG/GCE) modified with bismuth was plated *in situ* using the following procedure: The EG/GCE, Ag/AgCl, and Pt wire electrodes were immersed in an electrochemical cell containing 0.1 M acetate buffer (pH 4.5), 0.6 mg L^{-1} of bismuth, and the target metals ions; Bismuth and the target metals were simultaneously deposited on the surface of the electrode by treatment at –1.4 V for 300 s with stirring.

3.2.7 Procedure for Differential Pulse Anodic Stripping Voltammetry Analysis

The DPASV potential scan was carried out from –1.4 V to 0 V. Prior to the next cycle, a 60 s cleaning step was performed at 0.3 V in fresh supporting electrolyte, with stirring to remove the target metals and bismuth. All potentials are given versus the Ag/AgCl electrode.

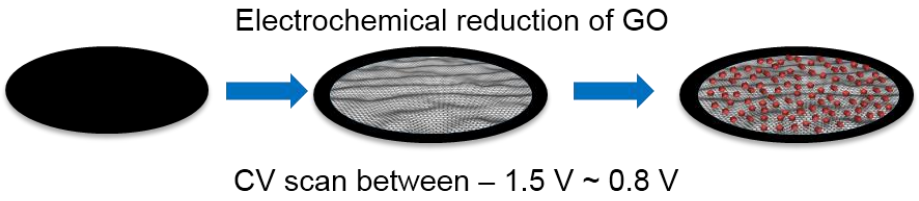

Figure 3. 1 Schematic of preparation of electrochemically deposited graphene/bismuth nanocomposite modified electrode.

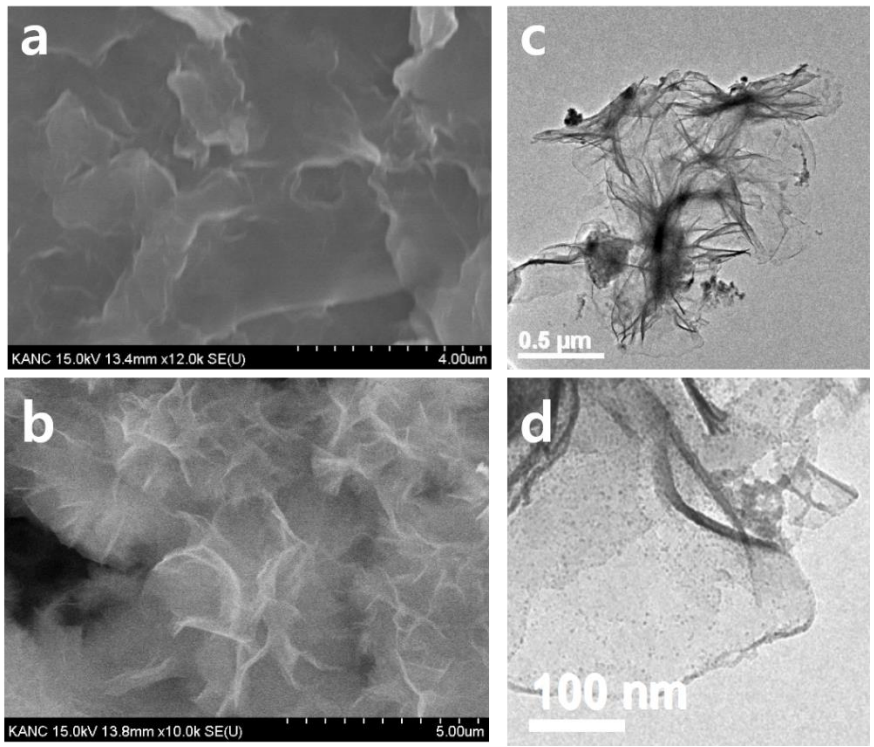

Figure 3. 2 SEM images of (a) GO and (b) EG samples. Also shown are TEM images of EG/Bi composite (c), (d).

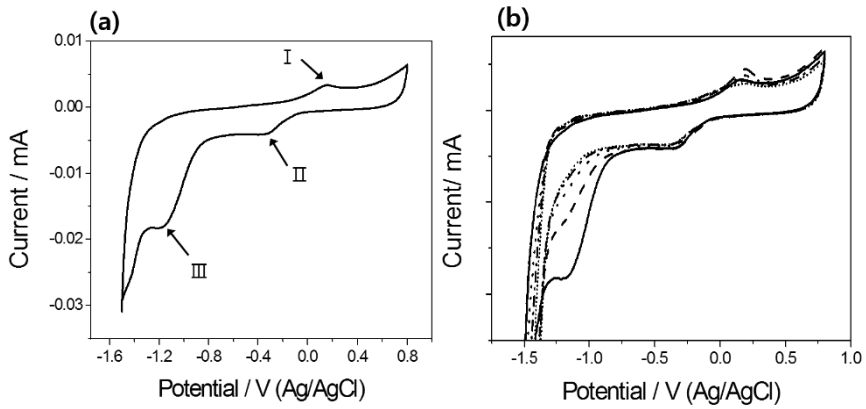

Figure 3. 3 A cyclic voltammogram of GCE in 5 mg ml $^{-1}$ GO

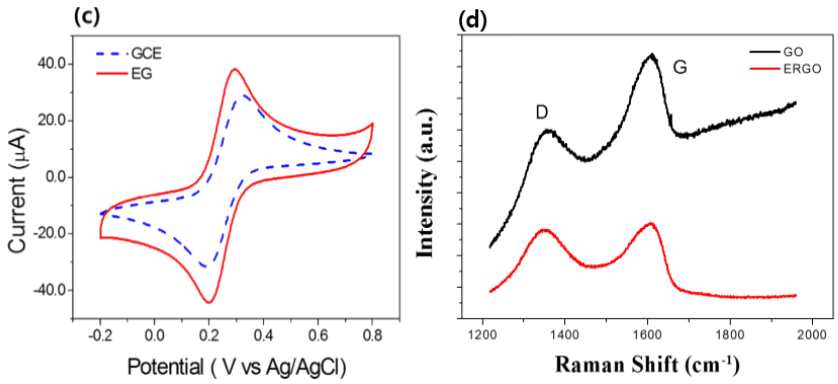

dispersion solution containing 0.1 M PBS (pH 7) at scanning rate of 50 mVs^{-1} (a). CVs for electrochemical reduction of GO on GCE in PBS solution (0.1 M) at a scan rate of 50 mVs^{-1} for five cycles (b). CVs obtained at a bare GCE and EG electrode in 0.1 M KCl solution containing 5 mM $K_3Fe(CN)_6$ + 5 mM $K_4Fe(CN)_6$ at a scan rate of 50 mVs^{-1}(c). Raman spectra of GO and EG (d).

Electrode substrate	Measurement technique	Detection range	Detection limit			Ref.
			Zn^{2+}	Cd^{2+}	Pb^{2+}	
Bi/CNT/GCE	SWASV	20 - 100	12.0	0.70	1.30	[8d]
Bi/CNT/SPE	SWASV	2 - 100	-	0.80	0.20	[17]
Bi/Graphene/MWCNT/GCE	DPASV	5 - 30	-	0.1	0.2	[18]
Bi/Nafion/Graphene/GCE	DPASV	0.5 - 50	-	0.02	0.02	[19]
Bi/EG/PG	SWASV	10 - 100	0.26	0.10	0.16	[20]
Bi/EG/SPE	SWASV	1 - 60	-	0.5	0.8	[21]
Bi/EG/GCE	DPASV	1 - 100	1.80	0.18	0.11	This work

*Bi: bismuth, CNT: carbon nano tube, DPASV: Differential pulse adsorptive stripping voltammetry, EG: electrochemically deposited graphene, GCE: glassy carbon electrode, MWCNT: multiwalled carbon nanotube, PG: pencil-graphite, SPE: screen - printed electrode, SWASV: square wave anodic stripping.

Table 3. 1 Comparison of the electrodes modified with EG/GCE and other materials for the detection of heavy metals.

Added	Found (μg L^{-1})[a]			Recovery (%)[b]			Found by ICP-MS[a]		
(μg L^{-1})	Zn^{2+}	Cd^{2+}	Pb^{2+}	Zn^{2+}	Cd^{2+}	Pb^{2+}	Zn^{2+}	Cd^{2+}	Pb^{2+}
5	4.7 ± 0.3	4.8 ± 0.4	4.2 ± 0.2	94.4	96.3	84.6	4.5 ± 0.1	4.2 ± 0.4	3.6 ± 0.4
10	9.5 ± 0.3	9.3 ± 0.6	9.1 ± 0.4	95.3	93.6	91.4	9.4 ± 0.2	8.7 ± 0.4	7.4 ± 0.5
15	4.6 ± 0.2	14.1 ± 0.3	12.9 ± 0.4	97.3	94.2	86.2	14.5 ± 0.5	14.7 ± 0.3	12.6 ± 0.3
20	9.6 ± 0.5	18.7 ± 0.4	17.2 ± 0.6	98.3	93.5	86.3	19.6 ± 0.3	18.2 ± 0.5	17.2 ± 0.2

[a] Mean of three repetitive measurements at a 95 % confidence level

[b] Mean ± standard deviation %

Table 3. 2 Results for the determination of trace heavy metal ions in tap water samples.

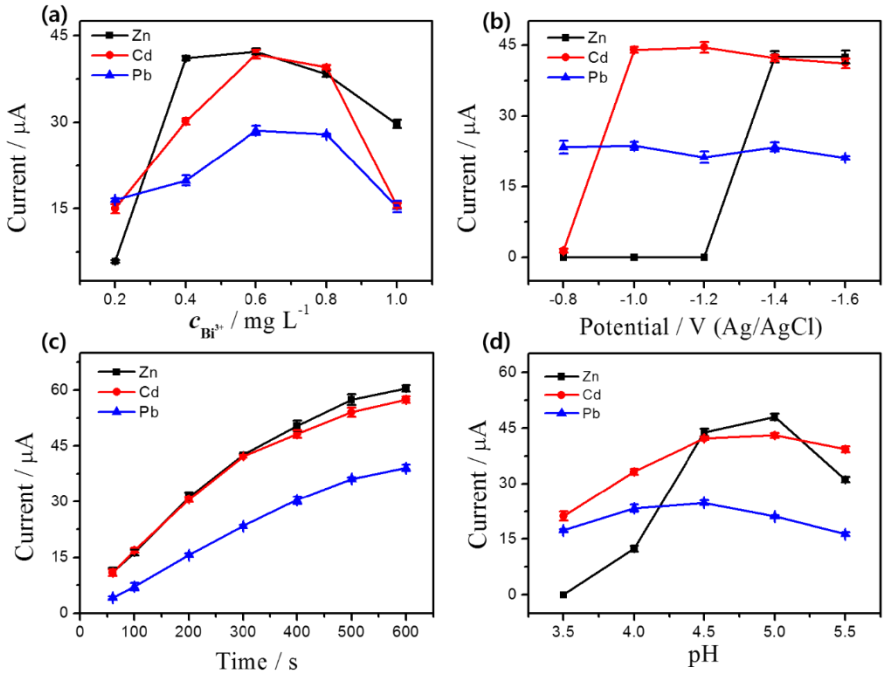

Figure 3. 4 The effect of (a) bismuth concentration, (b) deposition potential, (c) deposition time, and (d) pH value on the stripping peak current of 40 μg L^{-1} each of Zn^{2+}, Cd^{2+} and Pb^{2+} on an *in situ* plated EG/Bi composite film coated electrode in solution. Error bar: *n*=3.

3.3 Results and Discussion

3.3.1 Characterization of EG/Bi Composite

The preparation of electrochemically deposited graphene (EG)/bismuth nanocomposite modified electrode is illustrated in Figure 3.1. The prepared EG was characterized first by SEM and TEM. Figure 3.2 (a) and (b) shows the SEM image of GO and EG obtained by electrodeposition. Figure 3.2 (b) reveals a wrinkled texture associated with the presence of flexible graphene sheets. TEM images of the EG/Bi composite are shown in Figure 3.2 (c) and (d). From the TEM images, it can be seen that the morphologies and the structure of the EG/Bi composite were well formed.

3.3.2 Electrochemical Characterization

Figure 3.3 (a) and (b) show the cyclic voltammograms of GO electrolysis on GCE, where one anodic peak (I) and two cathodic peaks (II and III) are observed during the process. Repetitive cyclic voltammograms were obtained from the direct electrochemical

deposition of EG by reducing a GO colloidal solution (5 mg ml^{-1}) synthesized with the modified Hummers' method. The CV curve of GO on the GCE in 0.1 M PBS (pH 7) electrolyte solution was obtained by potential cycling between 0.8 V and –1.5V. Figure 3.3 (a) shows a cathodic current at –1.15 V with an observed onset at –0.8 V. The reduction current was clearly larger in these first cycles, with the wave attributed to the reduction of the hydroxyl and epoxy groups on the GO sheet. The CV curves in Figure 3.3 (b) prove that the electrodeposited graphene-modified GCE only exhibits peaks I and II, while peak III at –1.15 V decreases rapidly over five cycles. Therefore, cathodic peak III was attributed to the irreversible electrochemical reduction of GO, and as a result, the modified graphene electrode from GO was very stable and insoluble in aqueous solvents [15d, 16d]. The redox probe $Fe(CN)_6^{3-/4-}$, which is sensitive to surface chemistry of carbon-based electrodes [22], and was used to investigate the bare GCE and EG/GCE shown in Figure 3.3 (c). The current response of EG/GCE toward $Fe(CN)_6^{3-4-}$ was increase in both cathodic and anodic peak currents suggesting that the electrochemical active sites of GCE increased by EG surface modification [23]. Moreover, the narrowed the anodic–to-cathodic

peak separation (⊿Ep) for EG/GCE was lower than that bare GCE suggests the improved electron transfer kinetics by EG (⊿Ep = 95 mV), which ascribed to the reactive edge defects on graphene [24]. Therefore, EG/GCE was attributed to the higher conductivity, electroactivity, and faster electron transfer of graphene [15a]. Raman spectroscopy is an effective tool to characterize the structural change of GO after reduction. Raman spectra of GO and the EG are shown in Figure 3.3 (d). Both GO and EG exhibit G and D bands. It is well known that changes in the relative intensities of the D and G band (I_D/I_G) indicate changes in the electronic conjugation state of GO during reduction. In this study, the I_D/I_G ratio of 0.75 for GO is increased to 0.83 in EG, suggesting that smaller sp^2 domains are formed upon reduction of the exfoliated GO. GO also displays peaks at ~1357 cm^{-1} and 1610 cm^{-1}, corresponding to D and G modes, respectively. Following the electrochemical reduction of GO, the G band was found to have shifted from 1610 to 1605 cm^{-1}, indicating that electrochemical reduction of GO does occur.

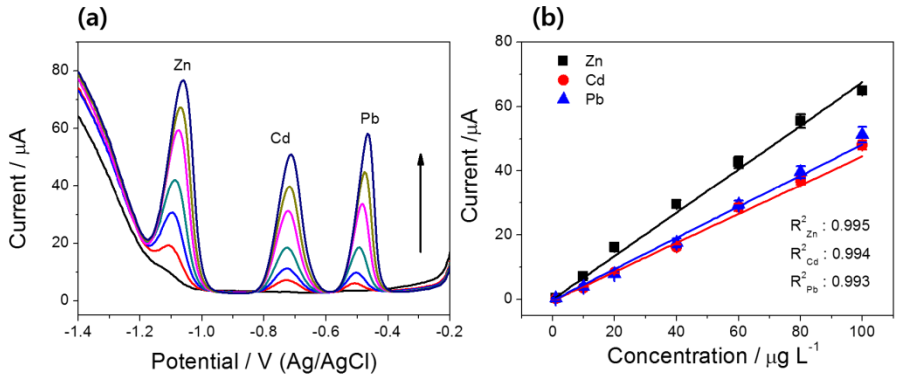

Figure 3. 5 (a) Stripping voltammograms for various concentrations(1, 10, 20, 40, 60, 80, 100 μg L^{-1} from bottom to top) of Zn^{2+}, Cd^{2+} and Pb^{2+} ions on the EG/Bi composite film electrode. (b) The calibration curves for the simultaneous analysis of Zn^{2+}, Cd^{2+} and Pb^{2+}. Error bar : *n*=3.

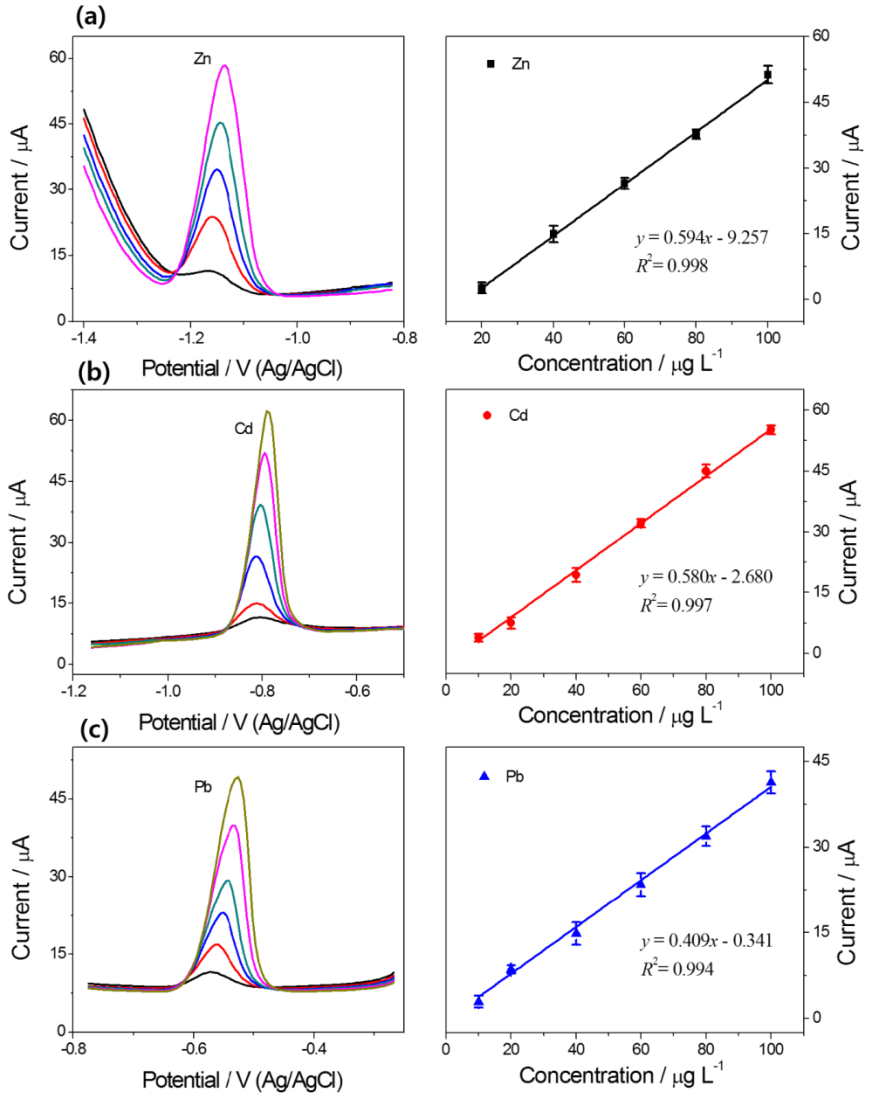

Figure 3. 6 Differential pulse anodic stripping voltammetry (left part) and corresponding calibration plots (right part) for individual analysis of Zn^{2+} (a), Cd^{2+} (b) and Pb^{2+} (c) obtained at EG/Bi composite film electrode. Error bar: n=3.

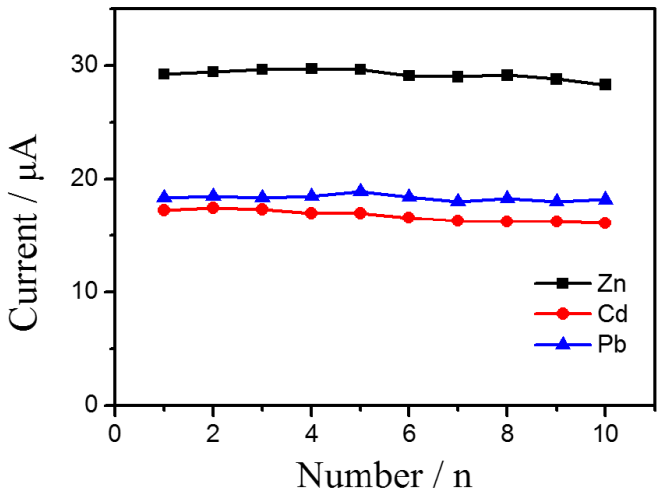

Figure 3. 7 The stability of 10 repetitive measurements of 40 μg L^{-1} Zn^{2+}, Cd^{2+} and Pb^{2+} on an *in situ* plated EG/Bi composite film coated electrode in solution.

Interference inos	Peak current (μA)			Relative signal change (%)		
	Zn^{2+}	Cd^{2+}	Pb^{2+}	Zn^{2+}	Cd^{2+}	Pb^{2+}
No interference ions	29.56	16.24	17.52			
Fe^{3+}	27.47	15.19	16.25	7.60	6.91	7.81
Co^{2+}	28.02	15.58	16.84	5.49	4.23	4.04
Ni^{2+}	27.94	15.24	16.91	5.80	6.56	3.60
Mn^{2+}	28.37	15.36	16.78	4.19	5.72	4.41
Cu^{2+}	28.36	15.29	16.23	4.23	6.21	7.94
Cr^{3+}	28.32	15.37	16.57	4.37	5.66	5.73

Table 3. 3 Effect of interference ions on the detection of 40 μg L^{-1} Zn^{2+}, Cd^{2+} and Pb^{2+}.

3.3.3 Optimization of Experimental Parameters

In order to get the best conditions for the DPASV determination of target metal ions, the different experimental conditions, such as the concentration of Bi^{3+}, deposition potentials, deposition times, and pH values, were optimized with consideration of the sensitivity and peak shape. These experiments were carried out in 0.1 M acetate buffer solution containing 40 μg L^{-1} of Zn^{2+}, Cd^{2+}, and Pb^{2+}.

The concentration of bismuth controlled the thickness of the bismuth film, in turn affecting the electrochemical response of the EG/Bi composite electrode. The influence of the bismuth ion concentration on the stripping signal of Zn^{2+}, Cd^{2+}, and Pb^{2+} was investigated (Figure 3.4 (a)). The peak heights for Zn^{2+}, Cd^{2+}, and Pb^{2+} increased with increasing bismuth concentration from 0.2 mg L^{-1} to 0.6 mg L^{-1} and decreased above 0.6 mg L^{-1}. Accordingly, the optimized concentration of bismuth was chosen as 0.6 mg L^{-1}.

The effect of the deposition potential on peak current of heavy metal ions was investigated in the potential range from −1.6 V to –0.6 V and the stripping current of the metal ions was obtained (Figure 3.4 (b)). As the deposition potential became more negative, the peak

currents of Cd^{2+} and Zn^{2+} increased up to –1.4 V, with no significant increase in the peak current of Pb^{2+}. The maximal peak height could be indicated at –1.0 V for lead and –1.4 V for Cd^{2+} and Zn^{2+} due to preferential reduction and deposition of metal ions at the electrode surface. Thus, a deposition potential of −1.4 V was considered optimal to achieve good sensitivity for all three heavy metal ions.

As shown in Figure 3.4 (c), the influence of the deposition time was studied over time intervals from 60 to 600 s. The peak currents increased linearly with prolonged deposition time. However, the slope of the curved plot tended to diminish for values up to 300 s due to the saturation effect of the bismuth film. Thus, 300 s was chosen to be the optimal pre-concentration deposition time.

The effect of pH on the stripping peak current was studied in 0.1 M acetate buffer solution, with pH values ranging from 3.5 to 5.5 (Figure 3.4 (d)). The best signals for Cd^{2+} and Pb^{2+} were observed at mildly acidic pH 4.5. In the case of Zn^{2+}, the highest peak current was observed at pH 5.0. To obtain good sensitivity for the target metal ions, pH 4.5 was used as the optimal pH value for subsequent experiments. The decrease of the peak current at lower pH can be attributed to protonation of graphene. At higher pH, the decrease in

the peak current is possibly due to formation of metal hydroxide complexes [17, 25].

3.3.4 Analytical Performance

The analytical performance of the EG/Bi composite electrode was investigated by simultaneous analysis of Zn^{2+}, Cd^{2+}, and Pb^{2+} concentrations from 1 µgL^{-1} to 100 µgL^{-1} in 0.1 M acetate buffer containing 0.6 mg L^{-1} Bi^{3+} solutions. The DPASV response for different concentrations of heavy metal ions is illustrated in Figure 3.5 (a). The peak currents were increased, with positive shifts of leak potentials, when concentrations of heavy metal ions were increased. This was due to the IR drop since the oxidation of metals became less reversible. Figure 3.5 (b) shows that the DPASV response and the resulting calibration plots are linear over the range 1 - 100 µg L^{-1} for Zn^{2+}, Cd^{2+}, and Pb^{2+}. The DPASV peak currents were obtained with correction to the base line, and then the calibration plots were evaluated from the peak currents. The corresponding calibration plots and correlation coefficients are $y = 0.676x - 0.085$ and $R^2 = 0.993$ for Zn^{2+}, $y = 0.450x - 0.4807$ and $R^2 = 0.994$ for Cd^{2+}, and $y = 0.490x -$

0.324 and R^2 = 0.993 for Pb^{2+} (*x*: concentration (μg L^{-1}), *y*: current (μA)), based on three times of the background noise (*S/N*=3). For comparison, the individual analysis of heavy metal ions was performed at conditions shown in Figure 3.6. The corresponding calibration plots and correlation coefficients are $y = 0.594x - 9.257$ and R = 0.998 for Zn^{2+}, $y = 0.580x - 2.680$ and R = 0.997 for Cd^{2+}, and $y = 0.409x - 0.341$ and R = 0.994 for Pb^{2+} (*x*: concentration (μg L^{-1}), *y*: current (μA)). From the calibration curves in Fig. 5 and 6, the detection limits of the metal ions were determined based on three times the background noise. The limits of detection were 1.80 μg L^{-1} for Zn^{2+}, 0.18 μg L^{-1} for Cd^{2+}, and 0.11 μg L^{-1} for Pb^{2+} for simultaneous analysis. In the case of individual analysis, the limits of detection were 2.05 μg L^{-1} for Zn^{2+}, 0.14 μg L^{-1} for Cd^{2+}, and 0.13 μg L^{-1} for Pb^{2+}.

The heavy metal ion detection performance of the EG/Bi composite sensor was compared with other reported Bi-modified electrodes (Table 3.1). The results show that EG/Bi exhibits a comparable performance for simultaneous determination of three heavy metal ions, nevertheless the EG-modified electrode is cost-efficient and easily fabricated.

A series of repetitive DPASV response measurements for 40 μg L^{-1} heavy metal ions in 0.1 M acetate buffer solution were performed to further evaluate the stability of the EG/Bi composite electrode. As shown in Figure 3.7, highly reproducible stripping currents were observed, with a relative standard deviation (RSD) of 1.48 % for Zn^{2+}, 3.11 % for Cd^{2+}, and 1.42 % for Pb^{2+}. Therefore, the EG/Bi composite electrode has an excellent stability for repetitive DPASV measurements.

3.3.5 Application to Real Environments

For the purposes of practical application, local tap water samples were collected and analyzed for trace heavy metal ions using the EG/Bi composite electrode. Different concentrations of trace heavy metal ions were added to the tap water and each sample analyzed three times. The mean recoveries (% ± SD) of the method were calculated, and are summarized in Table 3.2. These results were compared with those obtained using ICP-MS. The target metal ion concentrations were in close agreement with the results obtained with ICP-MS, demonstrating the potential for EG/Bi composite electrodes

for analysis of trace heavy metals in real samples

3.3.6 Interference Study

The interference study was performed by adding various potentially interfering metal cations including Fe (III), Co (II), Ni (II), Mn (II), Cu (II), and Cr (III) in 50 fold excess with target metal ions into a standard solution containing 40 μg L^{-1} Zn^{2+}, Cd^{2+} and Pb^{2+} under the optimized working conditions. The results obtained are lists currents of target metal ions in the absence (I_0) and presence (I_i) of interfering metal ions and the relative signal changes, I_i/I_0 −1, are shown in Table 3.3. We can see that most substance had little interference on the signal of 40 μg L^{-1}. The absolute values of relative signal changes were varied from 3.60 % to 7.94 %, which indicates a satisfying selectivity for the simultaneous determination of trace heavy metal ions.

3.4 Conclusion

An enhanced sensing platform, based on the direct electrochemical reduction of GO colloidal solution at glassy carbon electrodes, has been developed for the determination of zinc, cadmium, and lead by DPASV. The electrochemically deposited graphene/bismuth nanocomposite film-modified glassy carbon electrode exhibited high, sharp peaks for heavy metal ions, showing improved detection limits over other bismuth-modified electrodes, by incorporating the beneficial properties of EG (enhanced electron transfer, huge specific surface area, good conductivity, etc.) and good stripping character of bismuth. The synthetic strategy described in this work has several advantages. First, this method can be used to control film thickness quantitatively and form a stable film on the electrode surface without any further treatment; therefor, this would be a straightforward way to integrate EG film and EG/Bi composite electrode. Second, environmentally friendly electrochemical method has been demonstrated. A “green synthesis” of graphene film electrode under mild conditions has used. Third, this strategy provides easy and fast. We show that graphene films can be prepared on electrodes directly

from GO dispersions by one step electrodeposition. Finally, we reported that the sensor was successfully applied to the simultaneous and individual determination of target metal ions in concentrations ranging from 10 to 100 μg L^{-1}. In the best case, the detection limits of simultaneous analyses were 1.93 for Zn^{2+}, 0.16 for Cd^{2+}, and 0.09 for Pb^{2+}. Additionally, this green preparation method, being simple, fast, and free of chemical-reduction reagents, offers several advantages over other graphene fabrication techniques and expands the scope of graphene-based electrochemical sensing devices, with promise for wider applications in environmental analysis.

References

[1] a) Vallee, B. L.; Ulmer, D. D. *Annual Review of Biochemistry* **1972**, *41*, 91. b) Hynes, M. J.; Jonson, B. *Chemical Society Reviews* **1997**, *26*, 133. c) Paoliello, M. M. B.; De Capitani, E. M. *Environmental Research* **2007**, *103*, 288.

[2] Aragay, G.; Pons, J.; Merkoçi, A. *Chemical Reviews* **2011**, *111*, 3433.

[3] Pohl, P. *TRAC Trends in Analytical Chemistry* **2009**, *28*, 117.

[4] Caroli, S.; Forte, G.; Iamiceli, A. L.; Galoppi, B. *Talanta* **1999**, *50*, 327.

[5] a) Vydra, F.; Stulík, K.; Juláková, E.; Tyson, J. *Electrochemical stripping analysis*, Ellis Horwood Chichester **1976**. b) Wang, J. *Electroanalysis* **2005**, *17*, 1341.

[6] Florence, T. M. *Journal of Electroanalytical Chemistry and Interfacial Electrochemistry* **1970**, *27*, 273.

[7] a) Wang, J.; Lu, J.; Hocevar, S. B.; Farias, P. A.; Ogorevc, B. *Analytical chemistry* **2000**, *72*, 3218. b) Arduini, F.; Calvo, J. Q.; Palleschi, G.; Moscone, D.; Amine, A. *TRAC Trends in Analytical Chemistry* **2010**, *29*, 1295. c) Kefala, G.; Economou, A.; Voulgaropoulos, A.; Sofoniou, M. *Talanta* **2003**, *61*, 603.

[8] a) Xu, H.; Zeng, L.; Xing, S.; Xian, Y.; Shi, G.; Jin, L. *Electroanalysis* **2008**, *20*, 2655. b) Ding, L.; Liu, Y.; Zhai, J.; Bond, A. M.; Zhang, J. *Electroanalysis* **2014**, *26*, 121. c) Zhu, L.; Tian, C.; Yang, R.; Zhai, J. *Electroanalysis* **2008**, *20*, 527. d) Hwang, G. H.; Han, W. K.; Park, J. S.; Kang, S. G. *Talanta* **2008**, *76*, 301. e) Chen, L.; Su, Z.; He, X.; Liu, Y.; Qin, C.; Zhou, Y.; Li, Z.; Wang, L.; Xie, Q.; Yao, S. *Electrochemistry Communications* **2012**, *15*, 34. f) Yi, W. J.; Li, Y.; Ran, G.; Luo, H. Q.; Li, N. B. *Sensors and Actuators B: Chemical* **2012**, *166*, 544. g) Wei, Y.;

Yang, R.; Yu, X.-Y.; Wang, L.; Liu, J.-H.; Huang, X.-J. *Analyst* **2012**, *137*, 2183.

[9] a) Katsnelson, M. I. *Mater. Today* **2007**, *10*, 20. b) Zhu, Y.; Murali, S.; Cai, W.; Li, X.; Suk, J. W.; Potts, J. R.; Ruoff, R. S. *Advanced Materials* **2010**, *22*, 3906.

[10] a) Wu, S.; He, Q.; Tan, C.; Wang, Y.; Zhang, H. *Small* **2013**, *9*, 1160. b) Pumera, M.; Ambrosi, A.; Bonanni, A.; Chng, E. L. K.; Poh, H. L. *TRAC Trends in Analytical Chemistry* **2010**, *29*, 954. c) Shao, Y.; Wang, J.; Wu, H.; Liu, J.; Aksay, I. A.; Lin, Y. *Electroanalysis* **2010**, *22*, 1027.

[11] Novoselov, K. S.; Geim, A. K.; Morozov, S.; Jiang, D.; Zhang, Y.; Dubonos, S.; Grigorieva, I.; Firsov, A. *Science* **2004**, *306*, 666.

[12] Dato, A.; Radmilovic, V.; Lee, Z.; Phillips, J.; Frenklach, M. *Nano Letters* **2008**, *8*, 2012.

[13] Reina, A.; Jia, X.; Ho, J.; Nezich, D.; Son, H.; Bulovic, V.; Dresselhaus, M. S.; Kong, J. *Nano Letters* **2008**, *9*, 30.

[14] a) Stankovich, S.; Dikin, D. A.; Piner, R. D.; Kohlhaas, K. A.; Kleinhammes, A.; Jia, Y.; Wu, Y.; Nguyen, S. T.; Ruoff, R. S. *Carbon* **2007**, *45*, 1558. b) McAllister, M. J.; Li, J.-L.; Adamson, D. H.; Schniepp, H. C.; Abdala, A. A.; Liu, J.; Herrera-Alonso, M.; Milius, D. L.; Car, R.; Prud'homme, R. K. *Chemistry of Materials* **2007**, *19*, 4396.

[15] a) Guo, S.-X.; Zhao, S.-F.; Bond, A. M.; Zhang, J. *Langmuir* **2012**, *28*, 5275. b) Guo, H.-L.; Wang, X.-F.; Qian, Q.-Y.; Wang, F.-B.; Xia, X.-H. *ACS nano* **2009**, *3*, 2653. c) Zhou, M.; Wang, Y.; Zhai, Y.; Zhai, J.; Ren, W.; Wang, F.; Dong, S. *Chemistry-A European Journal* **2009**, *15*, 6116. d) Chen, K.; Chen, L.; Chen, Y.; Bai, H.; Li, L. *Journal of Materials Chemistry* **2012**, *22*, 20968. e) Liu, C.; Wang, K.; Luo, S.; Tang, Y.; Chen, L. *Small* **2011**, *7*, 1203.

[16] a) Wang, Z.; Zhou, X.; Zhang, J.; Boey, F.; Zhang, H. *The Journal of Physical Chemistry C* **2009**, *113*, 14071. b) Shao, Y.; Wang, J.; Engelhard, M.; Wang, C.; Lin, Y. *Journal of Materials Chemistry* **2010**, *20*, 743. c) Chen, L.; Tang, Y.; Wang, K.; Liu, C.; Luo, S. *Electrochemistry Communications* **2011**, *13*, 133. d) Kauppila, J.; Kunnas, P.; Damlin, P.; Viinikanoja, A.; Kvarnström, C. *Electrochimica Acta* **2013**, *89*, 84.

[17] Wang, Z.; Wang, H.; Zhang, Z.; Liu, G. *Sensors and Actuators B: Chemical* **2014**, *199*, 7.

[18] Huang, H.; Chen, T.; Liu, X.; Ma, H. *Analytica Chimica Acta* **2014**, *852*, 45.

[19] Li, J.; Guo, S.; Zhai, Y.; Wang, E. *Analytica Chimica Acta* **2009**, *649*, 196.

[20] Pokpas, K.; Zbeda, S.; Jahed, N.; Mohamed, N.; Baker, P. G.; Iwuoha, E. I. *Internationl Journal of Electrochemistry Science* **2014**, *9*, 736.

[21] Ping, J.; Wang, Y.; Wu, J.; Ying, Y. *Food Chemistry* **2014**, *151*, 65.

[22] Chen, P.; McCreery, R. L. *Analytical Chemistry* **1996**, *68*, 3958.

[23] Wang, D.-W.; Gentle, I. R.; Lu, G. Q. *Electrochemistry Communications* **2010**, *12*, 1423.

[24] a) Kampouris, D. K.; Banks, C. E. *Chemical Communications* **2010**, *46*, 8986. b) Brownson, D. A. C.; Banks, C. E. *Analyst* **2010**, *135*, 2768.

[25] Lv, M.; Wang, X.; Li, J.; Yang, X.; Zhang, C. a.; Yang, J.; Hu, H. *Electrochimica Acta* **2013**, *108*, 412.

Chapter 4. Iron oxide/Graphene/Bismuth Nanocomposite for Electrochemical Detection of Heavy Metal Ions

4.1 Introduction

Certain heavy metals such as iron, copper, manganese, and zinc in small quantities are nutritionally essential for a healthy life. However, some heavy metals show a tendency to bind with ligands of biological matter containing nitrogen, sulfur, and oxygen. Accordingly, even low concentrations of some heavy metal ions can cause serious health problems such as those affecting the central nervous system (Hg^{2+}, Pb^{2+}, As^{3+}); the kidneys or liver (Cu^{2+}, Cd^{2+}, Hg^{2+}, Pb^{2+}); or skin, bones, or teeth (Ni^{2+}, Cu^{2+}, Cd^{2+}, Cr^{2+}). The pollution caused by toxic heavy metals has drawn extensive attention worldwide. Although heavy metals can progressively accumulate through the food chain, they are readily excreted [1a, 1b, 2, 26]. Therefore, it is necessary to develop highly sensitive, rapid, and simple methods for the detection of these pollutants. At present, many analytical

methods, such as inductively coupled plasma mass spectrometry (ICP-MS) [27], atomic absorption spectroscopy [28], and flame atomic absorption spectrometry (FAAS) [29], are used to detect trace heavy metal ions. These methods usually require analytical techniques performed by skilled personnel and require expensive instruments. Many efforts are ongoing to develop a simple and rapid technique for trace-heavy-metal detection. Electrochemical methods have attracted extensive attention as an alternative to spectroscopic techniques because they offer advantages of quick analysis speed, simple instrumentation, low cost, and high sensitivity [30]. Anodic stripping voltammetry (ASV) has been extensively used to analyze trace metal ions due to an effective preconcentration step prior to the stripping measurements [7a]. Mercury-based electrodes are commonly used for AVS due to the unique ability of mercury to preconcentrate heavy metals [31]. However, because of its serious toxicity and difficult handling, new and more environmentally friendly mercury-free electrodes have replaced this electrode. Bismuth is a very attractive alternative material due to its comparable performance to mercury for electrochemical analysis. Moreover, the advantageous properties of bismuth are attributed to its ability to form a “fused alloy” with heavy

metals. Recently, there has been considerable interest in the study of bismuth-modified electrodes to improve the sensitivity of electrochemical detection methods [5b, 7a, 7c, 8f, 10b, 32]. A common approach is to incorporate carbon materials, including carbon nanotubes and graphene [8a, 8c, 8d, 30b, 33]. Moreover, graphene, a one-atom-thick planar sheet of sp^2-bonded carbon atoms, is a novel and fascinating carbon material due to its unique thermal, mechanical, and electrochemical properties. Graphene also has a larger specific surface area than other carbon-based materials, and this combination of physical properties enables graphene's application in a wide range of technological fields such as nanoelectronic devices, capacitors, and sensors [9b, 10]. The integration of nanoparticles and graphene has been reported by many researchers via various methods. Their enhanced properties provide wide applications, for example, in catalysis, biomedical fields, and energy storage [34].

Recently, the magnetic nanoparticle/graphene nanocomposite has attracted increasing interest because of its stability, large surface area, and catalytic activity. Thus, the magnetic nanoparticle/graphene composite is used in many applications such as a contrast agent for magnetic resonance imaging, magnetic separation, targeted drug

delivery, wastewater treatments, and energy storage [35]. However, magnetic nanoparticle/graphene composites have not been widely investigated for application in electrochemical sensing [36].

We recently reported a solventless thermal decomposition method to prepare iron oxide/graphene nanocomposites for application as lithium-ion battery anodes [37]. This method was simple, cheap, and scalable for mass production. It can be easily prepared by a simple heat treatment using a mixture of an iron–oleate precursor and graphene. After characterizing the as-prepared nanocomposite and confirming the stable formation of iron oxide nanoparticles on graphene, we modified a glassy carbon electrode (GCE) as an electrochemical sensing platform for sensitive and selective analysis of heavy metal ions. The experimental results indicated that this electrode exhibited a better electrochemical performance and higher electrocatalytic behavior response to heavy metal ions. Finally, this simple, low-cost, and highly sensitive sensor was used to determine the amounts of Zn^{2+}, Cd^{2+}, and Pb^{2+} in real samples.

4.2 Experimental Section

4.2.1 Chemicals

All reagents were analytical grade and used as received without further purification. Graphite powder (<20 μm), sodium acetate, acetic acid, iron(III) acetylacetonate ($Fe(acac)_3$) and oleic acid were purchased from Sigma-Aldrich (USA). Standard solutions of Bi^{3+}, Zn^{2+}, Cd^{2+}, and Pb^{2+} (1000 mg L^{-1}) were obtained from Sigma-Aldrich and diluted as required. Acetate (Ac) buffer solutions (HAc-NaAc, 0.1 M) with different pH values were prepared by mixing stock solutions of 0.1 M HAc and 0.1 M NaAc. All solutions were prepared with doubly-distilled water.

4.2.2 Characterization Methods

Transmission electron microscopy (TEM; JEM-3010, JEOL) and field-emission scanning electron microscopy (FE-SEM; JSM-6700F, JEOL) were used to examine the morphologies of the graphene and iron oxide/graphene (Fe_2O_3/G) composite. X-ray diffraction (XRD)

analysis was performed using a Rigaku Dmax 2500 diffractometer. The carbon content was revealed by thermos-gravimetric analysis (TGA) measurements, with a TA Instruments Q-5000 IR model at 20–700 ℃ and a heating rate of 10 ℃ min^{-1} in air flux.

4.2.3 Apparatus

Electrochemical experiments were performed with an Autolab potentiostat (Metrohm, USA). A modified GCE (3 mm in diameter, Bioanalytical Systems, Inc.) served as the working electrode, with the Ag/AgCl electrode (Bioanalytical Systems, Inc.) and platinum wire acting as a reference and a counter electrode, respectively.

4.2.4 Preparation of Reduced Graphene Oxide (RGO)

Graphene oxide (GO) was prepared from graphite powder (Aldrich, <20 micron) by an imorived Hummers method. Graphene was obtained by a thermal expansion of the GO under high vacuum. The GO was put into a round flask that was sealed at one end and the other end was connected to a high vacuum pump. The flask was

rapidly heated under a high vacuum. At about 200 ℃, a dramatic expansion of GO was observed. The final products were kept at 300 ℃ for 5 h.

4.2.5 Preparation of Iron-oxide Nanoparticles (F_2O_3)/Graphene (G) Nanocomposite

Graphene oxide (GO) was prepared from graphite powder by an improved Hummers' method. The as-prepared GO was thermally expanded to synthesize reduced GO by rapid heating to 250 ℃ in a tube furnace (heating rate: 13℃ min^{-1}) and the final product was washed several times with ethanol. Fe_2O_3/G composites were prepared by a solventless method according to a previous report. Briefly, $Fe(acac)_3$ (2 mmol) was mixed with oleic acid (6 mmol). These iron–oleate precursors were mixed in a mortar with 0.2 g of the as-prepared graphene without any solvent. The mixture was heated to 600 ℃ (heating rate: 10 ℃ min^{-1}) and maintained at that temperature for 3 h under a N_2 atmosphere.

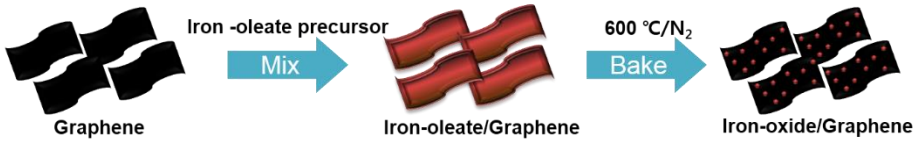

Figure 4. 1 Schematic of preparation of Fe_2O_3/graphene nanocomposite.

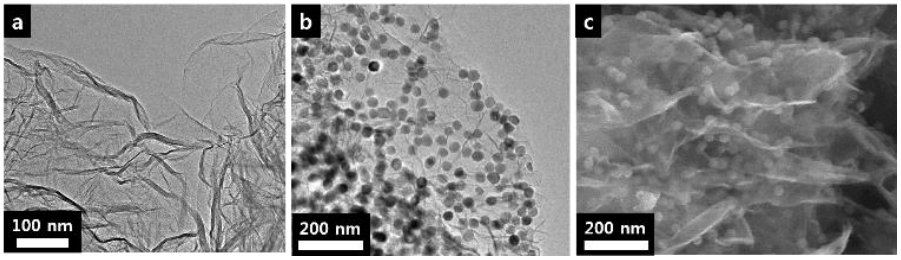

Figure 4. 2 TEM images of RGO (a), Fe_2O_3/G nanocomposite (b) and SEM image of Fe_2O_3/G nanocomposite (c).

4.2.6 Fabrication of Bismuth-coated Fe_2O_3/G Nanocomposite Modified Electrode

Prior to the modification, the GCE was polished with 1.0, 0.3, and 0.05 μm alumina slurries and then rinsed with doubly distilled water. The cleaned electrode was dried. Fe_2O_3/G (1 mg) was sonicated in a solution containing H_2O (1 mL) and ethanol (3.4 mL) for 10 min to form a homogenous solution. Then, 8 μL of the Fe_2O_3/G solution was added onto the GCE and dried for 5 min under an infrared heat lamp. For comparison, an RGO-modified electrode was fabricated using the same process.

4.2.7 Procedure for Differential Pulse Anodic Stripping Voltammetry Analysis

The Fe_2O_3/G/GCE modified with bismuth was plated *in situ* using the following procedure: the composite modified electrode, Ag/AgCl (3 M KCl), and Pt wire electrodes were immersed in an electrochemical cell containing 0.1 M acetate buffer (pH 4.5) and 0.2 mg L^{-1} of bismuth and the appropriate target metal ions. Differential

pulse anodic stripping voltammetry (DPASV) was used for the detection of trace heavy metals with a deposition potential of −1.4 V for 300 s with stirring. Anodic stripping of the electrodeposited metal was performed in the potential range varying from −1.4 V to −0.3 V under the following conditions: amplitude, 50 mV; pulse width, 50 ms; potential step, 4 mV; and pulse period, 0.2 s. Prior to the next cycle, the electrode was cleaned for 60 s at 0.1 V in a fresh supporting electrolyte with stirring to remove the target metals and bismuth.

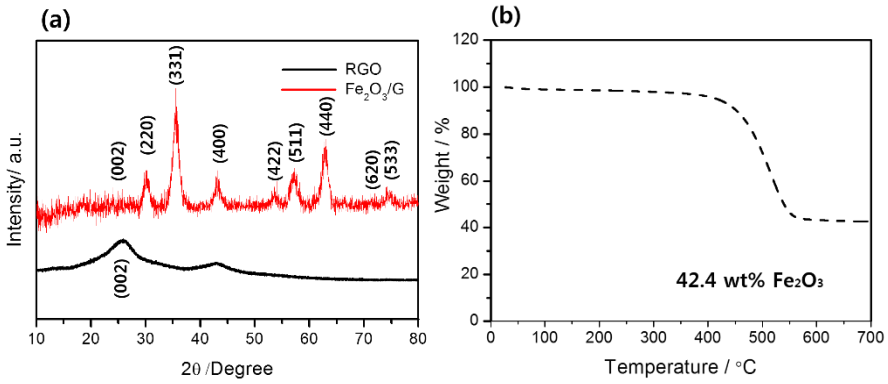

Figure 4. 3 XRD pattern of the RGO, Fe_2O_3/G nanocomposite (a) and TGA result of the Fe_2O_3/G nanocomposite (b).

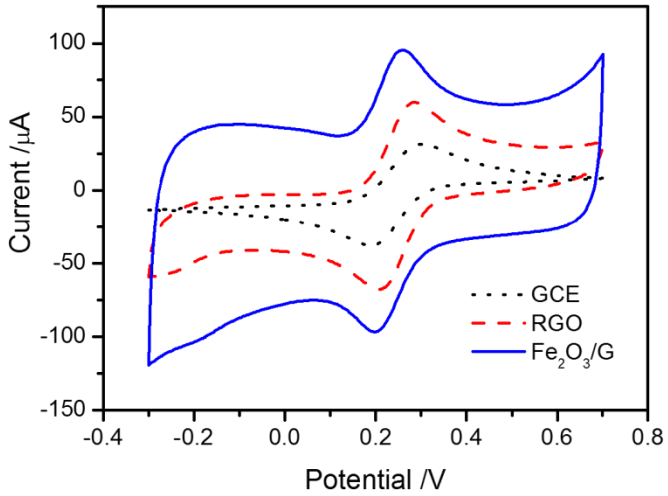

Figure 4. 4 CV curves of the bare GCE, and RGO or Fe_2O_3/G composite modified electrode in 1 M KCl solution containing 5 mM $Fe(CN)_6^{3-/4-}$; potential scan between 0.8 and −0.2 V; scan rate: 50 mVs^{-1}.

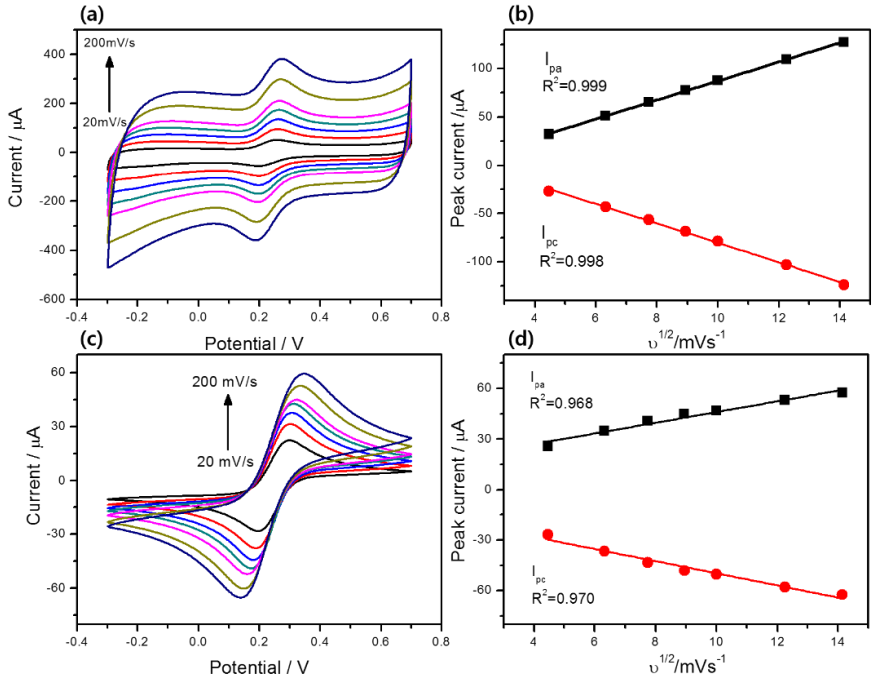

Figure 4. 5 CVs of the Fe_2O_3/G composite modified electrode (a) and bare GCE (c) with different scan rates of 20, 40, 60, 80, 100, 150 and 200 mV s^{-1} in 1 M KCl solution containing 5 mM $Fe(CN)_6^{3-/4-}$. (b and d) Plots of i_{pa} , i_{pc} *vs.* $v^{1/2}$ for the Fe_2O_3/G composite modified electrode (b) and bare GCE (d).

4.3 Results and Discussion

4.3.1 Characterization of Fe_2O_3/G Nanocomposite

The scheme of Fe_2O_3/G nanocomposite, as shown in Figure 4.1, is performed by solventless thermal decomposition method. SEM, TEM, TGA, and XRD were used to characterize the morphology and structure of the as-prepared Fe_2O_3/G composite. Figure 4.2 shows the TEM images and SEM image of RGO and the Fe_2O_3/G composite. Figure 4.2 (a) shows the typical wrinkled and sheet-like character of RGO. Figure 4.2 (b) and (c) show the TEM and SEM images of the Fe_2O_3/G composite, respectively. The images of the Fe_2O_3/G composite shows well-dispersed Fe_2O_3 nanoparticles that uniformly decorated the graphene sheets (average particle size = 30 nm); the folding nature of the graphene sheets is clearly visible. The crystal structures of RGO and the Fe_2O_3/G composite were further characterized by XRD in Figure 4.3 (a). The broad peak correspond to the reflection peak of the RGO. The diffraction peaks in Figure 4.3 (a, red) are consistent with the standard structure of maghemite (JCPDS card No. 39-1346). Due to the high XRD intensity of the iron

oxide nanoparticles and the broad peak of RGO, the peak from RGO is very hard to distinguish in the Fe_2O_3/G composite. The characteristics of thermal decomposition of the Fe_2O_3/G composite were studied by TGA in air atmosphere (Figure 4.3 (b)). The carbon contents of Fe_2O_3/G was measured to be 57.6 wt%.

4.3.2 Electrochemical Characterization

Cyclic voltammetry (CV) was used to investigate the electrochemical behavior of a bare GCE, and the electrodes modified with RGO or Fe_2O_3/G composite with a scan rate of 50 mV s^{-1} in 1 M KCl containing 5 mM $Fe(CN)_6^{3-/4-}$; these CV curves are shown in Figure 4.4. As can be seen, the peak currents obtained at RGO modified electrode (dash) were obviously larger than those at the bare GCE (dot), which were attributed to the fact that the electrochemical active sites of GCE increased by RGO surface modification. Moreover, the peak currents at the Fe_2O_3/G composite modified electrode were significantly larger than those at RGO modified electrode. Such increases could be explained in terms of the electrocatalytic activity and large surface area of Fe_2O_3/G composite.

The effect of scan rate on the Fe_2O_3/G composite modified electrode was investigated. CV experiments were performed at different scan rates using the Fe_2O_3/G composite modified electrode and bare GCE in 1 M KCl containing 5 mM $Fe(CN)_6^{3-/4-}$, respectively. Figure 4.5 (a) and (c) show that the peak currents for the redox reaction increase with the increasing scan rate. The plot of the anodic peak current (I_{pa}) and cathodic peak current (I_{pc}) with respect to the scan rate is shown in Figure 4.5 (b) and (d). Both the I_{pa} and I_{pc} are linearly related with the square root of the scan rate in the range of 20–200 mV s^{-1}.

The linear regression equations of the Fe_2O_3/G composite electrode are $I_{pa}(A) = 9.852 \times 10^{-6} v^{1/2} (mV\ s^{-1})^{1/2} - 1.118 \times 10^{-5}$ ($R^2 = 0.999$) and $I_{pc}(A) = -1.007 \times 10^{-5} v^{1/2} (mV\ s^{-1})^{1/2} - 2.029 \times 10^{-5}$ ($R^2 = 0.998$), respectively. The peak currents of the redox couples are directly proportional to the scan rate, indicating that the redox process occurring at the Fe_2O_3/G composite modified electrode was a surface-confined process.

The electrochemically effective surface area was estimated by cyclic voltammetry using $K_3[Fe(CN)_6]$ as a probe and according to the Randles–Sevcik equation [38]:

$$i_p = 2.69 \times 10^5 n A C_0 D^{1/2} v^{1/2} \quad (1)$$

where D and C_0 are the diffusion coefficient and bulk concentration of the redox probe, respectively. n is the number of electron transfer ($n = 1$), v is the scan rate and A is the effective surface area.

For 5 mM $K_3[Fe(CN)_6]$, $n = 1$, $D = 6.67 \times 10^{-6}$ cm^2 s^{-1}, as computed from eqn (1), the effective surface area of the Fe_2O_3/G composite modified electrode (0.082 cm^2) is nearly 1.86 times as large as that of bare GCE (0.044 cm^2), which enhances the charge transfer kinetics. In addition, the larger electrochemical surface active area is not only useful for enhancing the sensor sensitivity, but also beneficial for lowering the detection limit.

4.3.3 Analytical Performance

The first trial of the experiments is to compare the sensing behavior of Bi toward heavy metal ions. The stripping signals on the Fe_2O_3/G composite and Fe_2O_3/G/Bi composite electrodes were compared using DPASV in a 0.1 M acetate buffer solution (pH 4.5) containing 100 μg L^{-1} of Zn^{2+}, Cd^{2+}, and Pb^{2+} (Figure 4.6 (a)). Two weak stripping peaks from Cd^{2+} and Pb^{2+} were observed only when

the electrolyte did not contain any bismuth, while the peak belonging to Zn^{2+} was not found. In contrast, the stripping currents for target metal ions at the Fe_2O_3/G/Bi composite electrode were further enhanced after the addition of 0.2 mg L^{-1} Bi^{3+} into the solution. This result indicates that bismuth could significantly improve the analytical performance by the formation of a "fused alloy" with the target metals. Thus, the Fe_2O_3/G/Bi composite electrode had improved sensitivity. Figure 4.6 (b) shows the stripping signals of GCE, RGO, and Fe_2O_3/G by *in situ* plating of bismuth for target metal ion determination. The stripping voltammograms were measured under the same conditions as Figure 4.6 (a). The stripping peaks for the heavy metal ions at GCE/Bi were very low, probably due to the poor conductivity at the electrode surface. In contrast, the RGO/Bi modified electrode exhibited a higher stripping response toward the target-metal-ion detection, probably because RGO possesses a good conductivity and a large surface area that can increase the heavy metal loading amounts. The highest stripping peaks were observed at the Fe_2O_3/G/Bi composite electrode. The improvement in the stripping peak currents of the heavy metal ions on the Fe_2O_3/G/Bi composite electrode could be attributed to the

synergetic effects between graphene and the Fe_2O_3 nanoparticles. Graphene had a good electric conductivity, higher area-to-volume ratio, and enhanced electron transfer at the electrode surface. Also, highly monodisperse Fe_2O_3 nanoparticles were in close contact with graphene, and they acted as mutual spacers in the nanocomposite to prevent aggregation of the nanoparticles and restacking of the graphene layers. In addition, the combination of Fe_2O_3 and graphene may provide the necessary conduction pathways on the electrode surface and a better electrochemical behavior. The resulting Fe_2O_3 nanoparticles and graphene composite exhibit a high catalytic activity and contribute to a significantly improved analytical performance [39].

Simultaneous determination of Zn^{2+}, Cd^{2+}, and Pb^{2+} was performed on Fe_2O_3/G/Bi composite electrode using DPASV under the optimum conditions. Figure 4.7 (a) shows the stripping responses for the target metal ions from 0 to 100 µg L^{-1} in 0.1 M acetate buffer containing 0.2 mg L^{-1} Bi^{3+} solution. The peak currents increased with increasing concentrations of heavy metal ions. Figure 4.7 (b) shows that the resulting calibration plots were linear over the range 1–100 µg L^{-1}. The DPASV peak currents were obtained with correction to the base line, and then the calibration curves were evaluated from the peak

currents. The calibration curves were $y = 1.039x - 1.015$ and $R^2 = 0.990$ for Zn^{2+}, $y = 0.938x - 0.590$ and $R^2 = 0.994$ for Cd^{2+}, and $y = 0.731x - 0.476$ and $R^2 = 0.994$ for Pb^{2+} (x: concentration (μg L^{-1}), y: current (μA)), calculated based on six times the background noise ($S/N = 3$). The limit of detection was calculated to be 0.11 μg L^{-1} for Zn^{2+}, 0.08 μg L^{-1} for Cd^{2+}, and 0.07 μg L^{-1} for Pb^{2+}. We also detected the low concentrations of trace heavy metal ions over 0.4 − 8 μg L^{-1}. The stripping currents for low concentrations of heavy metal ions were illustrated in Figure 4.8. The resulting calibration plots for Cd^{2+} and Pb^{2+} were observed to be linear over the 0.4 to 8 μg L^{-1}, but Zn^{2+} was not liner over that range. The equation of calibration curve were $y = 0.265x + 0.003$ and $R^2 = 0.290$ for Zn^{2+}, $y = 0.797x + 0.054$ and $R^2 = 0.906$ for Cd^{2+}, and $y = 0.526x + 0.676$ and $R^2 = 0.945$ for Pb^{2+} (x: concentration (μg L^{-1}), y: current (μA)). The detection limits were calculated based on three times the background noise ($S/N = 3$). We have compared this composite electrode with other modified electrodes, and the results are listed in Table 4.1. The analytical performance of the Fe_2O_3/G/Bi composite electrode is comparable and even better than previous reports.

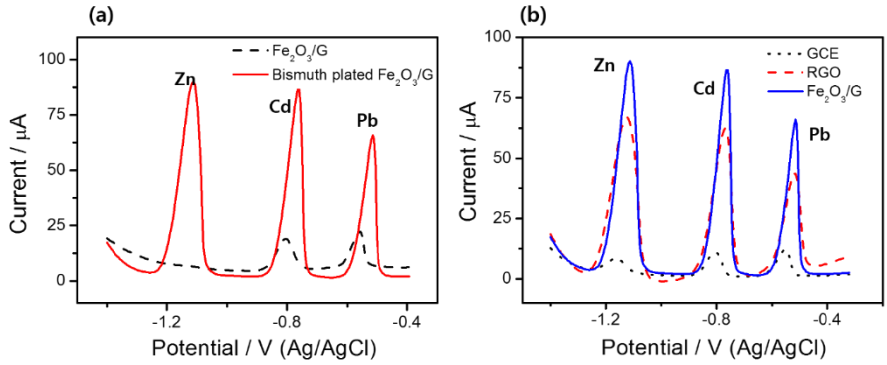

Figure 4. 6 (a) Effect of the presence of bismuth on Fe_2O_3/G nanocomposite modified electrode. (b) DPASV responses at GCE (black), RGO/GCE (red), and Fe_2O_3/G/GCE (blue). The test solution contains 100 µg L^{-1} of each of the target metals and 0.2 mg L^{-1} of Bi^{3+}.

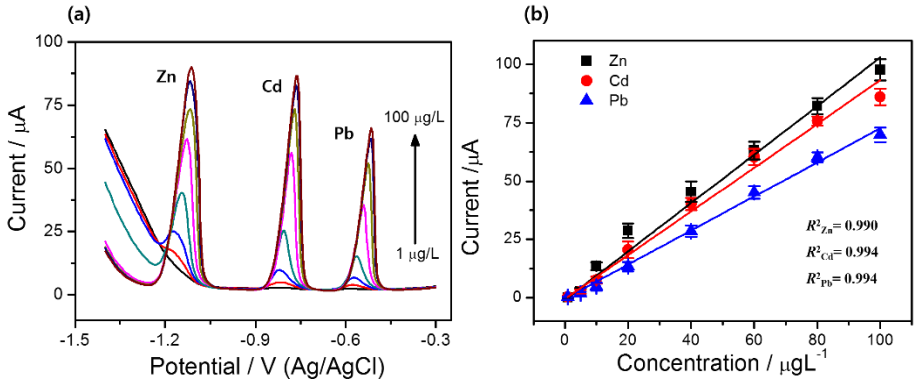

Figure 4. 7 (a) Stripping voltammograms for various concentrations (1, 10, 20, 40, 60, 80, 100 μg L^{-1} from bottom to top) of Zn^{2+}, Cd^{2+} and Pb^{2+} ions on the Fe_2O_3/G/Bi composite film electrode. (b) The calibration curves for the simultaneous analysis of Zn^{2+}, Cd^{2+}, and Pb^{2+}. Error bar: n=6.

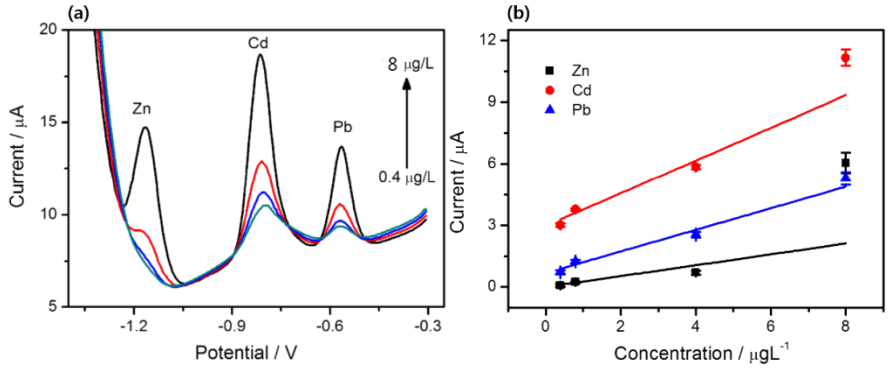

Figure 4. 8 (a) DPASV curves obtained of Zn^{2+}, Cd^{2+} and Pb^{2+} ions for low concentrations (0.4, 0.8, 4, 8 μg L^{-1} from bottom to top) on the Fe_2O_3/G/Bi composite electrode. (b) The corresponding calibration curves. Error bar: n=3.

4.3.4 Optimization of Experimental Parameters

To establish the most suitable experimental conditions for the DPASV measurement of Zn^{2+}, Cd^{2+}, and Pb^{2+} at the Fe_2O_3/G/Bi composite electrode, we optimized the pH, concentration of Bi^{3+}, deposition potential, and deposition time.

The effect of pH on the peak current of trace heavy metal ions in DPASV in the pH range of 3.0–5.5 is shown in Figure 4.9 (a). For Cd^{2+} and Pb^{2+} ions, the stripping peak currents increased by increasing the pH in the range of 3.0–4.5 and decreased at higher pH. In the case of Zn^{2+}, the highest peak current was observed at pH 5.0. The lower pH values resulted in reduction of the peak current due to protonation of hydrophilic groups of the graphene. At higher pH, the peak currents decreased due to the possible formation of metal hydroxide complexes. Thus, the optimum pH value during the measurements was determined to be 4.5.

Figure 4.9 (b) shows the effect of the bismuth concentration on the current response in the range of 0–0.8 mg L^{-1}. The stripping peak currents of the target metal ions displayed a clear dependence on the bismuth thickness. The peak currents increased rapidly with

increasing concentrations of bismuth from 0 to 0.2 mg L^{-1}. However, the stripping currents of the three metal ions decreased when the bismuth concentration was higher than 0.2 mg L^{-1}. This result indicates that a thick bismuth film might hinder the mass transfer of heavy metal ions during the stripping step. Therefore, the optimum concentration of bismuth was selected as 0.2 mg L^{-1} for the simultaneous determination of heavy metal ions.

We also studied the effect of the deposition potential and deposition time, as shown in Figure 4.9 (c) and (d). The deposition potential is a very important factor for improving the sensitivity of the DPASV measurement. The effect of the deposition potential was studied in the potential range varying from −1.8 V to −0.8 V. Figure 4.8 (c) shows that the stripping currents of the target metal ions exhibited a notable increasing trend with negative shifts of the deposition potential. The maximum peak height could be observed at −1.2 V for Cd^{2+} and Pb^{2+}, and at −1.4 V for Zn^{2+}. However, when the accumulation potential was more negative than −1.4 V, the stripping currents reduced because of the hydrogen evolution reaction at more negative potentials, which might damage the metal alloy deposition at the electrode surface. Thus, the deposition potential of −1.4 V was

chosen as the optimum value for the three heavy metals.

Finally, we investigated the effect of the deposition time, as shown in Figure 4.9 (d). The stripping peak currents increased linearly with a prolonged deposition time. However, at a deposition time longer than 300 s, the slope of the curved plot began to diminish, indicating that there was a saturation effect for the bismuth film and the amount of heavy metal ions on the electrode surface. Thus, 300 s was selected as the optimum deposition time.

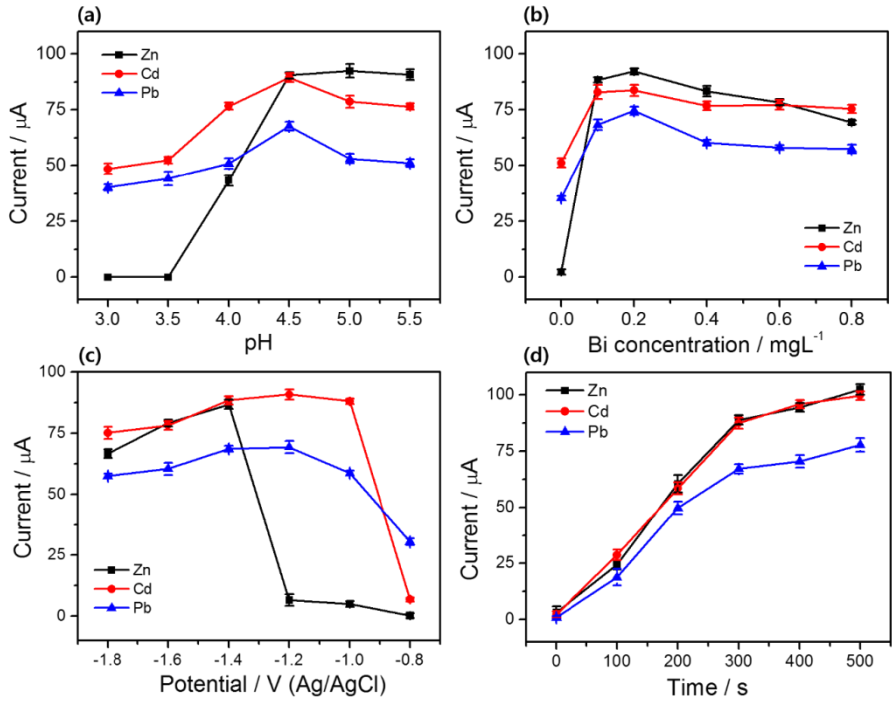

Figure 4. 9 The effects of pH (a), Bi^{3+} concentration (b), deposition potential (c), and deposition time (d) on the stripping peaks current of 100 μg L^{-1} heavy metal ions. Error bar: n=3.

Electrode substrate	Detection range (μgL^{-1})	Limits of detection (μgL^{-1})			Ref.
		Zn^{2+}	Cd^{2+}	Pb^{2+}	
G/AlOOH/GCE	200-800	-	0.03	0.09	[33]
Bi/G/MWCNT/GCE	5 – 30	-	0.10	0.20	[18]
DMSA/Fe_3O_4	1-50	-	-	0.50	[40]
Bi/NA/G/PANI	1-300	1.00	0.10	0.10	[41]
Bi/Au/G/Cys/GCE	0.5-40	-	0.1	0.05	[42]
NA/MgO/GCE	1-6.7		7.21	0.43	[8g]
G/Fe_3O_4/GCE	20 – 40	-	2.68	-	[43]
Fe_3O_4/MWCNT/GCE	1-130	-	-	0.50	[44]
Bi/NA/MWCNT/SPE	0.5-100 (Cd^{2+}; 0.5-80)	0.3	0.1	0.07	[45]
Bi/NA/IL/G/SPCE	0.1-100	0.09 (ngL^{-1})	0.06 (ngL^{-1})	0.08 (ngL^{-1})	[46]
Bi/Fe_2O_3/G/GCE	1-100	0.11	0.08	0.07	This work

Bi: bismuth, Cys: cysteine, DMSA: dimercaptosuccinic acid, G: graphene, GCE: glassy carbon electrode, IL: ionic liquid, MWCNT: multiwalled carbon nanotube, NA: nafion, PANI: polyaniline, SPE: screen-printed electrode, SPCE: screen-printed carbon electrode.

Table 4. 1 Comparison of the electrodes modified with Fe_2O_3/G/GCE and other.

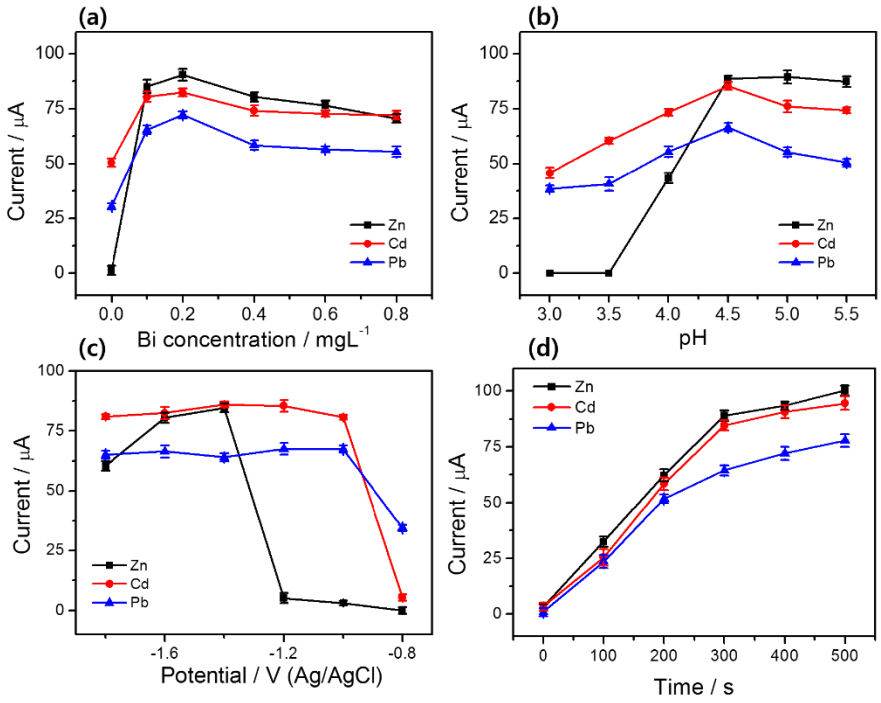

Figure 4. 10 The effects of Bi^{3+} concentration (a), pH (b), deposition potential (c), and deposition time (d) on the stripping peaks current of 100 μg L^{-1} heavy metal ions in tap water sample. Error bar: n=3.

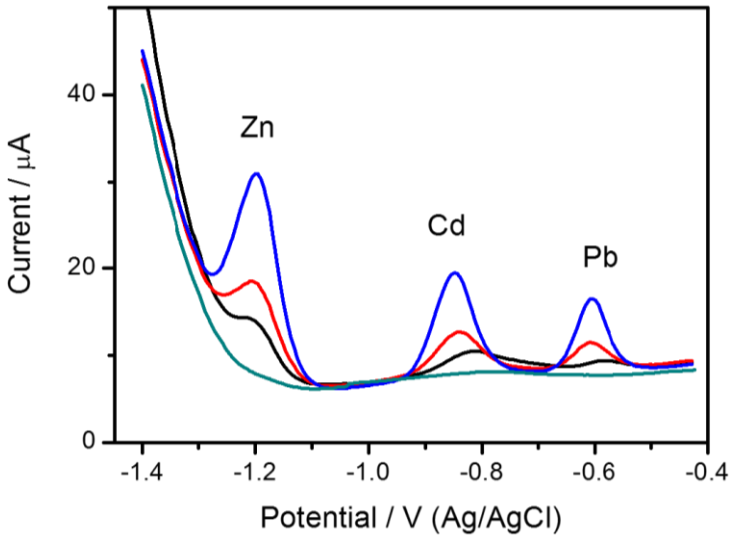

Figure 4. 11 DPASV for the determination of heavy metals in tap water. From below: sample and successive standard additions 5 μg L^{-1} of each of target metals.

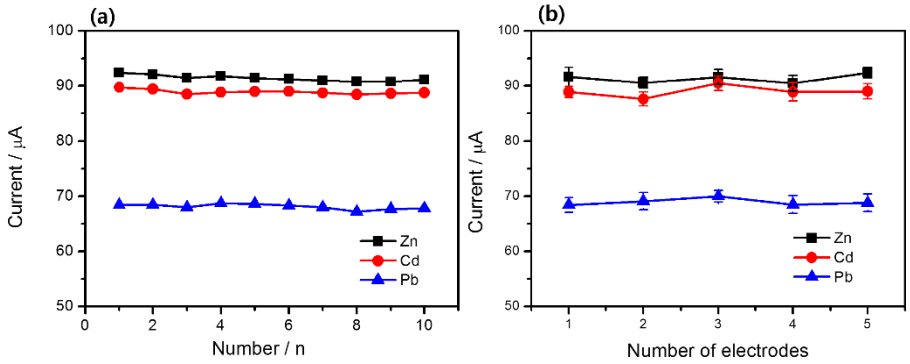

Figure 4. 12 Stripping peak current of target metal ions for repeated measurements (n=10) and different electrode in the solution of 100 μg L^{-1}. Error bar n=3.

4.3.5 Application to Real Environments

The Fe_2O_3/G/Bi composite electrode was applied to determine heavy metal ions in local tap water samples by using a standard addition method to show the practical applications of this method. All water samples were filtered with a 0.22 mm membrane. We optimized the pH, concentration of Bi^{3+}, deposition potential, and deposition time in tap water sample (Figure 4.10 a-d) and performed triplicate measurements of the DPASV response with different concentrations of trace heavy metal ions for the real sample. By comparison with the results shown in Figure 4.9, their values were no significant differences between the results. Figure 4.11 shows representative stripping voltammograms of samples obtained with composite electrode by method of standard additions in the tap water. The mean recoveries (%) of the method were calculated, and are summarized in Table 4.2. The same determinations were performed by ICP-MS. These comparative results suggest that there is satisfactory agreement, demonstrating the potential for the Fe_2O_3/G/Bi composite electrodes for analysis of trace heavy metals in real samples.

4.3.6 Reproducibility of the Fe_2O_3/G/Bi Modified Electrode

The developed electrode was evaluated by repetitive measurements of 100 μg L^{-1} heavy metal ions under optimized working conditions to study its reproducibility. The relative standard deviation from 10 successive measurements using a single electrode was measured and found to be 1.68% for Zn^{2+}, 0.92% for Cd^{2+}, and 1.69% for Pb^{2+}. The currents at same conditions was determined three times using different sensors prepared independently. The relative standard deviation was 0.89% for Zn^{2+}, 1.15% for Cd^{2+}, and 0.91% for Pb^{2+} for 5 different electrodes. The results show that the Fe_2O_3/G/Bi composite electrode has a good reproducibility (Figure 4.12).

4.3.7 Interference Study

The interferences study was performed by adding interfering metal cations, including Co^{2+}, Ni^{2+}, Mn^{2+}, Cu^{2+}, and Cr^{3+}, in 50-fold excess with the analytes to a standard solution containing 40 μg L^{-1} Zn^{2+}, Cd^{2+} and Pb^{2+}. The results of the metal cation toward the target heavy metal ions collected from the DPASV response currents are shown in

Table 3. The peak currents of the heavy metal ions in the absence (I_0) and presence (I_i) of interfering metal ions and the relative signal changes, $I_i/I_0 - 1$, are also summarized. Most substances provided little interference to the 40 μg L^{-1} signal. The absolute values of the relative signal changes varied from 2.31% to 8.46%, which suggests that the Fe_2O_3/G/Bi nanocomposite-modified electrode was not affected by other metal species. A good selectivity for Zn^{2+}, Cd^{2+} and Pb^{2+} is thus demonstrated for the present sensor, which is attributed to the selective transportation of Zn^{2+}, Cd^{2+} and Pb^{2+} from the sample solution to the electrode *via* the stronger affinity of Fe_2O_3/G/Bi composite for these ions [8e, 8g, 41].

4.4 Conclusion

A novel and highly sensitive electrochemical sensor for heavy metal ions determination was fabrication based on graphene supporting Fe_2O_3 nanoparticle composite modified electrode. The Fe_2O_3/G nanocomposite was synthesized from iron–oleate precursor and graphene by a solventless thermal decomposition method. The new nanohybrid material combined the unique electronic behavior of

graphene with the excellent catalytic properties of Fe_2O_3 nanoparticles by a synergistic integration of the two nanomaterials. Finally, the sensor was successfully applied to the simultaneous determination of the target metal ions in concentrations ranging from 1 to 100 µg L^{-1}, and the detection limits of the simultaneous analyses were 0.11 for Zn^{2+}, 0.08 for Cd^{2+}, and 0.07 for Pb^{2+}. Moreover, the Fe_2O_3/G composite modified electrode offered excellent stability in the electrochemical determination of heavy metal ions. In addition, the sensor was applied for the determination of Zn^{2+}, Cd^{2+}, and Pb^{2+} in real samples and the result was consistent with the results by ICP-MS. The proposed method will offer potential application for monitoring of heavy metals and other pollutants in a wide range of electrochemical sensing applications.

Original	Added	Found (µg L^{-1})[a]			Recovery (%)			Found by ICP-MS[a]		
	µg L^{-1}	Zn^{2+}	Cd^{2+}	Pb^{2+}	Zn^{2+}	Cd^{2+}	Pb^{2+}	Zn^{2+}	Cd^{2+}	Pb^{2+}
N.D	5	4.6 ± 0.4	4.3 ± 0.4	4.1 ± 0.4	92.3	86.2	82.6	4.7 ± 0.3	4.4 ± 0.2	4.6 ± 0.6
N.D	10	9.3 ± 0.2	9.2 ± 0.6	8.6 ± 0.6	93.4	92.5	86.6	9.4 ± 0.6	9.4 ± 0.4	9.2 ± 0.7
N.D	15	14.3 ± 0.2	14.1 ± 0.4	12.1 ± 0.5	95.3	94.4	80.7	14.4 ± 0.3	14.6 ± 0.3	14.1 ± 0.3

N.D, not detected

[a] Mean ± standard deviation %

Table 4. 2 Results for the determination of trace heavy metal ions in tap water samples.

Interference inos	Peak current (μA)			Relative signal change (%)		
	Zn^{2+}	Cd^{2+}	Pb^{2+}	Zn^{2+}	Cd^{2+}	Pb^{2+}
No interference ions	47.62	44.10	30.24			
Co^{2+}	44.21	42.46	28.47	7.16	3.44	3.72
Ni^{2+}	46.52	42.11	29.42	2.31	4.51	2.71
Mn^{2+}	45.34	43.03	28.76	4.79	2.43	4.90
Cu^{2+}	44.97	42.41	27.68	5.56	3.83	8.46
Cr^{3+}	46.08	42.64	28.17	3.23	3.31	6.84

Table 4. 3 Effect of interfering ions on the detection of 40 μg L^{-1} Zn^{2+}, Cd^{2+} and Pb^{2+}.

References

[1] a) Vallee, B. L.; Ulmer, D. D. *Annual Review of Biochemistry* **1972**, *41*, 91. b) Hynes, M. J.; Jonson, B. *Chemical Society Reviews* **1997**, *26*, 133. c) Paoliello, M. M. B.; De Capitani, E. M. *Environmental Research* **2007**, *103*, 288.

[2] Aragay, G.; Pons, J.; Merkoçi, A. *Chemical Reviews* **2011**, *111*, 3433.

[3] Pohl, P. *TRAC Trends in Analytical Chemistry* **2009**, *28*, 117.

[4] Caroli, S.; Forte, G.; Iamiceli, A. L.; Galoppi, B. *Talanta* **1999**, *50*, 327.

[5] a) Vydra, F.; Stulík, K.; Juláková, E.; Tyson, J. *Electrochemical stripping analysis*, Ellis Horwood Chichester **1976**. b) Wang, J. *Electroanalysis* **2005**, *17*, 1341.

[6] Florence, T. M. *Journal of Electroanalytical Chemistry and Interfacial Electrochemistry* **1970**, *27*, 273.

[7] a) Wang, J.; Lu, J. *Electrochemistry Communications* **2000**, *2*, 390. b) Arduini, F.; Calvo, J. Q.; Palleschi, G.; Moscone, D.; Amine, A. *TRAC Trends in Analytical Chemistry* **2010**, *29*, 1295. c) Kefala, G.; Economou, A.; Voulgaropoulos, A.; Sofoniou, M. *Talanta* **2003**, *61*, 603.

[8] a) Xu, H.; Zeng, L.; Xing, S.; Xian, Y.; Shi, G.; Jin, L. *Electroanalysis* **2008**, *20*, 2655. b) Ding, L.; Liu, Y.; Zhai, J.; Bond, A. M.; Zhang, J. *Electroanalysis* **2014**, *26*, 121. c) Zhu, L.; Tian, C.; Yang, R.; Zhai, J. *Electroanalysis* **2008**, *20*, 527. d) Hwang, G. H.; Han, W. K.; Park, J. S.; Kang, S. G. *Talanta* **2008**, *76*, 301. e) Chen, L.; Su, Z.; He, X.; Liu, Y.; Qin, C.; Zhou, Y.; Li, Z.; Wang, L.; Xie, Q.; Yao, S. *Electrochemistry Communications* **2012**, *15*, 34. f) Yi, W. J.; Li, Y.; Ran, G.; Luo, H. Q.; Li, N. B. *Sensors and Actuators B: Chemical* **2012**, *166*, 544. g) Wei, Y.;

Yang, R.; Yu, X.-Y.; Wang, L.; Liu, J.-H.; Huang, X.-J. *Analyst* **2012**, *137*, 2183.

[9] a) Katsnelson, M. I. *Materials Today* **2007**, *10*, 20. b) Zhu, Y.; Murali, S.; Cai, W.; Li, X.; Suk, J. W.; Potts, J. R.; Ruoff, R. S. *Advanced Materials* **2010**, *22*, 3906.

[10] a) Wu, S.; He, Q.; Tan, C.; Wang, Y.; Zhang, H. *Small* **2013**, *9*, 1160. b) Pumera, M.; Ambrosi, A.; Bonanni, A.; Chng, E. L. K.; Poh, H. L. *TrAC Trends in Analytical Chemistry* **2010**, *29*, 954. c) Shao, Y.; Wang, J.; Wu, H.; Liu, J.; Aksay, I. A.; Lin, Y. *Electroanalysis* **2010**, *22*, 1027.

[11] Novoselov, K. S.; Geim, A. K.; Morozov, S.; Jiang, D.; Zhang, Y.; Dubonos, S.; Grigorieva, I.; Firsov, A. *Science* **2004**, *306*, 666.

[12] Dato, A.; Radmilovic, V.; Lee, Z.; Phillips, J.; Frenklach, M. *Nano Letters* **2008**, *8*, 2012.

[13] Reina, A.; Jia, X.; Ho, J.; Nezich, D.; Son, H.; Bulovic, V.; Dresselhaus, M. S.; Kong, J. *Nano Letters* **2008**, *9*, 30.

[14] a) Stankovich, S.; Dikin, D. A.; Piner, R. D.; Kohlhaas, K. A.; Kleinhammes, A.; Jia, Y.; Wu, Y.; Nguyen, S. T.; Ruoff, R. S. *Carbon* **2007**, *45*, 1558. b) McAllister, M. J.; Li, J.-L.; Adamson, D. H.; Schniepp, H. C.; Abdala, A. A.; Liu, J.; Herrera-Alonso, M.; Milius, D. L.; Car, R.; Prud'homme, R. K. *Chemistry of Materials* **2007**, *19*, 4396.

[15] a) Guo, S.-X.; Zhao, S.-F.; Bond, A. M.; Zhang, J. *Langmuir* **2012**, *28*, 5275. b) Guo, H.-L.; Wang, X.-F.; Qian, Q.-Y.; Wang, F.-B.; Xia, X.-H. *ACS nano* **2009**, *3*, 2653. c) Zhou, M.; Wang, Y.; Zhai, Y.; Zhai, J.; Ren, W.; Wang, F.; Dong, S. *Chemistry-A European Journal* **2009**, *15*, 6116. d) Chen, K.; Chen, L.; Chen, Y.; Bai, H.; Li, L. *Journal of Materials Chemistry* **2012**, *22*, 20968. e) Liu, C.; Wang, K.; Luo, S.; Tang, Y.; Chen, L. *Small* **2011**, *7*, 1203.

[16] a) Wang, Z.; Zhou, X.; Zhang, J.; Boey, F.; Zhang, H. *The Journal of Physical Chemistry C* **2009**, *113*, 14071. b) Shao, Y.; Wang, J.; Engelhard, M.; Wang, C.; Lin, Y. *Journal of Materials Chemistry* **2010**, *20*, 743. c) Chen, L.; Tang, Y.; Wang, K.; Liu, C.; Luo, S. *Electrochemistry Communications* **2011**, *13*, 133. d) Kauppila, J.; Kunnas, P.; Damlin, P.; Viinikanoja, A.; Kvarnström, C. *Electrochimica Acta* **2013**, *89*, 84.

[17] Wang, Z.; Wang, H.; Zhang, Z.; Liu, G. *Sensors and Actuators B: Chemical* **2014**, *199*, 7.

[18] Huang, H.; Chen, T.; Liu, X.; Ma, H. *Analytica Chimica Acta* **2014**, *852*, 45.

[19] Li, J.; Guo, S.; Zhai, Y.; Wang, E. *Analytica Chimica Acta* **2009**, *649*, 196.

[20] Pokpas, K.; Zbeda, S.; Jahed, N.; Mohamed, N.; Baker, P. G.; Iwuoha, E. I. *Internationl Journal of Electrochemistry Science* **2014**, *9*, 736.

[21] Ping, J.; Wang, Y.; Wu, J.; Ying, Y. *Food Chemistry* **2014**, *151*, 65.

[22] Chen, P.; McCreery, R. L. *Analytical Chemistry* **1996**, *68*, 3958.

[23] Wang, D.-W.; Gentle, I. R.; Lu, G. Q. *Electrochemistry Communications* **2010**, *12*, 1423.

[24] a) Kampouris, D. K.; Banks, C. E. *Chemical Communications* **2010**, *46*, 8986. b) Brownson, D. A. C.; Banks, C. E. *Analyst* **2010**, *135*, 2768.

[25] Lv, M.; Wang, X.; Li, J.; Yang, X.; Zhang, C. a.; Yang, J.; Hu, H. *Electrochimica Acta* **2013**, *108*, 412.

[26] a) Järup, L. *British medical bulletin* **2003**, *68*, 167. b) Esteban-Vasallo, M. D.; Aragonés, N.; Pollan, M.; López-Abente, G.; Perez-Gomez, B. *Environmental health perspectives* **2012**, *120*, 1369.

[27] Schramel, P.; Wendler, I.; Angerer, J. *International archives of occupational and environmental health* **1997**, *69*, 219.

[28] Willis, J. *Analytical chemistry* **1962**, *34*, 614.

[29] Tokalioğlu, Ş.; Kartal, Ş.; Elci, L. *Analytica chimica acta* **2000**, *413*, 33.

[30] a) Aragay, G.; Merkoçi, A. *Electrochimica Acta* **2012**, *84*, 49. b) Zhu, L.; Xu, L.; Huang, B.; Jia, N.; Tan, L.; Yao, S. *Electrochimica Acta* **2014**, *115*, 471.

[31] Economou, A.; Fielden, P. *Analyst* **2003**, *128*, 205.

[32] a) Rehacek, V.; Hotovy, I.; Vojs, M. *Electroanalysis* **2014**, *26*, 898. b) Švancara, I.; Prior, C.; Hočevar, S. B.; Wang, J. *Electroanalysis* **2010**, *22*, 1405. c) Lezi, N.; Economou, A.; Dimovasilis, P. A.; Trikalitis, P. N.; Prodromidis, M. I. *Analytica chimica acta* **2012**, *728*, 1. d) Dimovasilis, P. A.; Prodromidis, M. I. *Analytica chimica acta* **2013**, *769*, 49. e) Lien, C.-H.; Hu, C.-C.; Chang, K.-H.; Tsai, Y.-D.; Wang, D. S.-H. *Electrochimica Acta* **2013**, *105*, 665. f) Riman, D.; Jirovsky, D.; Hrbac, J.; Prodromidis, M. I. *Electrochemistry Communications* **2015**, *50*, 20.

[33] Gao, C.; Yu, X.-Y.; Xu, R.-X.; Liu, J.-H.; Huang, X.-J. *ACS applied materials & interfaces* **2012**, *4*, 4672.

[34] a) Li, F.; Song, J.; Yang, H.; Gan, S.; Zhang, Q.; Han, D.; Ivaska, A.; Niu, L. *Nanotechnology* **2009**, *20*, 455602. b) Wang, Y.; Li, Z.; Wang, J.; Li, J.; Lin, Y. *Trends in biotechnology* **2011**, *29*, 205. c) Shang, L.; Bian, T.; Zhang, B.; Zhang, D.; Wu, L. Z.; Tung, C. H.; Yin, Y.; Zhang, T. *Angewandte Chemie International Edition* **2014**, *53*, 250.

[35] a) Yang, X.; Zhang, X.; Ma, Y.; Huang, Y.; Wang, Y.; Chen, Y. *Journal of Materials Chemistry* **2009**, *19*, 2710. b) Cong, H. P.; He, J. J.; Lu, Y.; Yu, S. H. *Small* **2010**, *6*, 169. c) Wang, C.; Feng,

C.; Gao, Y.; Ma, X.; Wu, Q.; Wang, Z. *Chemical engineering journal* **2011**, *173*, 92. d) Yang, K.; Hu, L.; Ma, X.; Ye, S.; Cheng, L.; Shi, X.; Li, C.; Li, Y.; Liu, Z. *Advanced materials* **2012**, *24*, 1868. e) Fu, Y.; Wang, J.; Liu, Q.; Zeng, H. *Carbon* **2014**, *77*, 710.

[36] a) Qu, S.; Wang, J.; Kong, J.; Yang, P.; Chen, G. *Talanta* **2007**, *71*, 1096. b) Peik-See, T.; Pandikumar, A.; Nay-Ming, H.; Hong-Ngee, L.; Sulaiman, Y. *Sensors (Basel)* **2014**, *14*, 15227. c) Wu, D.; Li, Y.; Zhang, Y.; Wang, P.; Wei, Q.; Du, B. *Electrochimica Acta* **2014**, *116*, 244. d) Bharath, G.; Madhu, R.; CHEN, S.-M.; Vediyappan, V.; Mangalaraj, D.; Nagamony, P. *Journal of Materials Chemistry A* **2015**.

[37] Jang, B.; Chae, O. B.; Park, S.-K.; Ha, J.; Oh, S. M.; Na, H. B.; Piao, Y. *Journal of Materials Chemistry A* **2013**, *1*, 15442.

[38] Allen J. Bard, L. R. F. *Electrochemical Methods: Fundamentals and Applications*, 2nd ed., Wiley **2011**.

[39] Teymourian, H.; Salimi, A.; Khezrian, S. *Biosensors and Bioelectronics* **2013**, *49*, 1.

[40] Yantasee, W.; Hongsirikarn, K.; Warner, C. L.; Choi, D.; Sangvanich, T.; Toloczko, M. B.; Warner, M. G.; Fryxell, G. E.; Addleman, R. S.; Timchalk, C. *Analyst* **2008**, *133*, 348.

[41] Ruecha, N.; Rodthongkum, N.; Cate, D. M.; Volckens, J.; Chailapakul, O.; Henry, C. S. *Analytica chimica acta* **2015**, *874*, 40.

[42] in *Multicomponent Reactions in Organic Synthesis*, Wiley-VCH Verlag GmbH & Co. KGaA, **2014**, pp. 471.

[43] Sun, Y.-F.; Chen, W.-K.; Li, W.-J.; Jiang, T.-J.; Liu, J.-H.; Liu, Z.-G. *Journal of Electroanalytical Chemistry* **2014**, *714-715*, 97.

[44] Haifeng, Y.; Yan, Y.; Junfang, L.; Xiaojing, L.; Guangcheng, X.; Qing, Z.; Chao, W. *Chemistry Letters* **2013**, *42*, 150.

[45] Fu, L.; Li, X.; Yu, J.; Ye, J. *Electroanalysis* **2013**, *25*, 567.
[46] Chaiyo, S.; Mehmeti, E.; Žagar, K.; Siangproh, W.; Chailapakul, O.; Kalcher, K. *Analytica chimica acta* **2016**, *918*, 26.

Chapter 5. Conclusion

The development of new composite electrode materials is an important issue in analytical chemistry. The proposed bismuth-based nanocomposite electrodes achieve good analytical performance for heavy metal detection. The remarkable stripping performance of the bismuth electrode is due to the ability of this metal to form “fused alloys” with other heavy metals, analogous to the formation of mercury amalgams. In addition, carbon nanomaterials such as graphene have been explored as electrode materials for the detection of heavy metal ions. Nanostructured electrodes have also been fabricated using composites of two or three materials, providing synergistic contributions from individual components.

This dissertation aimed at fabricating bismuth-based nanocomposites for the detection of heavy metal ions. To achieve this, we prepared a novel enhanced sensing platform based on porous graphene via simple activation of GO by KOH. The resultant AG exhibits a unique structure that makes it a potentially attractive material for the electrochemical determination of trace metal ions. The composite film integrates the unique properties of AG and the

advantages of bismuth electrodes, leading to enhanced sensitivity toward trace metal ions. The AG-NA/Bi composite was also used as an electrode material for the determination of metal ions in a real sample. Thus, the proposed method facilitates the monitoring of trace heavy metal ions and can be expanded to detect other environmental pollutants.

Further, an enhanced sensing platform based on the direct electrochemical reduction of GO colloidal solution at glassy carbon electrodes has been developed for the determination of zinc, cadmium, and lead by DPASV. The glassy carbon electrode modified with an electrochemically deposited graphene (EG)/Bi nanocomposite film exhibited intense sharp peaks of heavy metal ions, showing improved detection limits compared to other bismuth-modified electrodes due to the combined beneficial properties of EG (enhanced electron transfer, large specific surface area, good conductivity, etc.) and the good stripping character of bismuth. The synthetic strategy described in this work has several advantages. First, this method can be used to quantitatively control film thickness and form a stable film on the electrode surface without any further treatment, leading to a straightforward integration of the EG film and

the EG/Bi composite electrode. Second, the above method is environmentally friendly, employing “green” graphene film electrode fabrication under mild conditions. Third, this strategy is easy and fast to implement. We show that graphene films can be directly prepared on the electrodes using a one-step electrodeposition of GO dispersions. Additionally, this green preparation method, being simple, fast, and free of chemical reduction reagents, offers several advantages over other graphene fabrication techniques and expands the scope of graphene-based electrochemical sensing devices, showing promise for wider applications in environmental analysis.

Finally, a novel and highly sensitive electrochemical sensor for heavy metal ion determination was fabricated based on an electrode modified by a graphene-supported iron oxide nanoparticle composite. The iron oxide (Fe_2O_3)/graphene (G) nanocomposite was synthesized from the iron oleate precursor and graphene by solvent-free thermal decomposition. This novel nanohybrid combined the unique electronic behavior of graphene with the excellent catalytic properties of Fe_2O_3 nanoparticles due to their synergistic integration. The fabricated sensor showed excellent stability and was successfully applied to the simultaneous determination of Zn^{2+}, Cd^{2+}, and Pb^{2+} in

real samples, with results being consistent with those obtained by ICP-MS. The proposed method can be potentially used for the monitoring of heavy metals and other pollutants in a wide range of electrochemical sensing applications.

We have compared those composite electrodes with other modified electrodes, and the results are listed in Table 5.1.and 5.2. The analytical performance of the bismuth nanocomposite-modified electrodes is comparable and even better than previous reports.

Thus, the prepared bismuth-based nanocomposite enables the fabrication of highly sensitive electrode materials for the detection of heavy metal ions, with the results suggesting its tremendous potential for applications in other fields.

	RGO/Bi Composite	AG/Bi Composite (Chap. 2)	EG/Bi Composite (Chap. 3)	Fe_2O_3/G/Bi Composite (Chap. 4)
The effective surface area	0.068cm^2	0.072cm^2	0.080cm^2	0.082cm^2
The anodic to cathodic peak separation (ΔE)	92 mV	85 mV	95 mV	68 mV

Table 5. 1 Comparison of the effective surface area and peak separation with bismuth nanocomposite-modified electrodes.

Electrodes	Linear range (μg L^{-1})			LOD (μg L^{-1})		
	Zn^{2+}	Cd^{2+}	Pb^{2+}	Zn^{2+}	Cd^{2+}	Pb^{2+}
RGO/NA/Hg	0.5 – 5.0	0.5 – 5.0	0.5 – 5.0	0.14	0.13	0. 07
RGO/NA/Bi	–	0.44 – 178	2.4 – 241	–	0.18	0.09
CNT/Bi	20 – 100	20 –100	20 – 100	12	0.70	1.30
MWCNTs/NA/Bi	–	0.08 – 100	0.05 –100	–	0.04	0.03
RGO/AlOOH	–	200 – 800	200 – 800	–	0.03	0.09
ERGO/PG/Bi	10 – 100	10 – 100	10 – 100	0.26	0.10	0.16
AG/NA/Bi (Chap. 2)	5 – 100	5 – 100	5 – 100	0.57	0.07	0.05
EG/Bi (Chap. 3)	1-100	1-100	1-100	1.08	0.18	0.11
Fe_2O_3/G/Bi (Chap. 4)	1-100	1-100	1-100	0.11	0.08	0.07

Table 5. 2 Comparison of the electrodes modified with bismuth nanocomposite and other materials for the detection of heavy metals.

Bibliography

1. International Publications

1) **Sohee Lee**, Sungyool Bong, Jeonghyun Ha, Minjeong Kwak, Seung-Keun Park, Yuanzhe Piao,
"Electrochemical Deposition of Bismuth on Activated Graphene-Nafion Composite for Anodic Stripping Voltammetric Determination of Trace Heavy Metals",
Sensors and Actuators B: Chemical, **2015**, *215*, 62-69.

2) **Sohee Lee**, Seung-Keun Park, Eunjin Choi, Yuanzhe Piao,
"Voltammetric determination of trace heavy metals using an electrochemically deposited graphene/bismuth nanocomposite film-modified glassy carbon electrode",
Journal of Electroanalytical Chemistry, **2016**, *766*, 120-127.

3) Minjeong Kwak[1], **Sohee Lee[1]**, Dongwon Kim, Seung-Keun Park, Yuanzhe Piao ([1]These authors contributed equally to this work.)
"Facile synthesis of Au-graphene nanocomposite for the selective determination of dopamine",
Journal of Electroanalytical Chemistry, **2016**, *776*, 66-73.

4) **Sohee Lee**, Jiseop Oh, Dongwon Kim, Yuanzhe Piao

"A sensitive electrochemical sensor using an iron oxide/graphene composite for the simultaneous detection of heavy metal ions"

Talanta, **2016**, *160*, 528–536.

5) Seung-Keun Park, Seunghee Woo, **Sohee Lee**, Chae-Yong Seong, Yuanzhe Piao

"Design and Tailoring of Three-dimensional Graphene–Vulcan carbon–Bi2S3 Ternary Nanostructures for High-Performance Lithium-Ion-Battery Anodes",

RSC Advances, **2015**, *5*, 52687-52694.

6) Eunjin Choi, **Sohee Lee**, Yuanzhe Piao,

"A solventless mix-bake-wash approach to the facile controlled synthesis of core-shell and alloy Ag-Cu bimetallic nanoparticles",

CrystEngComm, **2015**, *17*, 5940-5946.

2. Domestic Publications

1) 이소희, 박원철

"전기 화학적으로 활성화된 glassy carbon 전극에서의 전압-전류 법을 이용한 Clenbuterol 측정"

Journal of the Korean Electrochemical Society, **2014**, *17*, 216-221.

3. International Conference

1) **Sohee Lee**, Yuanzhe Piao,

"Simultaneous Detection of Trace Heavy Metal Ions Using a Chemically Activated Graphene / Bi Nanocomposites Electrode by Differential Pulse Anodic Stripping Voltammetry"

The 225th ECS Meeting, Orlando, Florida, USA, May, 11-15, 2014.

2) **Sohee Lee**, Yuanzhe Piao,

"Determination of trace heavy metal by differential pulse anodic stripping voltammetry using a chemically activated graphene-bismuth nanocomposite electrode",

1st International Conference on Functional Integrated Nano Systems, Graz, Austra, December 3-5, 2014.

3) **Sohee Lee**, Yuanzhe Piao,

"Determination of Clenbuterol at electrochemically activated glassy carbon electrode"

2014 International Symposium on New Frontiers in Nano-Bio-Energy Convergence Science and Technology (ISNBE 2014), AICT,

Suwon, Korea, August 12-13, 2014.

4) **Sohee Lee**, Yuanzhe Piao,

"Voltammetric determination of trace heavy metals using an electrochemically deposited graphene/bismuth nanocomposite film modified glassy carbon electrode"

2015 International Symposium on New Frontiers in Nano-Bio Convergence Technology, AICT, Suwon, Korea, December 17-18, 2015. - ***Oral presentation***

5) Byungchul Jang, **Sohee Lee**, Yuanzhe Piao

"Preparation of Iron-oxide/Graphene Nanocomposite as Anode Material in Li-ion Secondary Batteries"

Carbon 2014, Jeju Island, Korea, June 29-July 4, 2014.

6) Eunjin Choi, **Sohee Lee**, Yuanzhe Piao,

"Robust thermal decomposition synthetic route to noble bimetallic alloy nanomaterials"

2015 International Chemical Congress of Pacific Basin Societies, Pacifichem 2015, Honolulu, HI, USA, December 15-20, 2015.

3. Patents

1) 박원철, 최은진, 이소희, “복합 금속 나노 입자의 제조 방법”, 출원번호: 10-2014-0051526.

4. Award

1) *Excellent Paper Presentation Award* at the 2013 Spring Meeting of the Korean Electrochemical Society
2) *Excellent Paper Presentation Award* at the 2014 Spring Meeting of the Korean Society of Industrial and Engineering Chemistry.

국 문 초 록

중금속은 대기 중에 미립자로서 부유하거나, 폐수의 형태로 방류되어 토양, 수자원 등 자연환경을 광범위하게 오염시키는 것으로 알려져 있다. 이 중 수은, 카드뮴, 크롬 등은 생활에서 자주 접할 수 있고, 독성이 강하기 때문에 주요 환경물질로 간주되고 있다. 중금속은 환경에 배출되면 생물 농축에 따라 사람에게까지 피해가 미치므로 그 심각성이 더해지고 있다. 소량의 중금속이더라도 체내에 축적이 되면 배설되지 않고 장기간에 걸쳐 건강에 해를 미친다. 예를 들어 수은과 납이 축적되는 경우 근육과 신경을 마비시키는 신경계 장애를 일으키고, 카드뮴은 골연화증을 일으키고 폐암을 발생시킬 수 있다. 아연은 적혈구의 활성저하를 일으켜 면역력이 저하된다. 이러한 문제들 때문에, 중금속의 검출과 분석은 매우 중요한 이슈로 여겨진다.

기존의 중금속 이온 분석방법으로는 유도 결합 플라즈마 질량분석법 (Inductively coupled plasma mass spectrometry: ICP-MS), 유도 결합 플라즈마 분광법 (Inductively couple atomic emission spectrometry: ICP-AES), 원자 흡수 분광 광도법

(Atomic absorption spectroscopy: AAS)등이 있다. 하지만 이러한 분석 방법은 샘플에 존재하는 중금속 이온들을 측정하기 위한 복잡한 전처리 과정과 고가의 분석 장비 사용이 요구되기 때문에 비용과 시간이 많이 소요된다는 단점이 있다. 이로 인해 측정 가능한 시료의 수는 제한적이고 측정하고자 하는 시료의 중금속 오염 정도를 정확하게 모니터링 하는데 어려움이 있다. 이와는 반대로 전기화학적 Stripping Voltammetry 기술은 샘플 내에 존재하는 중금속의 선택적 분리 및 농축이 가능하기 때문에 미량의 중금속 이온도 정량 분석이 가능하다. 결과적으로 전기화학적 방법을 통한 미량의 중금속 이온 검출 방법에 대한 분석법이 활발히 연구되고 있다. 일반적으로 사용되는 전기화학적 분석 방법으로는 Anodic stripping voltammetry 인데, 이는 작업 전극(working electrode) 으로 주로 수은을 사용 한다. 하지만, 분석 후 발생되는 유독성인 수은의 후처리 문제와 분석결과의 재현성을 위한 표면처리 문제, 그리고 공기 중에 노출되면 쉽게 변화하는 특성 등으로 인하여, 최근 수은을 함유하지 않은 무독성 및 친환경적인 대체 전극 개발에 많은 노력들이 이루어지고 있다. 현재 이러한 문제점을 해결하기 위하여 비스무스 (Bismuth; Bi)를 수은 대신 사용하여 중금속을 검출하려는 연구가 진행되고 있

다. 이러한 전기 화학적 분석 방법을 도입함과 동시에 전극용 물질로 전자전달 및 물질전달능력, 뛰어난 기계적, 구조적 성능 등을 가진 그래핀을 전극에 도입하여 우수한 민감도 및 내구성을 가진 센서를 제작하는 연구가 진행되고 있다.

본 학위 논문에서는 친환경적인 비스무스를 기반으로한 그래핀과 나노입자를 도입하여 비스무스 기반의 나노복합체 전극을 제조하고, 이를 활용하여 중금속 이온 검출에 대해 기술하였다.

첫째로, 화학적으로 활성화 시킨 그래핀을 비스무스와 복합체 개질 전극을 이용한 중금속 이온 센서를 개발하였다. 합성된 그래핀 옥사이드에 수산화칼륨을 이용하여 기공구조를 형성하고, 이를 통해 기존에 열적 환원을 통해 얻은 그래핀 보다 훨씬 큰 비표면적을 갖는 활성화된 그래핀을 얻었고, 이 활성화된 그래핀으로 작동 전극을 개질 하고 여기에 전기화학적으로 환원된 비스무스를 복합시켜 중금속 이온검출을 위한 전극을 개발하였다. 두번째로, 전기화학적으로 환원된 그래핀과 비스무스 나노복합체를 합성하고 이를 중금속 이온을 검출하였다. 그래핀 옥사이드를 수용액 상에서 작동전극에 직접 환원 시키고, 이후 비스무스를 같은 방식인 전기화학적 방법으로 환원시켜 복합체를 만들어 개질 전극을 개발

하였다. 이 전극을 이용하여 보다 쉬운 단계로 중금속 이온 검출을 위한 전극 개발을 하였다. 마지막으로, 열적 방법으로 합성된 그래핀과 산화철 나노입자를 용매없이 건식 상태에서 나노복합체를 합성하였다. 이를 또한 작동전극에 개질 하여 중금속 이온을 검출 하였다.

다양한 방법을 통해 그래핀 및 나노입자를 복합재료로 형성하고 이를 중금속 이온 검출 전극 재료로 적용하였을 때, 기존소재 대비 월등한 성능 향상 및 내구성 향상을 확인 할 수 있었다.

주요어: 비스무스, 나노복합체, 중금속 이온 검출, 그래핀, 양극 벗김 전류법, 전기화학 센서, 개질 전극.

학 번: 2011-22758